AD_____

Award Number: W81XWH-12-2-0071

TITLE: Novel in vitro/ex vivo animal modeling for Filovirus aerosol infection

PRINCIPAL INVESTIGATOR: Ayesha Mahmood, Ph.D.

CONTRACTING ORGANIZATION: Sanofi Pasteur VaxDesign Corporation
Orlando, Florida, 32826

REPORT DATE: September 2013

TYPE OF REPORT: Annual Report

PREPARED FOR: U.S. Army Medical Research and Materiel Command
Fort Detrick, Maryland 21702-5012

REPORT DOCUMENTATION PAGE

Form Approved
OMB No. 0704-0188

1. REPORT DATE	**2. REPORT TYPE**	**3. DATES COVERED**
September 2013	Annual Report	15 August 2012- 14 August 2013

4. TITLE AND SUBTITLE
Novel in vitro/ex vivo animal modeling for Filovirus aerosol infection

5a. CONTRACT NUMBER

5b. GRANT NUMBER
W81XWH-12-2-0071

5c. PROGRAM ELEMENT NUMBER

6. AUTHOR(S)
Ayesha Mahmood, Ph.D.

Email: Ayesha.Mahmood@sanofi.com

5d. PROJECT NUMBER

5e. TASK NUMBER

5f. WORK UNIT NUMBER

7. PERFORMING ORGANIZATION NAME(S) AND ADDRESS(ES)
Sanofi Pasteur VaxDesign Corporation
Orlando, Florida, 32826

8. PERFORMING ORGANIZATION REPORT NUMBER

9. SPONSORING / MONITORING AGENCY NAME(S) AND ADDRESS(ES)
U.S. Army Medical Research and Materiel Command
Fort Detrick, Maryland 21702-5012

10. SPONSOR/MONITOR'S ACRONYM(S)

11. SPONSOR/MONITOR'S REPORT NUMBER(S)

12. DISTRIBUTION / AVAILABILITY STATEMENT
Approved for Public Release; Distribution Unlimited

13. SUPPLEMENTARY NOTES

14. ABSTRACT
The overall objective of this work is to develop in vitro modular systems to dissect immune responses relating to upper and lower respiratory tract. This approach simplifies the airway physiology to mucosal epithelial interfaces responsible for primary tissue immunological responses to host infections and disease pathogenesis. This report summarizes the work relating to the collaborative research effort between the military USAMRIID labs and Sanofi Pasteur, to investigate the application of the Mucosal Tissue Equivalent (MTE) module of the MIMIC® system for the development of in vitro influenza and filovirus disease models. The cellular composition of the MTE module consists of human and non-human primate species of interest for filovirus infection. The research findings from the five human and four NHP MTE modules indicate non-equivalence of primary cell and cell line form and function. The primary human MTE demonstrates superior morphology, vesicle cycling and antigen presentation cell stimulation. The MTE tissue related innate response, in terms of cytokine and chemokine profiles and viral infection and defense related genes, was also not equivalent in the various MTE motifs. The NHP tissue models showed the greatest degree of permeability and varying growth rates. This developmental work is in the process of evolution into in vitro disease models. The baseline morphological and functional read-outs described in this report may serve as a guide for therapeutic development for highly pathogenic filovirus strains.

15. SUBJECT TERMS- none provided

16. SECURITY CLASSIFICATION OF:			**17. LIMITATION OF ABSTRACT**	**18. NUMBER OF PAGES**	**19a. NAME OF RESPONSIBLE PERSON**
a. REPORT	**b. ABSTRACT**	**c. THIS PAGE**			USAMRMC
U	U	U	UU	92	**19b. TELEPHONE NUMBER** *(include area code)*

Table of Contents

Page

Introduction……..4

Body…….....5

Part I: *In vitro* human tissue models.. ……..…..…..7

Part II: *In vitro* non-human primate tissue models……....43

Key Research Accomplishments……...……...…….……50

Reportable Outcomes……...……..…..……..55

Conclusion……..…….…….…56

Reference……60

Appendices…….…63

A0: Filovirus Morphology……..…...…….....64

A1: Quantitative PCR data and supporting cytokine and chemokine in the human lung tissue models…….....65

A3: Appendix 2: 2013 Biomedical Engineering Society Meeting presentation documentation……..……92

INTRODUCTION

The overall objective of this work is to develop *in vitro* modular systems to dissect immune responses relating to upper and lower respiratory tract. This approach simplifies the airway physiology to mucosal epithelial interfaces responsible for primary tissue immunological responses to host infections and disease pathogenesis. This report summarizes the work relating to the collaborative research effort between the military USAMRIID labs and Sanofi Pasteur, to investigate the application of the Mucosal Tissue Equivalent (MTE) module of the MIMIC® system for the development of *in vitro* influenza and filovirus disease models. The cellular composition of the MTE module consists of human and non-human primate species of interest for filovirus infection. This work is relevant to the US Military due to the potential bioterrorism threat of pathogenic filovirus strains in the military and civilian populations.

BODY:

This report summarizes the year one research findings in the development of nine human and non-human primate MTE models. This work elaborates on the role of tissue form and function by directly comparing primary cell sources and commercially available cell lines of interest for filovirus inflection.

Five human models were evaluated in terms of form and function. The human tissue modules were composed of primary cells from upper (nasal epithelium) and lower (alveolar epithelium and alveolar epithelium/endothelium bilayer) airway. A549 and CRL-1848 epithelial cell lines of human origin were compared against the primary human mucosal MTE. The tissue form (morphology) was evaluated in terms of high resolution electron microscopy, vesicle formation, and tissue permeability. For the human MTE, more extensive immunological functional assays were used to assess responses in terms of cellular activity by the addition of TLR agonists, influenza vaccine antigen and inactivated filovirus strains. These experimental approaches were inspired by human airway physiology. The pulmonary mucosal interface is involved in orchestrating an innate immune response from recognition of pathogen from the epithelial cell surface to cytoplasmic pattern recognition receptors, which in-turn trigger surfactant and mucin production, interferons, and cytokines and chemokines at the site of infection, which is in direct contact with vasculature and mucosal associated lymphoid tissues. Thus functionally relevant *in vitro* readouts were designed to show the ability of the *in vitro human* tissue models to accurately reflect primary tissue function in terms of gene expression of defense related proteins, cytokine and chemokine response and antigen presenting cell maturation. We have successfully addressed project specific aims related to design and primary tissue function of the respiratory epithelium with the addition of immune cells, to build complexity into our modular mucosal tissue models, to begin the transition to influenza disease model work.

Four non-human primate (NHP) tissue models were evaluated for form and basic tissue function. The cellular composition of the NHP MTE included *Macaca mulatta, monkey, rhesus* (4MBr-5), *Tadarida brasiliensis, bat, free-tailed* (TB 1 Lu), *Mus musculus* (LA4), and *African Green Monkey* (Vero) cell lines. The experimental studies for the NHP models included basic tissue staining to assess confluencey and viability, permeability studies and basic vesicle cycling function.

This annual report summarizes the Sanofi Pasteur work relating to specific aims and sub-tasks for the current and up-coming year. Specifically, we have addressed the following tasks:

3.2 Develop MIMIC model of lung epithelium (4QFY13)
- 3.2.1 Develop MTE module with cell lines
- 3.2.2 Develop MTE module with primary cells

3.3 Assess virus infectivity of MTE module (4QFY14)
- 3.3.1 Assess MTE module following influenza vaccination

The human tissue model developmental work is reported in PART I of this report; it addresses Specific Aim 3.2 and 3.3.1. The non-human primate work is shown in Part II; it addresses Specific Aim 3.2.2. There are a total of nine MTE epithelium variations. Table 1 shows functional readouts for the nine human and non-human primate read-outs for the work. The green denote the experiments that were performed. Whereas, the red dots denote experiments that were omitted based on available resources.

			PART I				PART II				
			NHP cell line tissue model				Primary human airway models			Human cell line models	
			4-MBr-5 Rhesus Monkey Bronchial	Tb1 Lu Bat Lung	Vero African Green Monkey Kidney	LA-4 Murine Lung Adenocarcinoma	Alveolar Epithelium	Nasal Epithelium	Alveolar Bilayer Epithelium / endothelium	A549 Lung Carcinoma	CRL1848 Lung Carcinoma
Airway Tissue	Tissue Integrity	Viability	●	●	●	●	●	●	●	●	●
		Confluencey (live/dead staining)	●	●	●	●	●	●	●	●	●
		High resolution TEM (differentiated epithelium)	●	●	●	●	●	●	●	●	●
		Short-term FITC Dextran permeability (10KDA, 70KDa, 500KDa)	●	●	●	●	●	●	●	●	●
	Vesicle / membrane function	Membrane activity (epithelium dye uptake)	●	●	●	●	●	●	●	●	●
		Active vesicle cycling (time-lapse confocal imaging)	●	●	●	●	●	●	●	●	●
	Gene expression	PRR: TLR gene expression- TLR agonists	●	●	●	●	●	●	●	●	●
		PRR: TLR expression- Irradiated filovirus interaction	●	●	●	●	●	●	●	●	●
		Cytosolic PRR: RIG-I and NOD1- inactive filovirus	●	●	●	●	●	●	●	●	●
		Surfactant protein genes expression- inactive filovirus	●	●	●	●	●	●	●	●	●
		Mucin protein gene expression- inactive filovirus	●	●	●	●	●	●	●	●	●
	Secretory factors	Cytokine and chemokine response- TLR agonist-3,-4	●	●	●	●	●	●	●	●	●
Airway Tissue Plus Immune Cells Innate Immune Response	DC Phenotype (CD14, HLA-DR)	Bacterial antigen Inactive *Staphylococcus aureus*	●	●	●	●	●	●	●	●	●
		Influenza vaccine (FluMist®, Fluzone®)	●	●	●	●	●	●	●	●	●
	Secretory factors	Cytokine and chemokine response Bacterial antigen- inactive *Staphylococcus aureus*	●	●	●	●	●	●	●	●	●
		Cytokine and chemokine response Influenza vaccine- FluMist®, Fluzone®	●	●	●	●	●	●	●	●	●

Table 1: Design of experiments grid for human and non-human primate tissue models

PART I: *In vitro* human tissue models: Form and function

Background: Experimental logic based on human physiology

For the identification of tissue architecture and basic cellular function, human tissue models composed of primary cells from the upper and lower airway along with cell lines were directly compared. Specifically, the models included primary cells from nasal epithelium, alveolar epithelium, and alveolar epithelium /endothelium along with A549 and CRL-1848 cell lines. The simple idea of “morphology drives biology” was explored repeatedly to compare the various cell type containing tissue models.

The tissue form and functional readouts for this work were inspired by human physiology. The pulmonary epithelium is one on the largest mucosal surfaces for pathogen entry. This mucosal tissue is involved in a variety of host mechanisms against large to small foreign matter pathogens. These are known to directly interact with the pulmonary epithelium and vascular endothelium. The variety of host response is dependent on pathogen recognition. The antigen uptake efficiency is based on its interaction with mucosal surface and cytoplasmic pattern recognition receptors, defense surfactant and mucin proteins that initiate the innate cellular response through secretory cytokine and chemokines responsible for leukocyte recruitment at the infection site and number of physiological pathways leading to a systemic response (Grieber, 2008; Yang, 2008; Ariki, 2012). The morphological differences between the models were identified in terms of high resolution transmission microscopy and fluorescently labeled dextran permeability studies. The functional readouts for the human tissue models included some basic vesicle cycling studies, secretory cytokine and chemokine levels, quantification of select genes involved in antigen / pathogen recognition, defense protein secretion, and immune responses. The design of our *in vitro* human tissue models has been simplified to address form and biological complexity of human airways.

The disease model work on human tissue models was initiated by using inactive filovirus strains and commercially available influenza vaccines. The mechanism and efficiency of virus entry and disease pathogenesis is related to how the pathogen interacts with the host cells. These readouts can be used as a guide for vaccine discovery and disease pathogenesis evaluation. For understanding these interactions, inactive virus particles served as a guide to safely characterize the initial key interactions between the virus and mucosal cells. To this end, the human tissue model work was focused on identifying classic pathogen entry genes of interest including pattern recognition receptors, host defense proteins and interferon pathway related genes for virus entry along with a handful of genes associated with bacterial entry.

Recognizing the importance of pattern recognition (PRR) function in host entry and therapeutic discovery, our rationale for exploring the innate response to known TLR

agonists was to define baseline function in terms of secretory factors along with sub-cellular factors like PRR and host defense related genes. The innate immune response relies on cellular pattern recognition receptors' (PRR) ability to recognize pathogen associated molecular pattern (PAMP) structures on the surface of the pathogen. The toll-like receptor (TLR) family is the most recognized type pattern recognition receptors (Grieber, 2008; Greene, 2005), followed by Nod-like receptors, RIG-1 receptor family, and others. The PRR family is associated with inflammation pathways including cytokine and chemokine responses, and lymphocyte recruitment which connects the local tissue to systemic host response to infection leading to adaptive immune response. The TLR family is composed on integral transmembrane glycoproteins found on the cellular surface and on the endosome and lysosome membranes. They interact with the pathogen associated PAMP molecules resulting in intracellular signal transduction of multiple host defense mechanisms. Toll like receptors-3, -7, -8, and -9 recognize nucleic acids and are associated with endosomal membranes; this is of relevance to filovirus entry. TLR3 recognize dsRNA in the intracellular compartments. TLR 7 and 8 are activated by ssRNA. Whereas, TLR 1, -2, -3, -4 and 6- recognize cellular membrane glycoprotein PAMP. Besides the TLR family, the intracellular cytostolic pathogens and their ssRNA, dsRNA, and DNA are recognized by retinoid acid-inducible gene I (RIG-1) family and nucleotide-binding oligomerization domain (NOD)-like receptors of the of PRR structures. For viral infection, the RIG-I sense cytoplasmic RNA is associated with type I interferon response induced by viral entry. Protein kinases are also activated by the IFN response and work alongside the RIG-I RNA helicases. NOD1 and NOD2 are the most recognized of NLR family members involved triggering inflammatory response due to recognition of bacterial peptidoglycan (Optitz, 2010; Xiang, 2010). Thus, the genomic work was inspired by pathogen recognition biology, defense proteins and interferon related pathways.

The functional characterization of the *in vitro* upper and lower airway model began with simple vesicle cycling studies, which evolved into an exploration of TLR agonist induced gene expression of innate immunity related genes and secreted cytokines and chemokine levels in the culture supernatants. The side-by-side comparison of primary cells vs. cell lines allowed for direct comparison of cellular intrinsic properties as they relate to mucosal infection and primary cellular defense mechanisms. These preliminary experiments were designed to demonstrate the baseline tissue related genomic activity for bacterial and viral antigen entry leading to immune cell recruitment and systemic response. The interaction between the pulmonary mucosa and respiratory antigen is initiated by pattern recognition receptors. TLR-3 and TLR4 are found on the alveolar endothelial and epithelial tissue. The classic example of pathogen associated molecular pattern (PAMP) associated with gram positive bacterial membrane is lipopolysaccharide (LPS) stimulation of TLR-4. Toll like receptor-3 activation is associated with viral dsRNA and synthetic poly(I:C). TLR2 ligands are involved in both gram positive and gram negative bacteria, along with mycoplasma, and yeast. Whereas, TLR 7 and TLR 8 recognize the ssRNA in most viruses along with anti-viral compounds like imiquimod

(Greene 2005). TLR9 is activated by bacterial DNA and unmethylated CpG. Thus, for broad-spectrum analysis of other TLR ligands and perhaps similarities to inactive viral or bacterial antigen profiles, the study included Pam3CSK4 (TLR1/TLR2), R848 (TLR7/TLR8), Gardiquimod (TLR7), CpG2006 (TLR9), Poly (I:C) (TLR3), and LPS (TLR4). Inactive filovirus strains of Bundibugyo, Ebola, Marburg, and Zaire whole virus were also tested along with influenza vaccine antigen (FluMist®, Fluzone®) to identify the innate endogenous and exogenous response for the influenza and filovirus disease models.

The experimental approaches to the MTE module define the baseline level of tissue related form and function. Our multi-step approach to characterization of related physiological pathways permits direct comparison of endogenous and exogenous pathways. The following sections are divided into specific studies with the same form and function theme to connect biology *in vitro* biology to the physiological knowns.

Human tissue models: Experimental methods

Tissue morphology and functional assays

Cell culture

Primary human nasal and alveolar cells (Promocell), A549 (ATCC), and CRL-848 (ATCC) were expanded in T-175 flasks in airway cell media. Passage 4 cells were used for tissue model studies. The primary tissue models were prepared by seeding 50,000 cells on a trans-well bucket coated wtih collagen and laminin in 10% serum containing 1:1 (v/v) Media199 and DMEM with 1% penicillin-streptomycin (sigma). After 3hr incubation, the multiwall plates were placed on the rocker at a rate of one cycle per minute. Media was exchanged every 48hr until the cells were confluent. For the cell lines, cell seeding density was 35,000cells/per well. Tissue layer formation was observed between 3-4 days for the cell lines and 5-7days for the primary cells. Media was removed from the apical side of tissue constructs and placed on a rocker at a rate of 1cycle per minute for 3 hour. The experiments were staggered to take into account the growth rates so the stimulations were done on differentiated tissue constructs.

High resolution Transmission Electron Microscopy (TEM)

The confluent tissue layers were fixed in 2.5% gluteraldehyde overnight. The samples were stained with 2% Osmium tetroxide (1hr) and Enbloc stained with 4% uranyl acetate (1hr). The tissue was dehydrated with ethanol and propylene oxide (1hr) and embedded in Epon resin. The resin blocks were cut and stained with uranyl acetate and lead citrate. The virus suspension was negatively stained with 2% phosphotungstic acid prior to visualization on EM grids. High resolution transmission electron microscopy was used for comparing the primary and cell line tissue models.

In vitro vesicle cycling via time-lapse tissue imaging

FM-143FX, a lipophilic styryl dye, was used to label cellular vesicle membranes. The dye (1ug/ml) was added to the apical side of live differentiated tissue. Fluorescence microscopy images were captured every 2 minutes for a period of 10-15 minutes for time lapse studies.

Innate mucosal tissue response: Treatment conditions

Innate mucosal responses were generated by applying treatment media to the apical side of the tissue constructs. After 24hr exposure, the culture supernatants and tissues were collected and immediately frozen at-30^{o}C.,. Lysis buffer was added to the tissue construct prior to storage. For each condition and tissue model, three sets of constructs were prepared. The concentration of various antigen were identical, to directly compare the tissue response from primary cells and human cell lines. Cell lysis buffer was introduced to the tissue constructs for RT-PCR studies. Specifically, FV1 (Sudan-lot012010AIK), FV2 (MAR-lot 5Nov2009), FV3 (EBOV-95-lot1), FV4 (BDBV-lot1Jun2010) were tested at a concentration of 100ng/ml TLR agonists included Pam3CSK4, Poly (I: C), LPS, R848, Gardiquimod, and CpG2006 were tested at 50ng/ml. With the exception of LPS (Sigma), all TLR agonists were purchased from Invivogen. 2010-2011 FluMist® (live attenuated) and Fluzone® (inactive intramuscular) were tested at 1:500 dilution of the vaccine. *Staphylococcus aureus* bioparticles were tested at a concentration of 1million particles per ml. The benzopyrene (0.5ug/ml) and nicotine (0.162ug/ml) combination was tested as a control smoke irritant.

Tissue morphology with inactive filovirus introduction

Please refer to Appendix A0 for the methods and results. The purpose of the study was to verify the starting material. This is not directly related to project specific aims.

Tissue "Leakiness" or permeability studies

FITC-dextran permeability studies were designed to measure tissue integrity. The tissue models were prepared as described above, in serum containing media. For permeability studies, base media (M199) was used for human and NHP tissue cell layers to remove residual media and cellular debris. 700ul was added to the receiver bucket and the apical side was exposed to air interface for 2hr. Eight serial dilutions for FITC-dextran (MW 10KDa, 70KDa, 500KDa; Sigma-Aldrich) were made and added to the apical side of the construct. Eight tissue constructs were sacrificed per time point (30, 180, 360min) after apical and basal media was collected and read at 485nm/535nm

wavelength. The data was reported in terms on concentration (mg/ml) based on the standard curve for each dextran.

Mucosal cytokine & chemokine response

Millipore 14-plex kits were used to quantify the baseline tissue response. The bead analytes include Interleukin-1a, -1b, -6, -8, -10, -12(p40), -12(p70), granulocyte macrophage colony stimulating factor (GM-CSF), monocyte chemotactic protein-1 (MCP-1), macrophage inflammatory protein (MIP-1a, MIP-1b), macrophage derived chemokine (MDC), interferon gamma-induced protein (IP-10), interferon (IFN-alpha2), and tumor necrosis factor (TNF-alpha). The culture supernatants were diluted with X-vivo and tested along with kit standards and controls. The observed results are reported in picograms per milliliter and based on the standards provided in the kits.

Quantitative PCR analysis of human mucosal tissue

Qiazol lysis buffer containing frozen tissue samples were homogenized in two cycles with the TissueLyser II (Qiagen) (20 Hz, 3 minutes). The samples were then pooled (6 replicates for treated samples and 12 replicates for no-treatment controls) into 1.5ml microcentrifuge tubes (Fisher), labeled, and stored at -20°C. To define baseline levels, RNA extraction was performed on the no treatment controls using the RNeasy Plus Mini Kit (Qiagen). RNA concentrations and purities were assayed by NanoDrop 2000 spectrophotometry. The quality of extracted RNA was then confirmed using an Agilent RNA 6000 Nano Kit (Agilent Technologies) along with the Agilent 1500 BioAnalyzer (Agilent Technologies). This process was later repeated for the treated samples. The RNA quality and concentration was determined prior to the qPCR reactions. cDNA synthesis was then performed with the RT² First Strand Kit (Qiagen) using 400ng of each sample. Per reaction protocol, the cDNA synthesis reactions were placed on ice while preparing the PCR components master mix. 37ul of cDNA synthesis reaction was added to a tube containing 185ul of 2X RT² SYBR Green qPCR Mastermix (Qiagen); samples were run in sets of 12. For each reaction, the volume was brought up to 370ul by the addition of 148ul of RNase-free water (Qiagen). The cycler (Applied Biosystems) generated the final Ct values. The genes of interest included pattern recognition receptors (TLR1, TLR2, TLR3, TLR4, TLR7, TLR9, DDX58/RIG-1, NOD1/CARD4), interferon responsive genes (SOCS1, STAT1, JAK2), defense response genes to bacteria (IFNB1, IFNG, MYD88, TNF), viral defense response genes **(**IFNAR2, IFNB1TYK2, EIF2AK2/PRKR, IRF3, TICAM1/TRIF, TNF), JAK/STAT signaling genes (STAT1, JAK2, TYK2), drug metabolism genes (CYP1A1,CYP1B1, GSTP1), and defense mechanism proteins (SFPD, SFPC, MUC1, MUC5AC). The delta-delta Ct method was used with the no treatment control as a baseline measure to generate the heat maps.

Innate tissue response of human tissue models with monocyte addition

Treatment conditions

The exposure time (24hr) and concentration of various antigens were identical to directly compare the tissue response from primary cells and human epithelial cell lines. The 2010-2011 FluMist® (live attenuated intranasal) and Fluzone® (split inactive intramuscular influenza) vaccines were tested at 1:250 dilution. *Staphylococcus aureus* bioparticles were tested at a concentration of 2 million particles per ml. For each condition, four sets of constructs were prepared for each tissue model per donor.

Antigen presenting cell collection and phenotyping

For the human constructs, monocytes were isolated from freshly thawed PBMCs. EasySep CD14 magnetic selection columns were used for monocyte collection. Prior to immune cell addition, antigen treatments prepared in X-vivo media were applied to each MTE based on the treatment conditions described above. Two hours after treatment, one million isolated monocytes were applied to differentiated tissue constructs. The MTE modules were incubated overnight for extravasation through the tissue constructs. The antigen presenting cells were harvested from the receiving bucket and prepared for flow cytometry analysis. The harvested antigen presenting cell population was stained with live/dead aqua, CD14, HLA-DR, CD80, CD83, and CD86 antibodies. Flow cytometric analysis was performed and gated on the live cell population. Cell surface marker expression of dendritic cells was determined by gating CD14, HLA-DR, CD80, CD83, and CD86.

Secretory cytokine and chemokine response

Millipore 14-plex kits were used to quantify the baseline tissue responses. The bead analytes were identical to the tissue interrogation section described above.). For innate response profiling, four replicate treatment conditions treatment wells were collected at 24hr from 10 donors (40 total). The culture supernatants were diluted with X-vivo and tested along with kit standards and controls. The observed results were reported in concentration, picogram per milliliter.

Results and discussion

Part I: Human MTE tissue models (specific aims 3.2.1; 3.3.1)

The experimental findings from the human tissue models described below are divided into sections to demonstrate MTE form and function. Experimental results follow the logic of MTE form in terms of 1) TEM imaging to compare cellular organelles and tissue health, 2) vesicle cycling, 3) tissue "leakiness" or FITC-Dextran permeability. The innate tissue response was characterized by the addition of TLR agonists along with bacterial (staphylococcus aureus) and viral (influenza and filovirus) antigen. The mucosal tissue

			Primary human airway models			Human cell line models	
			Alveolar Epithelium	Nasal Epithelium	Alveolar Bilayer Epithelium / endothelium	A549 Lung Carcinoma	CRL1848 Lung Carcinoma
Airway Tissue	Tissue Integrity	Viability	+	+	+	+	+
		Confluencey (live/dead staining)	+	+	+	+	+/-
		High resolution TEM (differentiated epithelium)	+	+	+	-/+	-/+
		Short-term FITC Dextran permeability (10KDA, 70KDa, 500KDa)	+/-	+/-	-	+	+
	Vesicle / membrane function	Membrane activity (epithelium dye uptake)	++	++	++	+/-	+/-
		Active vesicle cycling (time-lapse confocal imaging)	++	++	++	-	-
	Gene expression	PRR: TLR gene expression- TLR agonists	+/-	+/-	++	+/-	-/+
		PRR: TLR expression- Irradiated filovirus interaction	-/+	-	+/-	-/+	++
		Cytosolic PRR: RIG-I and NOD1- inactive filovirus	-	-/+	++	-	++
		Surfactant protein genes expression- inactive filovirus	-/+	-/+	+/-	+/-	+/-
		Mucin protein gene expression- inactive filovirus	-	-/+	+/-	+	+
	Secretory factors	Cytokine and chemokine response- TLR agonist-3,-4	+/-	+/-	-/+	+	+

Table 2: Summary of human MTE module mucosal tissue response

related readouts included 4) secretory factors (cytokines and chemokines), and 5) gene expression. The human lung MTE was further analyzed with the addition of immune cells and later re-visited to characterize innate immune response via 6) secretory cytokines and chemokines, and 7) activation of antigen presenting cell surface markers. The generalized results for the human MTE construct studies are summarized in Table 2. The following sections will elaborate the research findings. Some examples include the ability of human primary cells MTE to demonstrate superior morphology, and permeability profiles, along with vesicle cycling function, when compared against the cell lines. The alveolar bilayer MTE shows the highest degree of TLR family gene expression. The cytokine and chemokine response was higher in the A549 and CRL-1848 cell lines.

Morphological differences between human primary cells and cell lines via Transmission Electron Microscopy (TEM) and vesicle cycling

High resolution TEM and vesicle cycling studies were designed to visualize the differentiated tissue organelles and vesicle formation with and without the presence of surfactant or lipid containing vesicles. In general, TEM observations showed that the primary airway constructs exhibit healthy organelles, differentiated tissue, and more active vesicle cycling compared to the cell line tissue models (Figures 1-5). This was further confirmed by confocal microscopy using membrane and vesicle dye addition (Figures 6 & 7). The rate of vesicle formation was further confirmed with time-lapse confocal microscopy. Thus, these basic cell biology studies demonstrate that our primary cells and culture conditions exploit differentiated cellular morphology and function in concordance with what is expected in human airway physiology. (Feherenbach, 2001; Herzpg, 2008). Furthermore, the vesicle cycling funciton was confirmed by TEM and confocal microscopy; this basic funtion is of relavance to virus entry and pathogen specific PRR function. Thus, the morpholgy described in this section is realted to the biology in the following set of studies.

The primary alveolar epithelial MTE modules exhibit healthy cellular organelles including large nuclei, rough endoplasmic reticulum, mitochondria and ribosomes within surfactant containing vesicles (Figure 1). In general, the presence of surfactant was visualized by the appearance of concentric structures by lamellar bodies within vesicles. Various stages of active vesicle formation, from membrane pinching to vesicle release can be observed in Figure 1a, b, c, and d. The apical villi show the active epithelial interface for antigen interaction. Figure 1f shows a high resolution image of vesicles containing surfactant and endosome like structures similar to in-vivo physiology. The presence of lamellar body containing surfactant vesicles is indicative of a differentiated alveolar epithelium with Type II cell function which is critical for pathogen entry through the lower airway. The lower airway contains two types of epithelial cells. Type I epithelial cells support the mechanical process of breathing and homeostasis. Type II alveolar epithelial cells are considered pseudo-epithelial cells, as they actively take part in antigen uptake and transport via vesicles with the aid of lipid membranes and surfactants to facilitate the transport to and from the open airways. The presence of

Type II epithelial cells and surfactant vesicles in the primary cell MTE demonstrates a visual of the mucosal immune function (Feherenbach, 2001; Herzog, 2008).

Primary alveolar bilayer constructs also contained healthy organelle structures with presence of vesicles formation at the outer membrane (Figure 3a, b, f). A variety of vesicle structures were found with empty (v), lipid filled (lv) and surfactant or lamellar body containing (sv) microstructures. The presence of surfactant and lipid filled vesicles is indicative of type II epithelial cells which are involved in picking up antigen and producing surfactant from the lower airway. The electron microscopy observation of the alveolar bilayer moving vesicles, from one cell to the next, mimics the physiological function of active vesicle cycling and is directly related to antigen pick-up and pathogen clearance (Herzog, 2008).

Similar to the alveolar epithelial construct, the primary nasal epithelial tissue (Figure 2) contains healthy nuclei, rough ER, and golgi structures with vesicles containing surfactant and lamellar bodies (marked sv). Active vesicle cycling across the cells is shown in figure 2e. Surfactant and dense endosome like structures were also observed

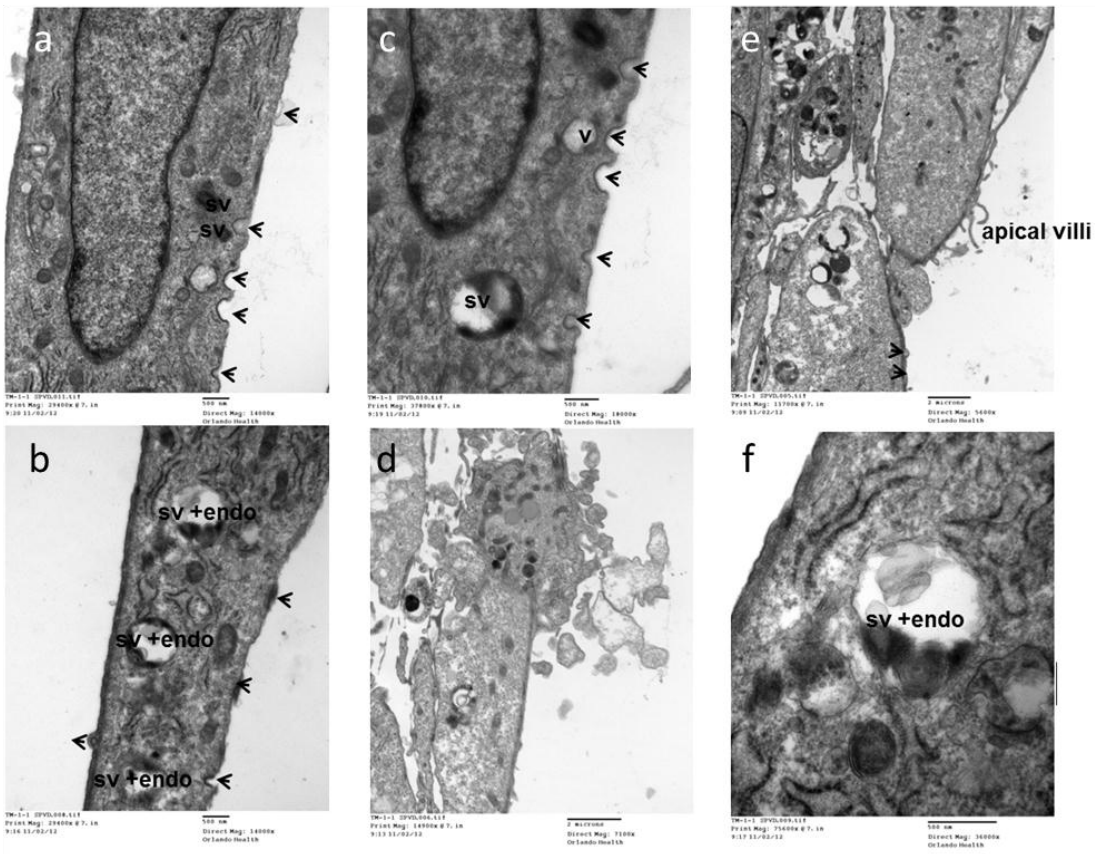

Figure 1: Electron microscopy imaging of differentiated primary alveolar epithelial tissue demonstrates active vesicle cycling *sv=surfactant vesicle with lamellar body like structures, endo=dense endosome like structures within the vesicles

(figure 2f). The nasal constructs contained a larger proportion of vesicles without lamellar bodies which we have identified as lipid filled vesicles (lv).

A549 cell line tissue constructs contained highly vescularized cells with relatively large nuclei and less defined cellular organelles, relative to the primary cell models described above. Figure 4a also showed the presence of keratosis-like organization in one construct; this may be an attribute of this cancerous cell line. The presence of microvilli at the apical surface (Figure 4e) is indicative of an active epithelial interface. However, the health of the cell appears to be compromised. We speculate that the “rocking” condition used to differentiate the pulmonary tissue models at the air-liquid interface may be responsible for this exaggerated vesicle formation activity in the A549 cell line; however, this could also be attributed to the intrinsic nature of the carcinogenic cell line.

The CRL-1848 tissue model contained a high density of empty vesicles similar to the

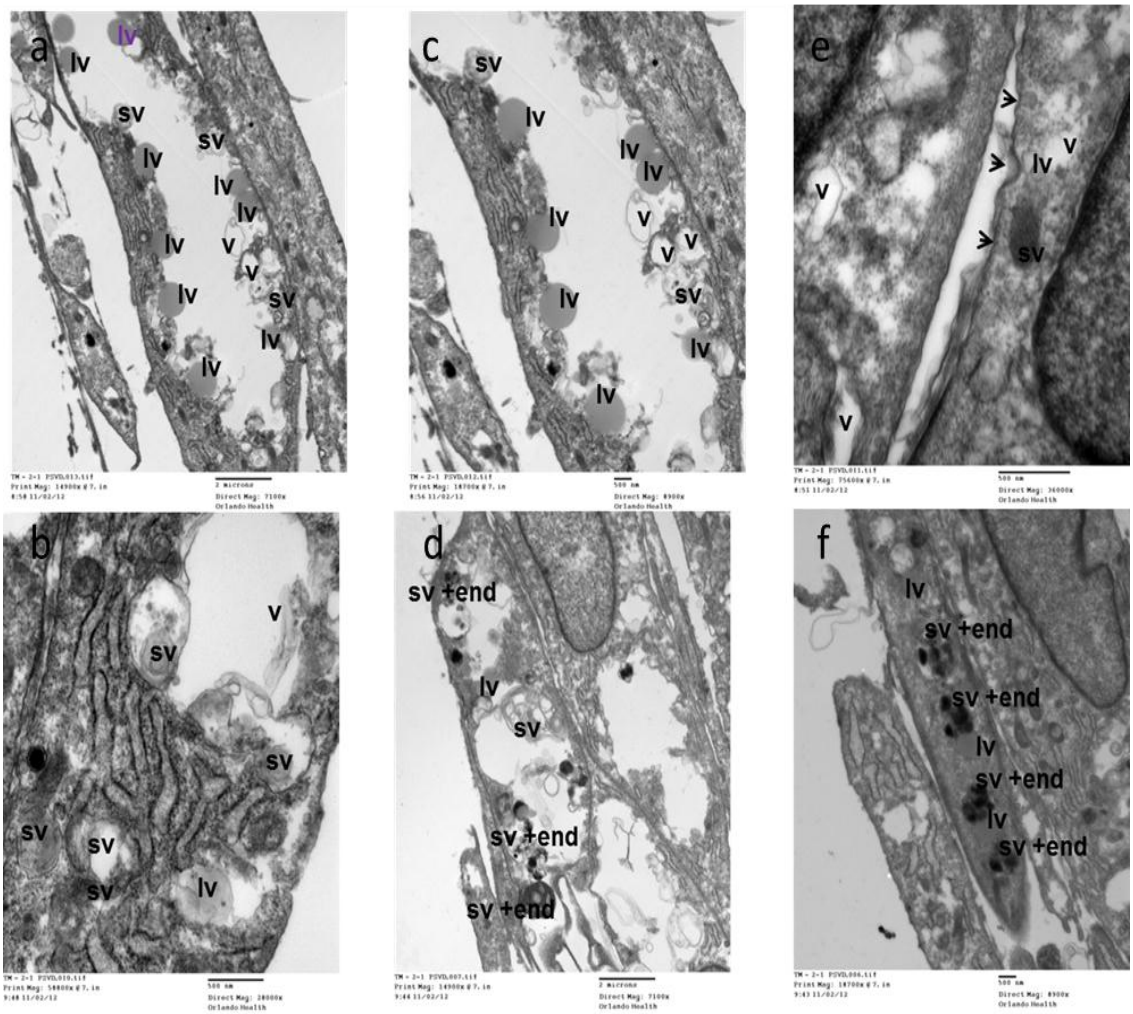

Figure 2 Electron microscopy imaging of differentiated primary nasal epithelial tissue demonstrates active vesicle cycling lv=lipid vesicles, non-lamellar body vesicles with dense fluid identified as lipids *sv=surfactant vesicle with lamellar body like structures, v=empty vesicles, endo=dense endosome like structures within the vesicles

A549 cell line described above. However, this tissue also displayed the presence of marginally healthier nuclei ribosomes and endoplasmic reticulum (Figure 5 a, b, e). Figure 5b shows a large vesicle like structure which contains ruminants of a dying or dead cell. Similar to the A549 model Figure 5f shows a differentiated and highly vascularized cell on the periphery. Under the tested conditions, both the cell lines have unusual microstructures with little or no presence of vesicles containing surfactant or lipids.

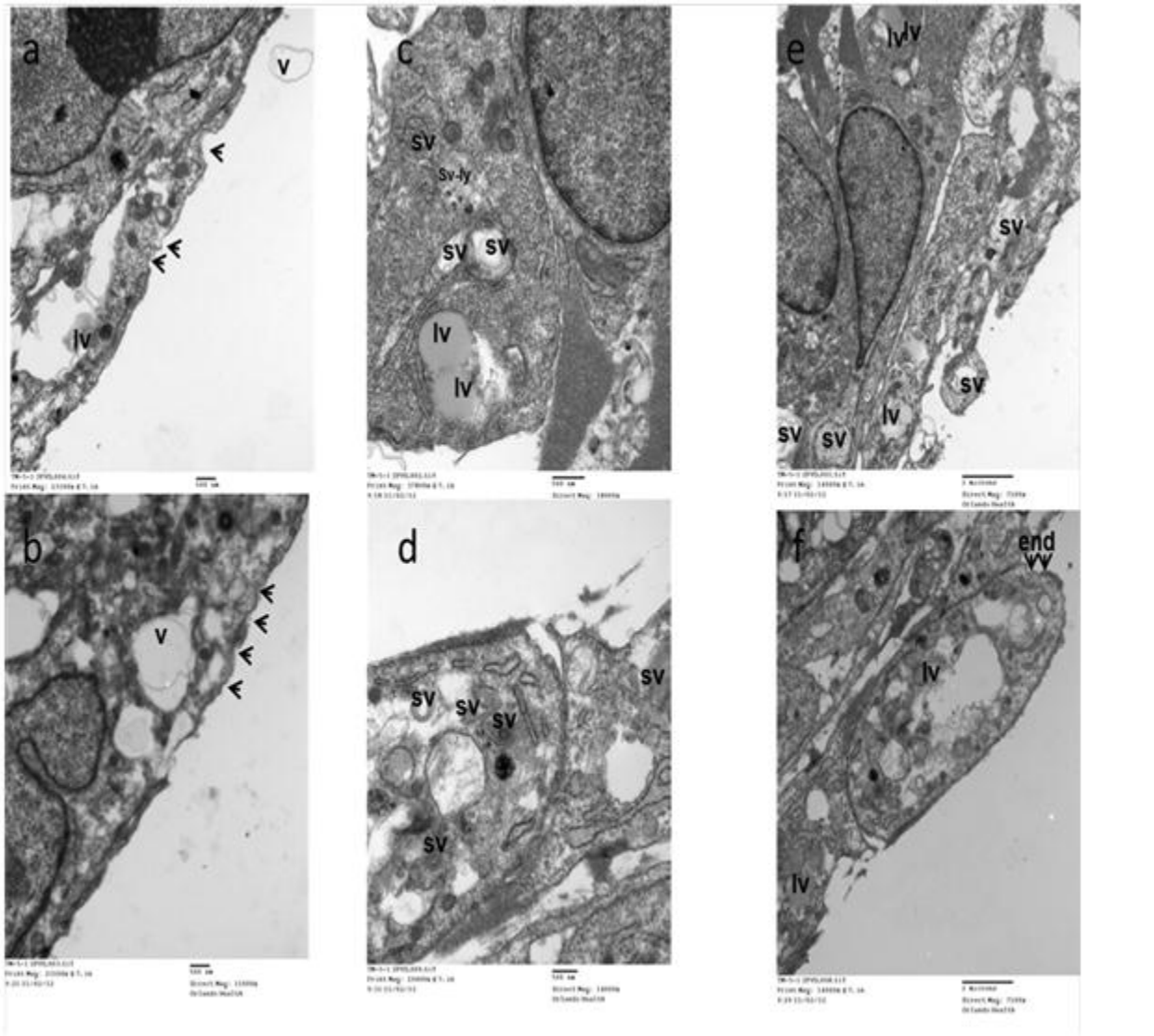

Figure 3 Electron microscopy imaging of differentiated alveolar bilayer tissue constructs demonstrates active vesicle cycling (a, b, f). This tissue contains empty vesicles along with surfactant and lipid filled structures. * lv=lipid vesicles, non-lamellar body vesicles with dense fluid identified as lipids, sv=surfactant vesicle with lamellar body like structures, v=empty vesicles, endo=dense endosome like structures within the vesicles

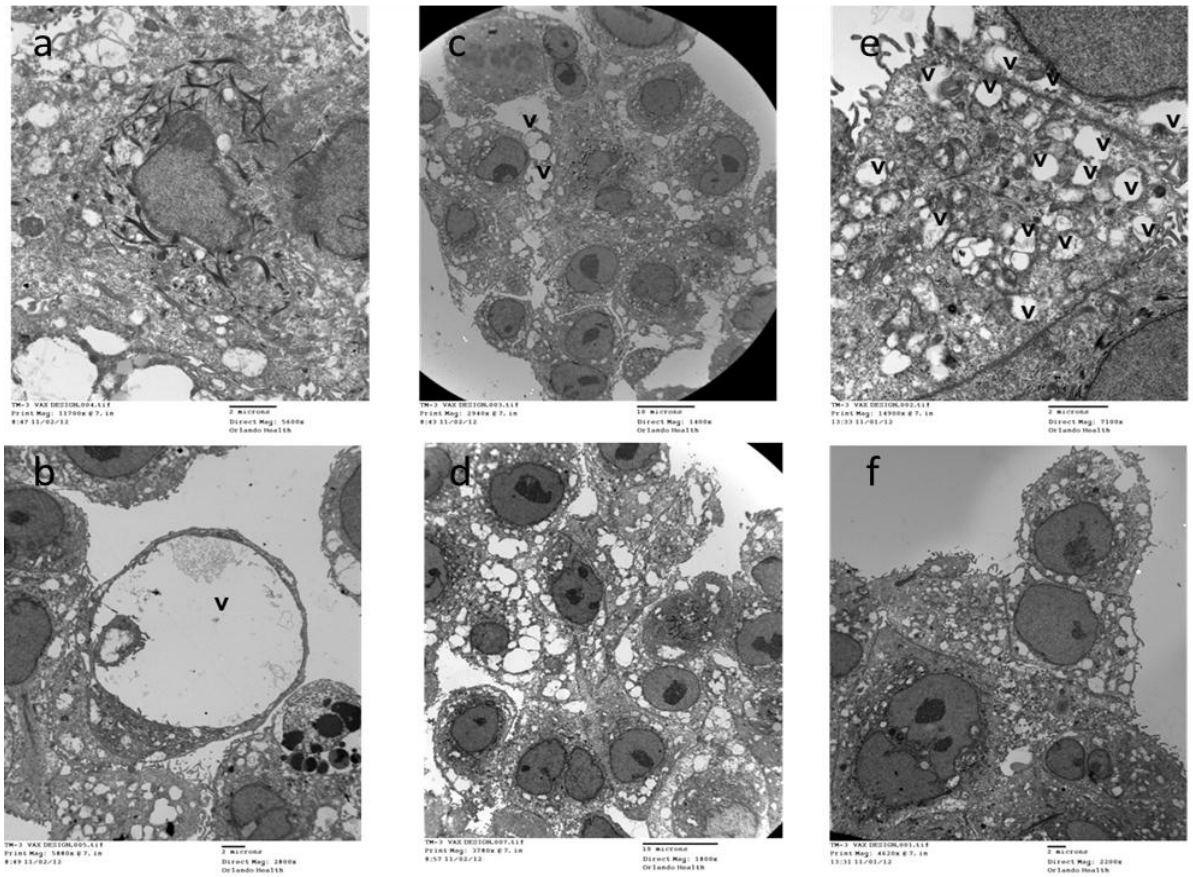

Figure 4 Electron microscopy imaging of human A549 cell line shows relatively larger nuclei and a higher ratio of empty vesicles with presence of organized structures similar to keratin peals found in carcinoma (a). Differentiated cells on the apical side (c) are filled with empty vesicle of small and b) relatively larger sizes. This can be observed with other tissue section regions (d, f)

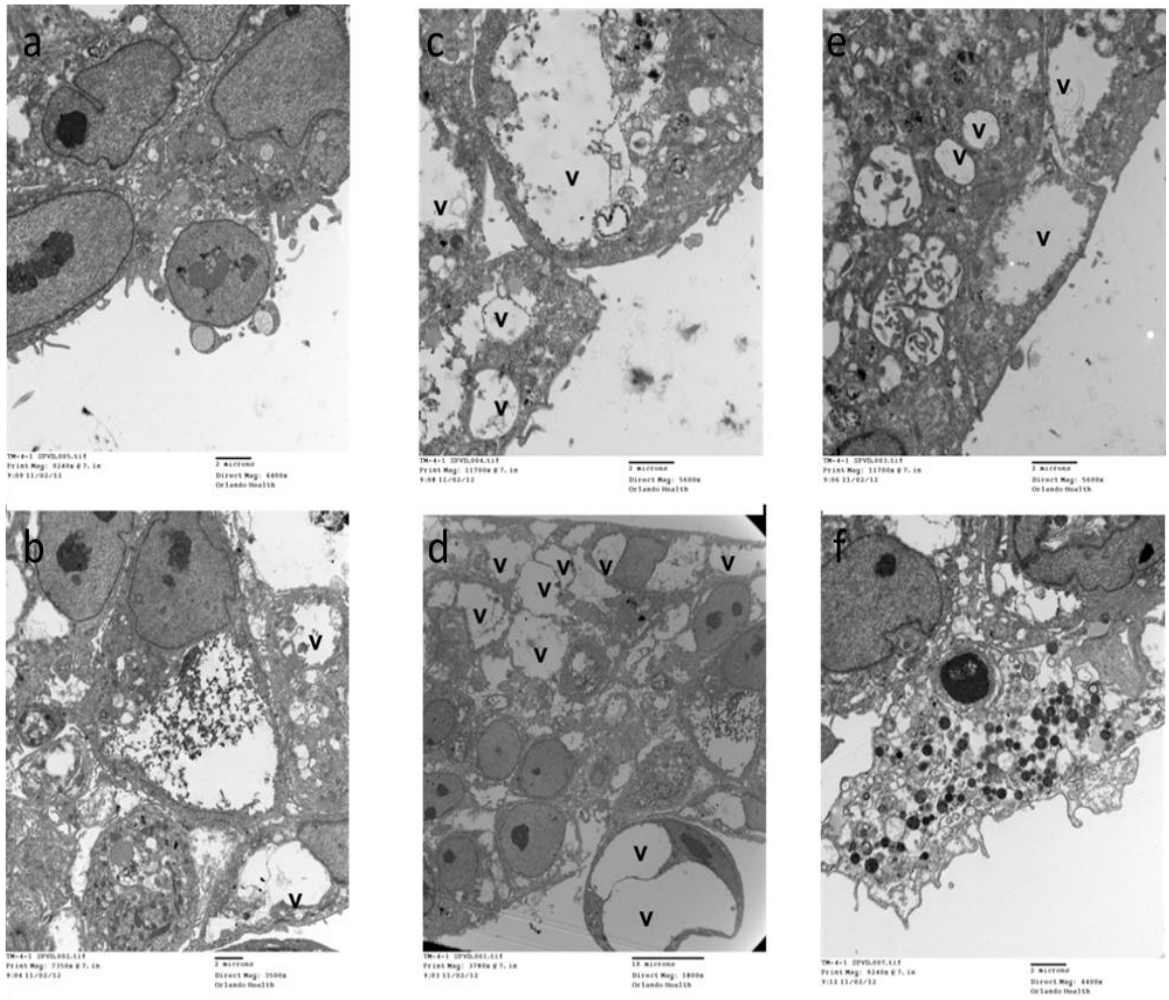

Figure 5: CRL1848 tissue constructs exhibit a highly vescularized morphology (b,c,d,e) with defined nuclei (a,b), and ribosomes and endoplasmic reticulum (b,e). On the apical side f) cell contain microvilli and highly vescularized cytoplasm with endosome-like structures. This cell (f) also appears to be pyknotic and dying

Basic vesicle cycling funciton in human tissue models via fluoresence microscopy of cellular vesicles

Similar to the elelctron microscopy results, the primary cells exhibited more active vesicle formation. Compared to the A549 and CRL-1848 human cell lines the round dense vesicle-like stuctures (Figure 6c) on the apical side of the confluent tissue (Figure 6a) are densly packed in the primary alveolar and nasal tissue. The membrane dye does have some residual background fluoresnce from the cellular membrane. However, the presence of the round vesicle stucutres with a bighter yellow appearce confirms the movement of the styrl dye in the form of a vesicle. The images clearly show that the primary cells contain a dense number of these vesicles in their cytoplasm.

Time lapse imaging of vesicle cycling across the tissue constructs showed a similar trend in vesicle formation (Figure 7). The images for the primary cell show the presence of bright vesicles as early as 2 minutes post exposure to FM-143FX dye. This direct

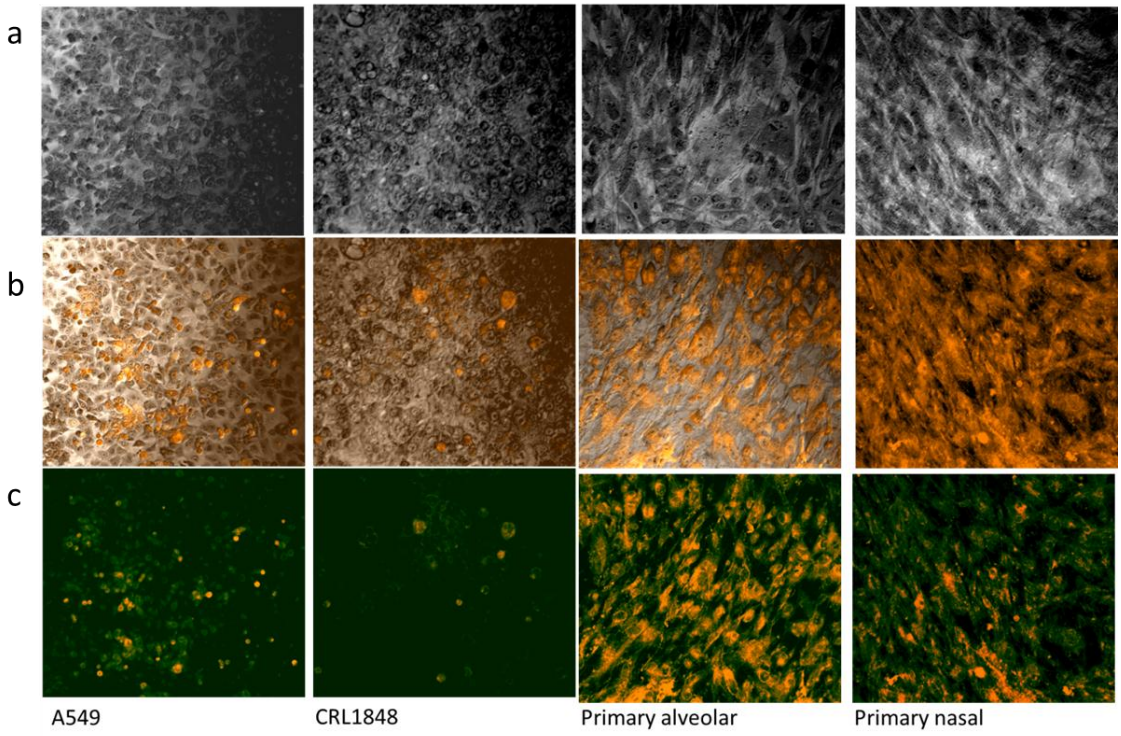

Figure 6: Light (a) and c) fluorescence microscopy along with simultaneous visualization of both light and confocal images at 6 minutes post streyl dye FM-143FX exposure. (b) the superimposed light microscopy image with the fluorescence image to demonstrate vesicle concentration in the area of interest.

comparison shows the relatively higher vesicle cycling function of the primary alveolar and nasal epithelial cells when compared to the A549 and CRL848 cell lines. It is important to note that the TEM images of the primary cells showed the presence of more differentiated epithelium with lipid or surfactant-like vesicle structures. We speculate that the same specialized vesicle structures are involved in the trafficking of our probe. It was also interesting to note there was a slight lag in the alveolar bilayer model vesicle cycling. The alveolar epithelium alone and in the presence of an endothelium showed a larger ration of lamellar body or surfactant carrying vesicles. It is possible that the dye is interacting with surfactant or mucin-like protein prior to entry.

Leakiness of human tissue models: FITC-Dextran permeability studies

The FITC-dextran experiments, with three different molecular weights, were designed to characterize the confluencey through the measurement of short term “leakiness” of the tissue constructs. This is of relevance to determine the degree of active process of monocyte extravasation through the tissue, to drive the innate response post infection and also can be used to assess how various factors (drugs, pathogens, allergens, irritants) influence vascular permeability. For example, how anti-histamines reduce vascular leakage following allergen insult, etc.

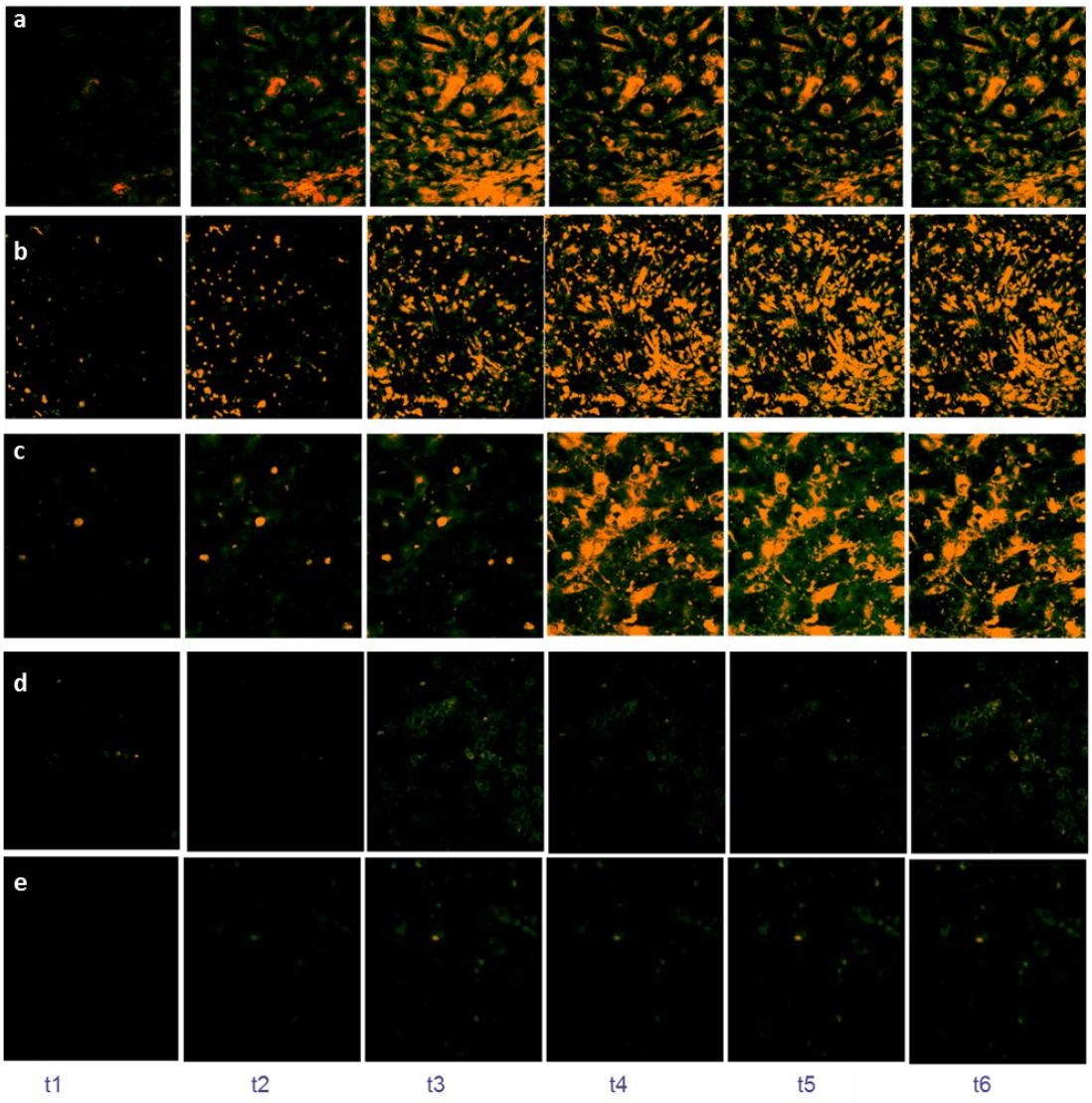

Figure 7: Direct comparison of vesicle cycling kinetics via visualization through time-lapse confocal microscopy of human airway tissue models with 2 minute time intervals a) Primary alveolar, b) primary nasal, c) primary alveolar bilayer, d) CRL-1848 cell line, e) A549 cell line

For the permeability studies, the experimental set-ups and kinetic sampling was identical for the primary cells and cell lines, for consistency and direct comparison of the MTE modules, The basal measure of the FITC dextran molecules (10Ka, 70KDa, 500KDa) serves as the most reliable measure of permeability since non-specific binding to the trans-well material, and attachment or metabolism of the molecule by the cells was not measured.

The basal FITC-dextran measure indicates the most non-confluent tissue constructs were composed of human CRL-1848 cell line (Figure 8). These findings correlate with the previous qualitative confocal imaging results in which gaps were observed in the cultured tissue. For the human primary cell tissue models, the permeability study results suggest that the alveolar bilayer model was the least permeable and therefore the most confluent with tight gap junctions as is observed in normal human respiratory conditions (Figure 8). While this was anticipated, the results also suggest the alveolar epithelium has a similar low permeability profile for this study. However, the two alveolar MTE modules are not equivalent. This idea was not supported by the next set of experiments with the dendritc cell maturation as a marker of the quality of the extravasation processes, which is directly related to tissue confluencey.

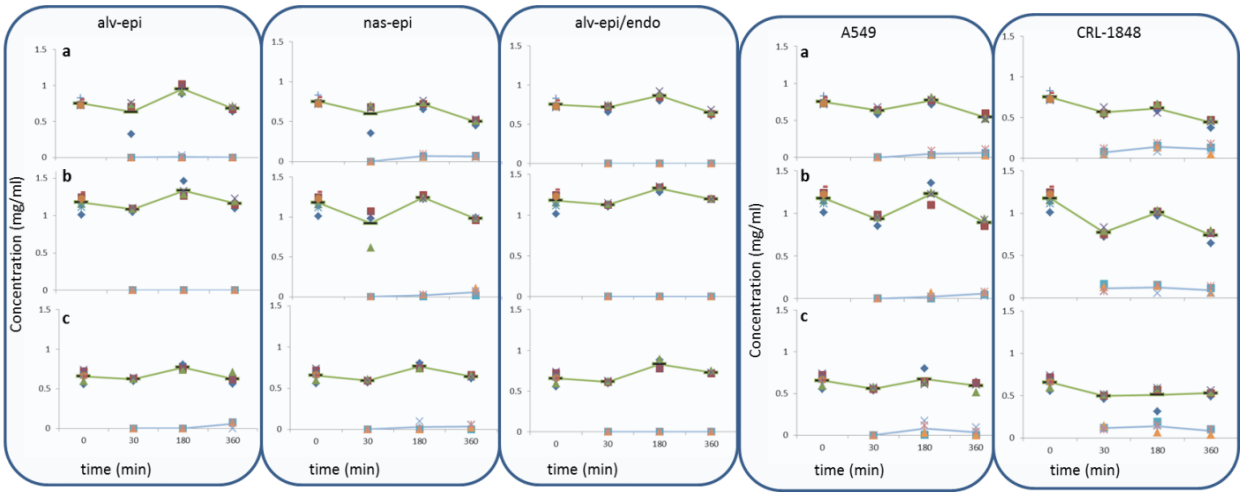

Figure 8: FITC-dextran permeability in human lung tissue models a) 10KDa, b) 70KDa, c) 500KDa. (green=apical average; blue=basal).

Both A549 and CRL-1848 were more permeable to FITC-dextran when compared against the primary cell MTE modules. The CRL-1848 cell line showed a high FITC-dextran permeability when compared to the A549 cell line and the primary human cell constructs. This finding was a confirmation of the initial morphological observations under the microscope. A leaky tissue motif is not biomimetic since it permits non-selective antigen and cellular entry from the epithelial mucosa. These finding are in accord in vivo studies where FITC dextran measurement in BAL fluid after intravascular

administration has been recognized as a measure of lung acute lung injury or disease related tissue permeability (Briot, 2008; Bayat, 2000, Gurey, 1998).

There was no apparent permeability dependency on FITC-dextran molecular weight (10KDa, 70KDa, 500KDa) for the primary cells, A549, or CRL1848 cell lines. Future experiments may include relatively higher molecular weights of fluorescently labeled particles to decipher the relative size of the open mucosal surface. The degree of tissue "leakiness" is an estimate of how the cell-cell contact. We also recognize that this may not be a controllable process in tissue cultures with cell lines of cancerous origin and population drifting growth rates.

Human tissue model innate cytokine and chemokine response to selected respiratory stimulants

The experimental approach to characterize the basic tissue response to known respiratory TLR agonists and inactive pathogen or vaccine was to better understand the innate immune responses and function of our *in vitro* MTE models. The secretory factors in the respiratory local tissue environment are involved in cell signaling, recruitment of antigen presenting cells in the airways which may aid in the design of aerosolized vaccine.

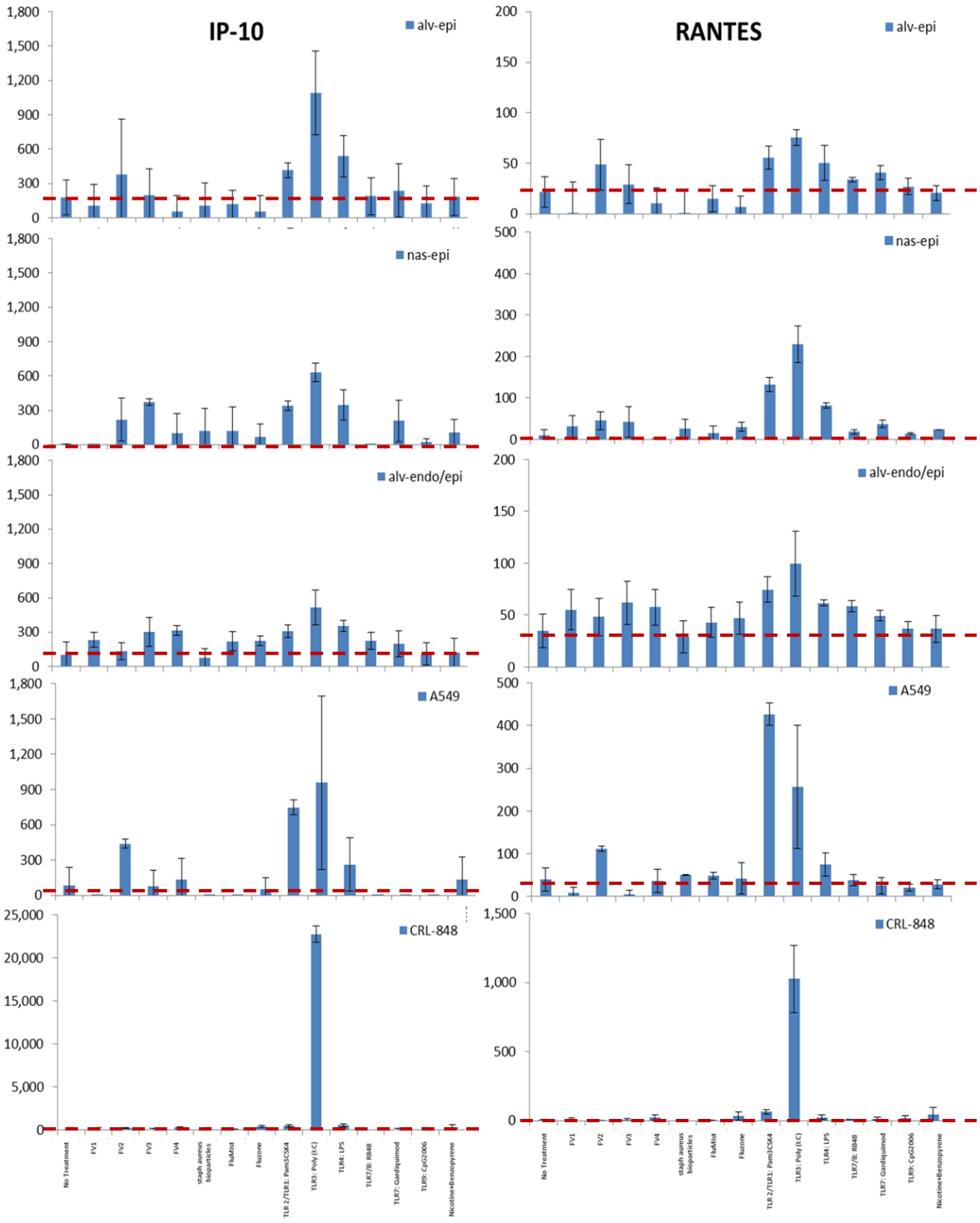

Figure 9: Soluble IP-10 and RANTES levels in culture supernatants from the pulmonary tissue models with highest activity from the Poly (I:C), followed by LPS (TLR4) and PamCSK4 (TLR2/1), respectively. CRL-848 constructs only showed TLR3 stimulation from Poly (I:C).

*FV1 (Sudan-lot012010AIK), FV2(MAR-lot 5Nov2009),FV3 (EBOV-95-lot1), FV4 (BDBV-lot1Jun2010)

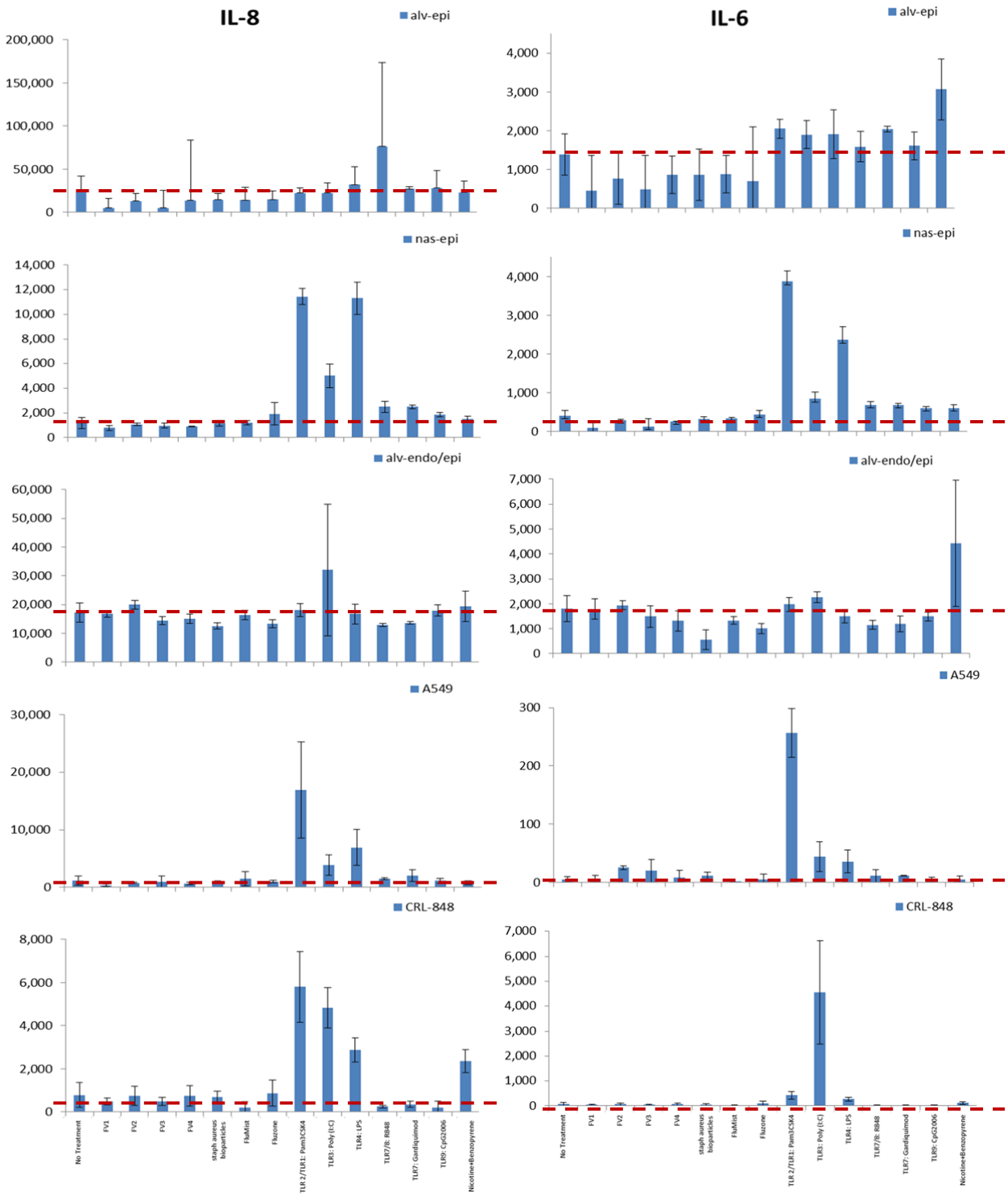

Figure 10: Tissue related Interleukin 6 and Interleukin 8 production in culture supernatants from the pulmonary tissue models.

*FV1 (Sudan-lot012010AIK), FV2(MAR-lot 5Nov2009),FV3 (EBOV-95-lot1), FV4 (BDBV-lot1Jun2010)

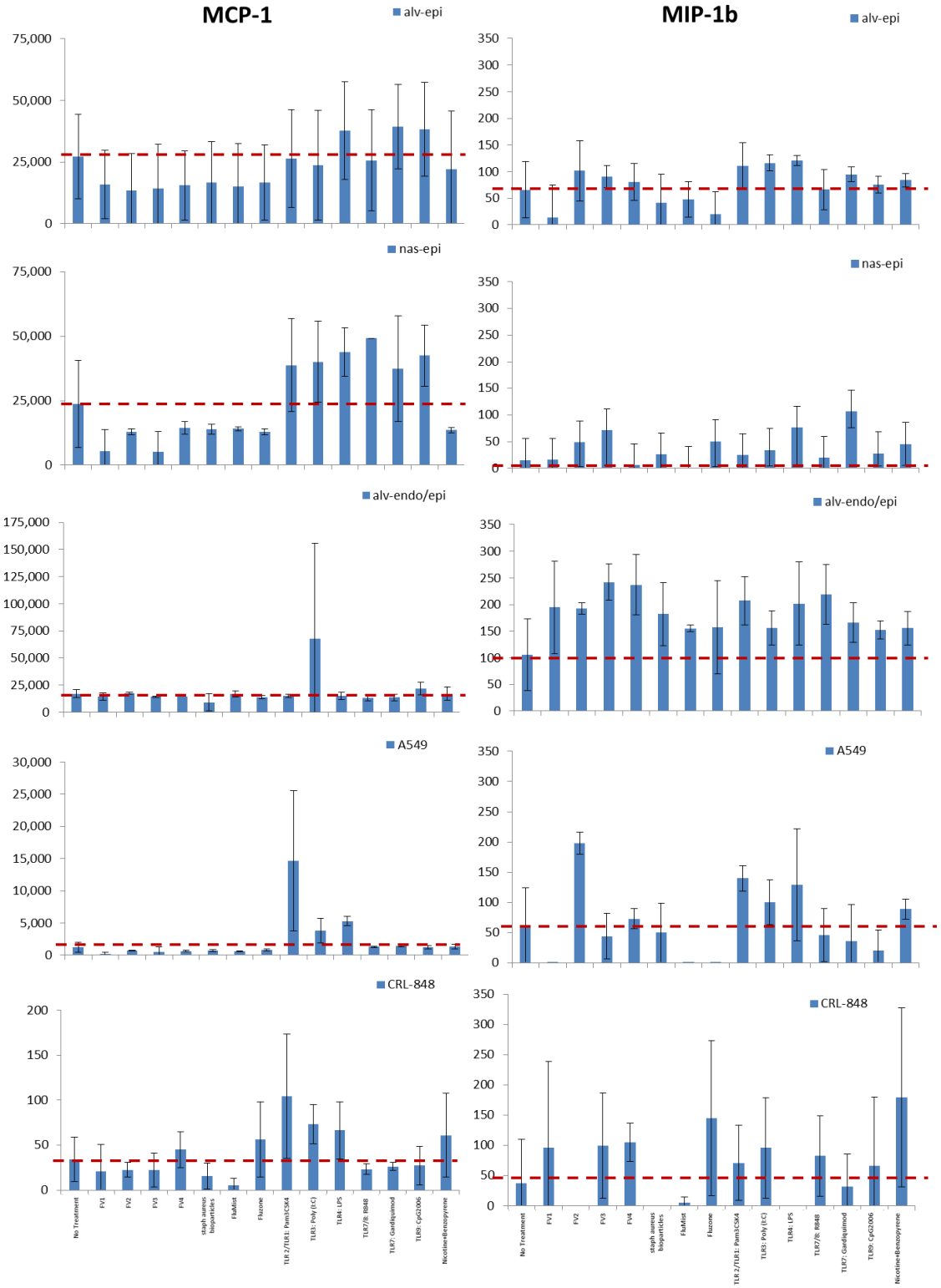

Figure 11: Monocyte Chemotactic Protein (MCP-1) and Macrophage Inflammatory Protein (MIP-1beta) in the culture supernatants

*FV1 (Sudan-lot012010AIK), FV2(MAR-lot 5Nov2009),FV3 (EBOV-95-lot1), FV4 (BDBV-lot1Jun2010)

This broad spectrum interrogation of TLR ligand based activity, in terms of soluble cytokine and chemokine levels in the culture supernatants, suggests that TLR 3 (Poly I:C) levels are highest in the airway tissue models. The TLR3, TLR4, and mild TLR2 response is in accordance with ex-vivo work by Ritter et al and others (Ritter 2005; Greene, 2005). The overall trends for the stimulated cultures showed Interferon gamma related protein (IP-10) and RANTES production by the primary cell tissue models and showed similar trends for TLR 3 (Poly I:C), TLR4 (LPS) and TLR2/1 PamCSK4, respectively (Figure 9). For tissue related Interleukin-8, the A549 and CRL848 cell lines showed TLR2, TLR3, and TLR 4 activity above the no treatment controls.

In contrast, the primary nasal constructs stimulated with TLR2, TLR3, TLR4, and showed a minor stimulation from R848, Gardiquimod, and CPG2006 (TLR7, TLR8, TLR9; Figure 10) as compared to the airway model. Based on its anatomical location, we postulate that the nasal mucosa has a higher degree of exposure to a variety of antigen type and therefore less responsive to some antigen. A noted example of this is rhinovirus induced cytotoxicity in the bronchial epithelium is not observed in the nasal epithelium (Vareille, 2011).

The alveolar bilayer construct showed TLR-3 activity to Poly(I:C). Compared to the other tissue models, this is a relatively limited response at the tested dose. However, this data set only represents the 24hr time point and does not include the addition of immune cell component to the differentiated lung tissue. The kinetics of cytokine release, effects of surfactant presence, and it's interaction with the additional endothelial layer needs to be considered.

The secretion of Monocyte Chemotactic Protein-1 (Figure 11) was higher for the epithelial constructs composed of alveolar and nasal primary cells for all the TLR agonist treatments when compared to the cell lines. The addition of the various filovirus strains reduced the soluble cytokine in the culture supernatant. It is interesting to note that in the alveolar bilayer constructs the level of MCP-1. This was similar to the no-treatment controls for all treatment controls, with the exception of Poly (I:C). The cell lines showed consistent activity of TLR 2, 3, and 4. Compared to epithelium alone constructs, the Macrophage inflammatory protein levels (Figure 11) were highest for the alveolar bilayer constructs and for all the treatments for all the stimulants including inactive virus and TLR ligands. FV2, inactive EBOV showed some activity for all the tissue models. The primary nasal epithelial cells produced the least level of MIP-1beta. While there was TLR2/1, TLR3 and TLR 4 activity for the A549 cell line. The CRL848 tissue also showed similar trends with the exception of LPS or TLR4 stimulation.

Based on the cytokine and chemokine data alone, we cannot draw conclusions on the effect of inactive filovirus strains for the cell lines and some minor differentials of inflammatory or chemotactic cytokine for the primary cells cultures. In comparing the two influenza vaccines, Fluzone® showed a mild response in MIP-1alpha, IL-10 and IL-12 (p70). The low dose antigen introduction of the vaccine and staph aureus particles was not sufficient for generating a significant soluble cytokine response. We recognize

that there is a kinetic factor and immune cell recruitment is involved in the release of these cytokines and chemokines. Therefore, the same panel of secretory factors was re-tested in the human MTE modules with the addition of immune cells.

The genomic profiling of human tissue models provides a complimentary analysis to draw conclusions based on transcriptomic expression of genes relating to the pattern recognition family, host defense, and surfactant production.

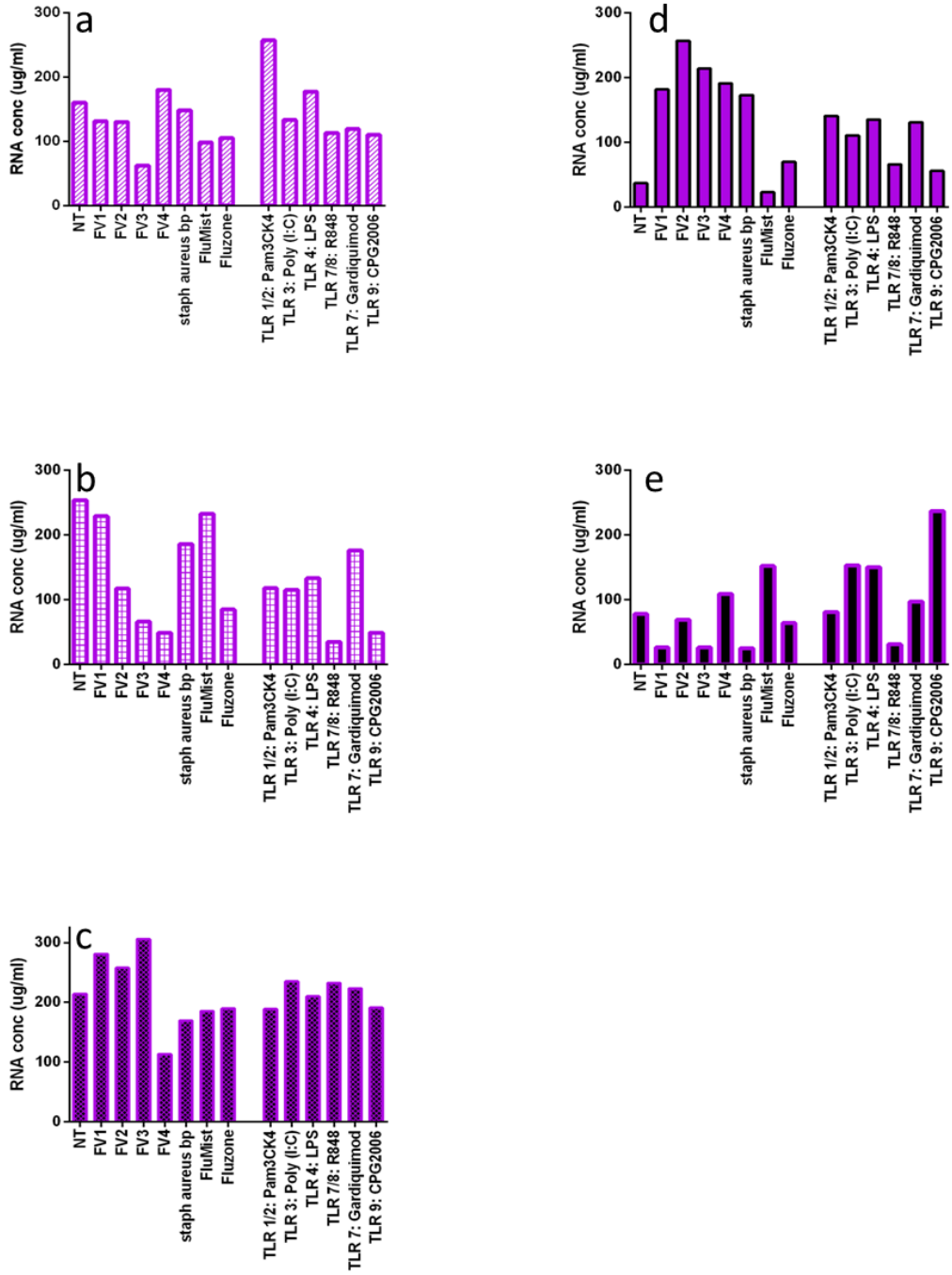

Figure1 2: Total RNA recovery a) alveolar epithelium, b) nasal epithelium, c) alveolar bilayer, d) A549, d) CRL-1848 *FV1 (*Sudan*-lot012010AIK), FV2(MAR-lot 5Nov2009),FV3 (EBOV-95-lot1), FV4 (BDBV-lot1Jun2010)

Genomic profiling of human tissue models via quantitative PCR

RNA Quantity and Quality

In general, the avleolar bilayer tissue constructs had the highest concentration of RNA relative to the other human models (Figure12). The A549 extracts contained more RNA compared to CRL-1848. While the RNA quality was acceptable for all the tested constructs, there was no real trends or conclusions to rate one tissue model superior to another (Figure13). The acceptable quality and quanitity of material allowed us to design the cDNA synthesis and qPCR set-ups.

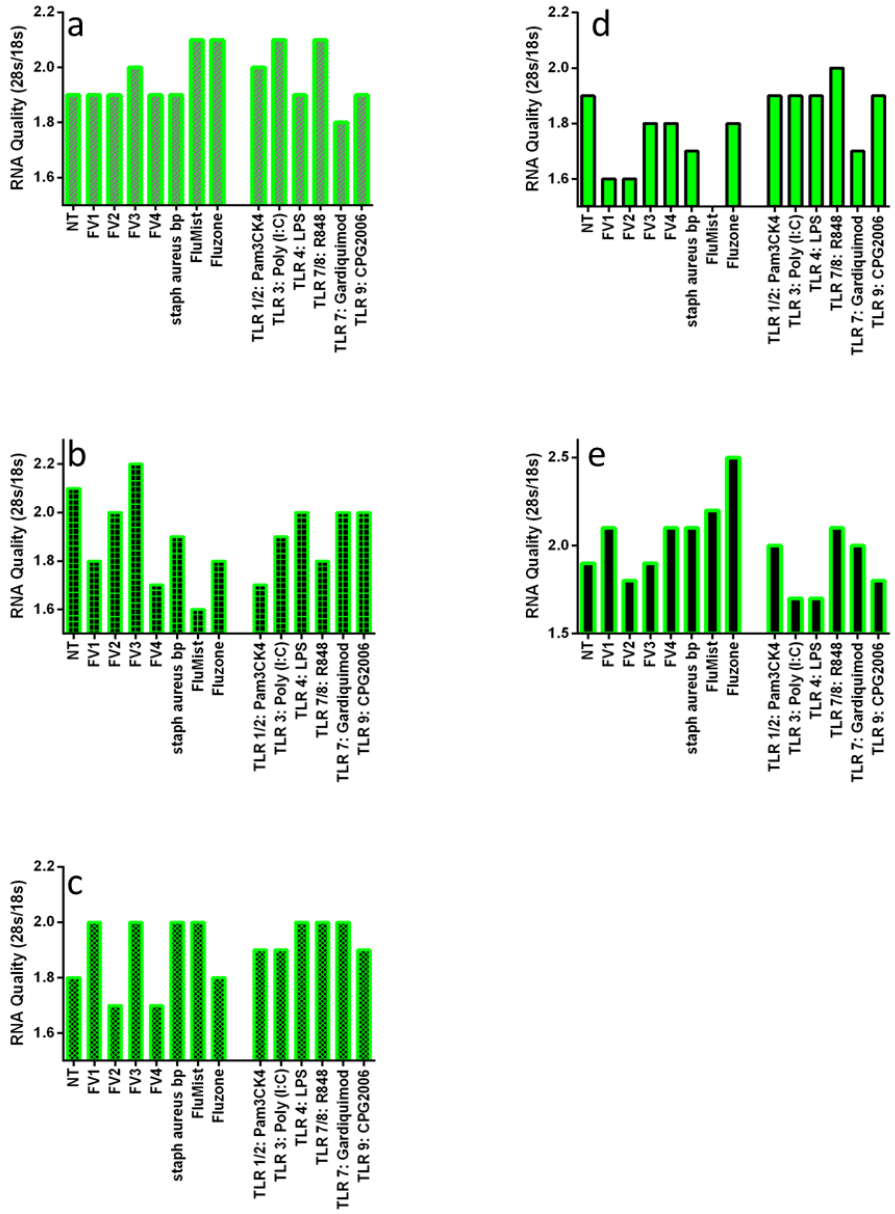

Figure 13: Recovered RNA quality measurement a) alveolar epithelium, b) nasal epithelium, c) alveolar bilayer, d) A549, d) CRL-1848

*FV1 (*Sudan*-lot012010AIK), FV2(MAR-lot 5Nov2009),FV3 (EBOV-95-lot1), FV4 (BDBV-lot1Jun2010)

The extraction had sufficient quality and quantitiy of RNA to directly proceed with the qPCR reactions. We speculate that this may be significanly alterered in the live filovirus studies, based on the pathogenic nature of the strains. The extraction of quality RNA is critical for transcriptomic evaluation of various cell populations. The A260:A280 ratio from BioAnalyzer readout was used to determine the quality of RNA, where a value of 1.7 or higher was considered acceptable. Also, the RNA Integrity number was used for identifying the quality of intact RNA. In general, the RNA Integrity Number (RIN) values were in the acceptable range (7-10). The electropherograms produced sharp peaks corresponding to the 18S and 28S ribosomal fragment, where the agarose gel electrophoresis yielded distinct bands. We anticipate reduced genomic quantity and quality with live virus infections; this will require larger scale set-ups.

Genomic Expression

The qPCR data in terms of Ct values was nomalized to the no treatment condition. The experimental house keeping genes including ACTB, HGDC, RTC and PPC. These genes are related to basic cellular function and cDNA syntheis and serve as internal qPCR plate controls. To normalize the data, the treatment Ct values were subtracted from the reference Ct values. To extrapolate the fold change from the Ct values, the delta-delta Ct method was used. The graphs for the various treatment groups are in Appendix A1. The heat maps were generated from the qPCR data by color assignment to the numeric fold change values. The red color is indicative of gene up regulation. Whereas, the negative expression was assigned a blue color coding. The tissue models and treatments were then split into the various innate immune response families for side-by-side comparision of the various tissue models.

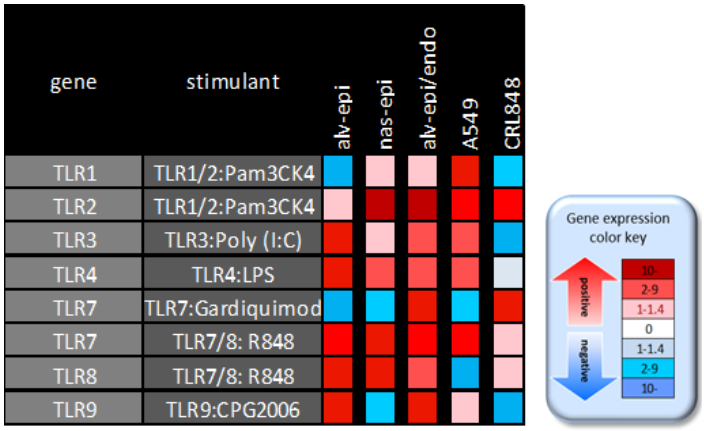

Figure14: Human airway tissue pattern recognition gene expression post TLR agonist introduction

The heat maps were generated from the qPCR data by color assignment to the numeric fold change values. The red color is indicative of gene up regulation. Whereas, the negative expression was assigned a blue color coding. The tissue models and treatments were then split into the various innate immune response families for side-by-side comparisions of the various tissue models. The results have been broken down in terms of gene families related to physiological responses.

Tissue Specific TLR gene expression

The TLR agonist stimulation served as internal controls to quantify the degree of gene expression based on cellular origin for the particular pattern recognition site. The TLR agonist related PRR expression served as a baseline for MTE module activity. The selected dose for the TLR agonist was based on our previous experience with the particular stimulant. We recognize that the degree of response depends on the dose and exposure time despite our controlled criteria.

The direct MTE tissue model comparison indicates that the alveolar bilayer model exhibits the highest level of TLR activity, followed by alveolar epithelium, A549 cell line, nasal epithelium and CRL-1848 respectively (Figure 14). The data suggests that the addition of alveolar endothelial layer to the epithelium improved the TLR7, TLR2 and TLR1 activity and this may be relevant to therapeutic development using the MTE module.

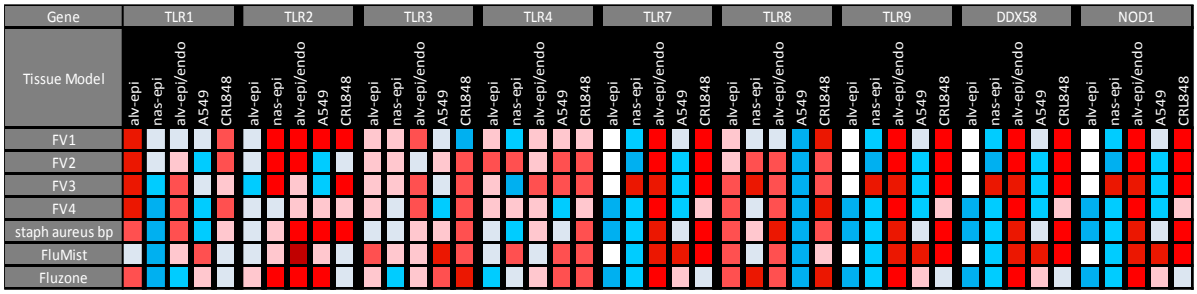

Figure 15: Tissue model pattern recognition gene expression to filovirus antigen *FV1 (*Sudan*-lot012010AIK), FV2(MAR-lot 5Nov2009),FV3 (EBOV-95-lot1), FV4 (BDBV-lot1Jun2010)

Transcriptomic Evaluation of PRR, Microbial Detection and Clearance Genes

After defining the baseline levels of TLR activity, we tested the transcriptomic activity of the *Sudan, Marburg, Ebola Bundibugyo*, *Staphylococcus Aureus* bioparticles, Fluzone™, and Flumist™ (Figure 16, 17, 18). Of the primary cells, the TLR -2, -3, -7, -8, -9 along with RIG-1 (DDX58) and NOD1 activity was highest in the bilayer tissue constructs. The nasal constructs showed mild stimulation to TLR3 and little to no activity for TLR -7,-9, RIG-I, and NOD1. This suggests that while the viral antigen activity is not as recognizable to the nasal mucosal as the tested TLR agonists. This is in agreement with the previous section on mucosal secretory cytokine and chemokine response by the nasal MTE and Vareille et al. It is also important to consider the correlation between pathogen entry and efficiency and recognize that the pathogen particles are highly irradiated and inactive.

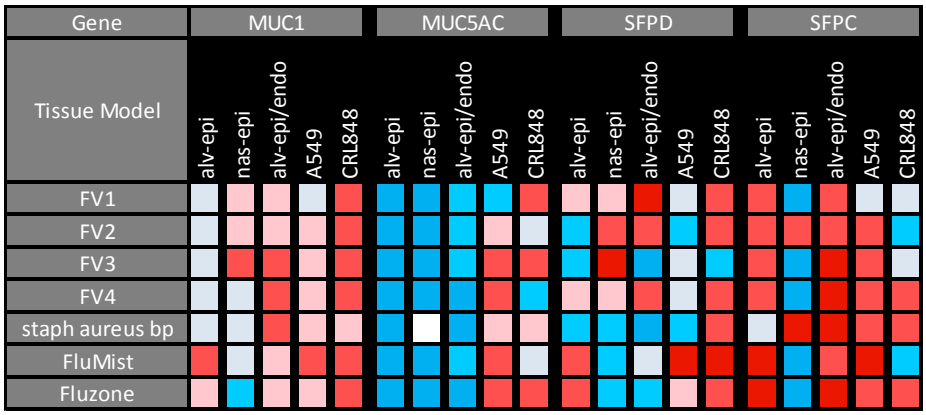

Figure 16: Tissue defense protein secretion by the human tissue models
*FV1 (*Sudan*-lot012010AIK), FV2(MAR-lot 5Nov2009),FV3 (EBOV-95-lot1), FV4 (BDBV-lot1Jun2010)

The CRL-848 showed higher than anticipated level of PRR related gene activity. However, the heat map trends and intensity for the primary cells was different than the human cell lines. The RIG-I (DDX58) and NOD1 activity suggests that the lower airway constructs interact with the virus particles on the cellular surfaces and at the cytostol level. This RLR activity is a precursor to the NF-kB activation. It is to be noted that there is a kinetic degradation of RIG-I from the interferon response via a negative feedback balance (Figure 15).

In the previous section, we summarized the tissue cytokine and chemokine responses as it relates to TLR activity. The highest activity was observed for TLR3, followed by mild TLR-7 and -9 for the primary cells. The genomic data demonstrates intracellular PRR activity which is associated with vesicle and endosomal activity, as described in morphology section. This is of particular importance to viral antigen pick-up and transport processes involved in classic disease pathogenesis and host defense mechanisms (Grieber, 2008; Greene, 2005),

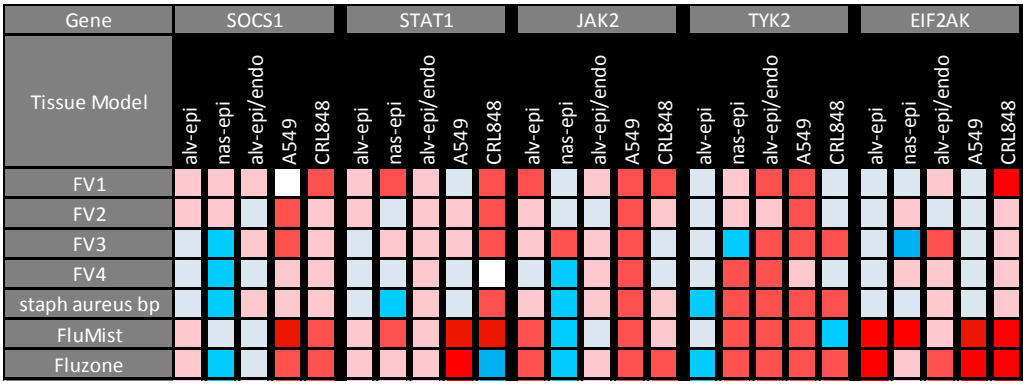

Figure 17: Viral or bacterial antigen infection / entry related genes
*FV1 (*Sudan*-lot012010AIK), FV2(MAR-lot 5Nov2009),FV3 (EBOV-95-lot1), FV4 (BDBV-lot1Jun2010

Signal transduction from the TLR family can be broadly classified into MyD88 or TRIF domain (Opitz B,2010; Yamamoto, 2002; Mogensen, 2009). MyD88 dependent

signaling induces pro-inflammatory response and can be triggered by all the TLRs with the exception of TLR3. Whereas, TRIF stimulates the type I interferon response which is associated with the interferon regulatory genes (IRF3 / 7), via endosomal activity triggered by TLR3 (dsRNA) and TLR 7 (ssRNA). Anti-viral IRF3 activation was observed

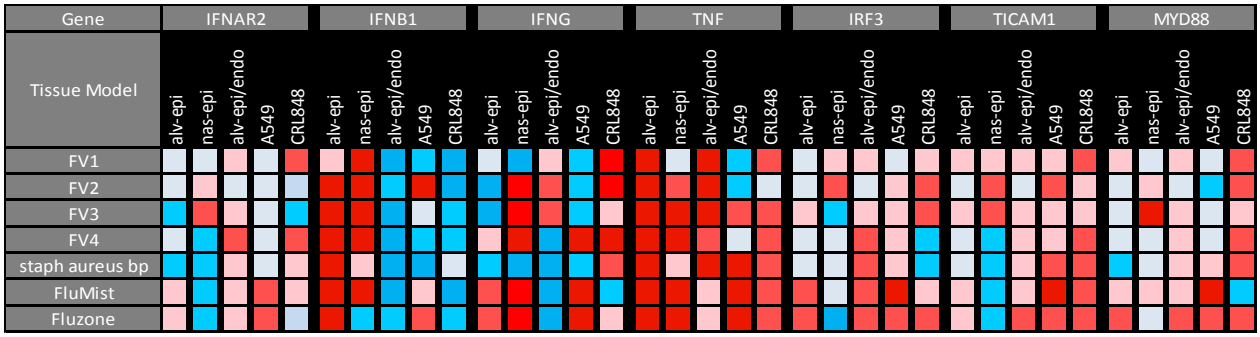

Figure 18: Host defense related genes for infection

*FV1 (*Sudan*-lot012010AIK), FV2(MAR-lot 5Nov2009),FV3 (EBOV-95-lot1), FV4 (BDBV-lot1Jun2010)

in the alveolar bilayer models and A549 cell line. We also selected TICAM1gene analysis. This gene is an adaptor protein containing Toll/interleukin1 receptor for TLR and signal transduction proteins via intracellular signaling. TICAM1 only interacts with TLR3 (dsRNA) and is associated with interferon beta response for virus. Primary cell tissue models showed mild MYD88 and TICAM activity, along with a weak interferon response. This is somewhat opposite of CRL-848 cell line. There was a detectable TNF response for all the human tissue models over the no-treatment control condition. Thus, we have pieces of both the MyD88 and TRIF pathway related gene expression differences in the primary cells when compared against cell lines which shows they are a closer mimetic to human respiratory physiology.

Interferon activity is generally considered a hallmark of viral infection and host defense related mechanisms. Interferon activity triggers surface glycoprotein related Janus Kinase (JAK) family, non-receptor tyrosine kinase (TYK) and leads to the activation of signal transducers and activators of transcription (STAT). We specifically looked at JAK2, stress associated EIF2AK and STAT1 and found activation of TYK2 more detectable than JAK2 and STAT1 for the alveolar bilayer models. A549 performed well for the cell lines with significant TYK2 and JAK2 activity and mild STAT1 up-regulation. The kinetics of interferon activity is generally considered a hallmark of viral infection. In this case, we anticipate significant differences between live filovirus infection and our findings with inactivated viral particles. This response may be similar to VLP type of therapeutics. However, it needs to be verified further.

The gene expression of defense proteins was quantified to directly compare primary human models to A549 and CRL-1848 cell lines; Figure 16. For inactive virus induced mucin protein production, the primary cells did not up-regulate MUC5AC compared to MUC1. This was in contrast to the A549 and CRL848 cell lines. MUC1 is produced at various mucosal sites throughout the body. Whereas, MUC5AC is associated with COPD, hyperactive carcinomas and a number of cell lines (Lau, 2004) and can explain

these observations and provides further data to suggest that cell lines are not representative of normal human respiratory physiology as is observed with primary cells in our bilayer MTE models. Higher levels of surfactant protein C relative to protein D were observed in both primary and cell line constructs. It is to be noted that surfactant protein D was detected at a higher level for the CRL1848 constructs. Surfactant protein C and D were found in the lower airway. Surfactant protein D is associated with the inflammatory response. The anti-inflammatory effects of MUC1 were demonstrated by in-vitro studies in both bacterial (*Pseudomonas aeruginosa*) and viral infection experiments (respiratory syncytial virus, RSV) in the A549 lung cancer cell line. (Li, 2010). Another unrelated study in the same cell line (A549) showed that surfactant producing protein D (SFP-D) was able to modulate allergen uptake and the resulting pro-inflammatory cytokine release in a cell specific manner (Schleh, 2012). It is difficult to directly compare our work against these studies. The electron microscopy images of the non-stimulated human MTE modules showed surfactant like vesicles in the primary cells and this was not observed in the A549 and CRL-1848 cell lines. We hypothesize that the level of cellular response, in terms of secretory factors and genomic expression is dependent on dose, kinetics, and type of antigen exposure. A TEM based morphological evaluation may confirm these genomic readouts to tie form and functional readouts similar to TLR family and endosome activity. The results from the PRR genes and defense protein expression in primary cell models may be used as a guide to design therapeutics.

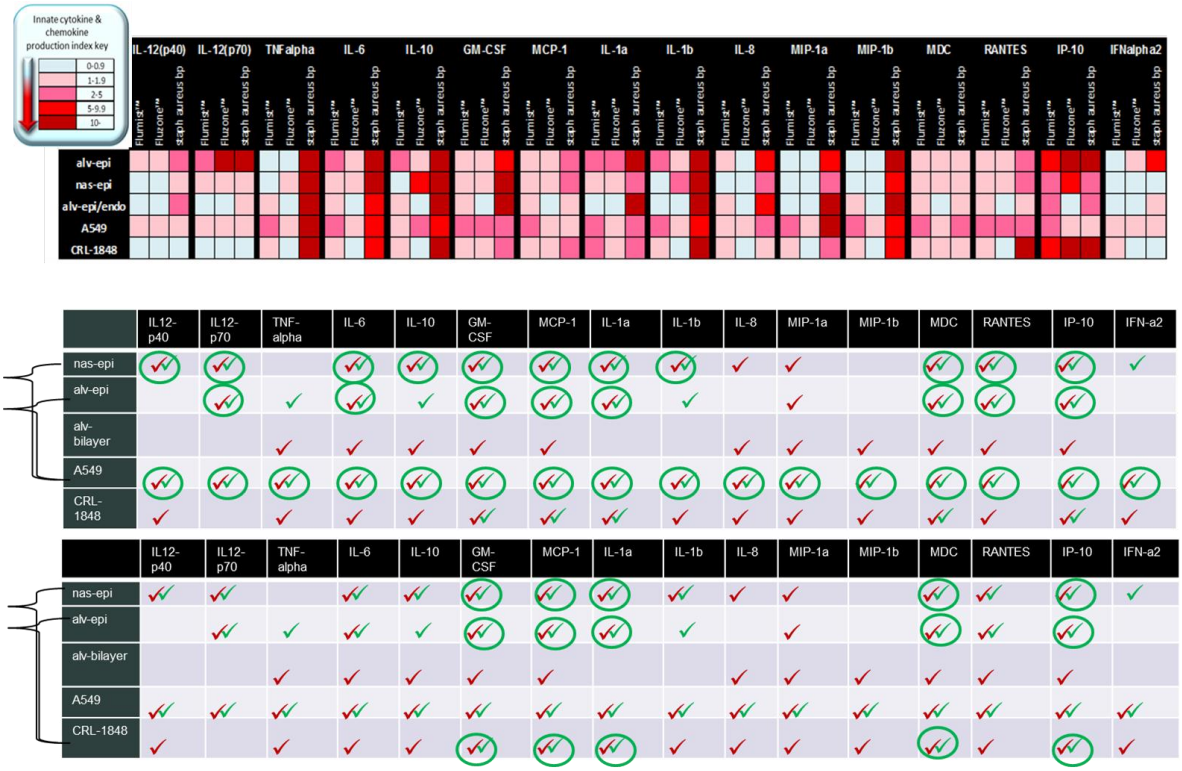

Figure 19: Influenza vaccine induced innate cytokine and chemokine response via quantitative data based a) big-picture heat map, b) A549 cell line comparison to three primary cell based MTE models , c) direct comparison of CRL-1848 to primary cell based MTE models

Characterization antigen presenting cell and secretory factors in human tissue models with influenza vaccine antigen (specific aim 3.3.1)

The *in vitro* lung mucosal module design and functional readouts are inspired by human physiological pathways relating to pattern recognition gene expression, vesicle formation, antigen uptake, surfactant and mucin production, along with cytokine and chemokine responses. Human peripheral blood mononuclear cells are then applied to the apical side of the MTE where monocytes migrate through the epithelium or endothelium and naturally differentiate into antigen presenting dendritic cells (DCs). The addition of immune cells to the mucosal tissue equivalent (MTE) module begins with naturally extravasated monocyte addition to the upper and lower airway tissue motif. The lung MTE module consists of a confluent epithelium from either a primary cell, or a cell line source. The migrated antigen presenting cells are collected in the transwell buckets. The antigen is introduced to the epithelial interface to mimic the mucosal contact with the external environment where the pathogen or therapeutic agents reside. The cellular differentiation or APC activation and maturation was analyzed by phenotyping of the antigen presenting cell

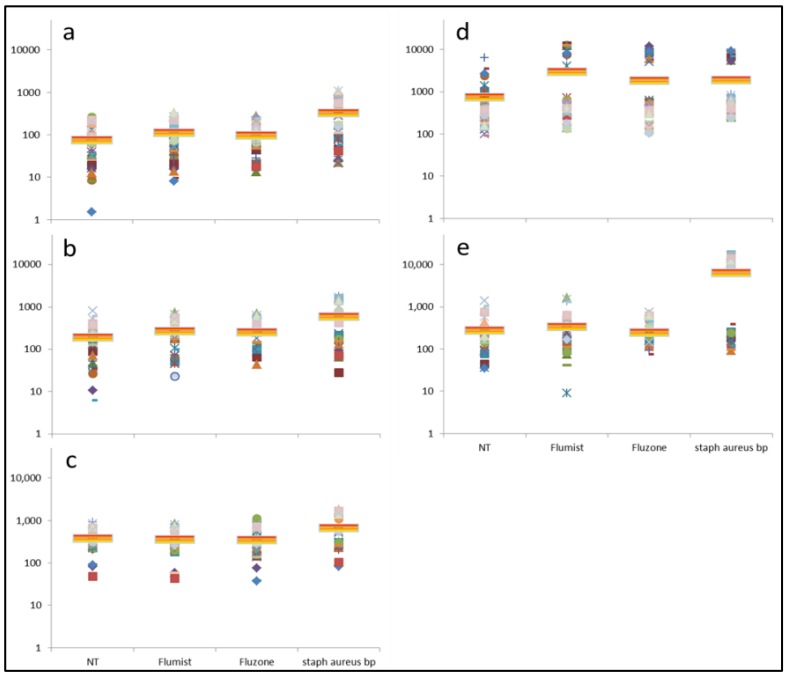

Figure 20: RANTES(pg/ml) production in a) alveolar epithelium, b) nasal epithelium, c) alveolar bilayer, d) A549 cell line, and e) CRL-1848 cell line tissue models.

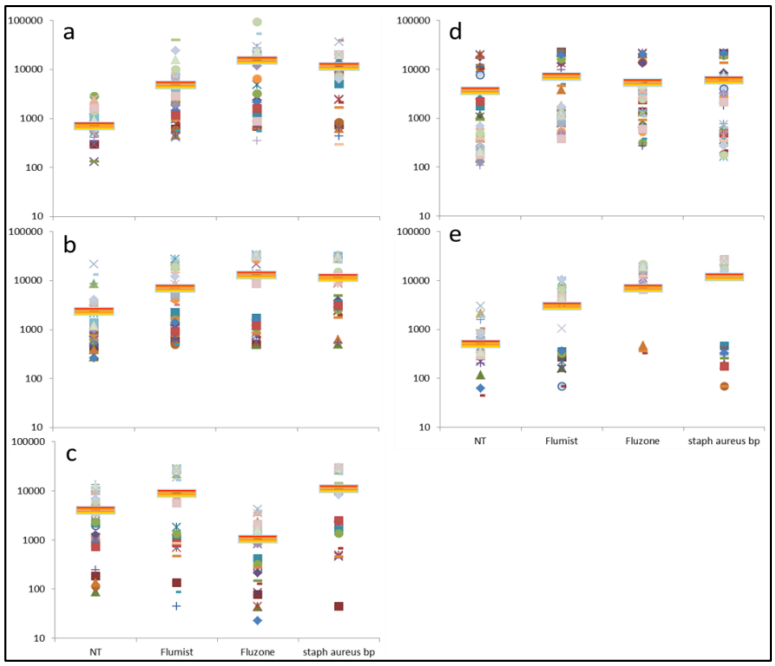

Figure 21: IP-10 (pg/ml) production in a) alveolar epithelium, b) nasal epithelium, c) alveolar bilayer, d) A549 cell line, and e) CRL-1848 cell line tissue models.

population by flow cytometry. Here, the dendritic cell maturation state is gated on the expression of co-stimulatory molecules MHC expression along with CD14, HLA-DR, CD80, CD86, and CD83 in the live cell population. The culture supernatants were used for cytokine and chemokine analysis to characterize partial secretory innate response. The type of antigen, dose, and cell type population in the modular system can be used to better understand the contribution and additive cellular response in the system.

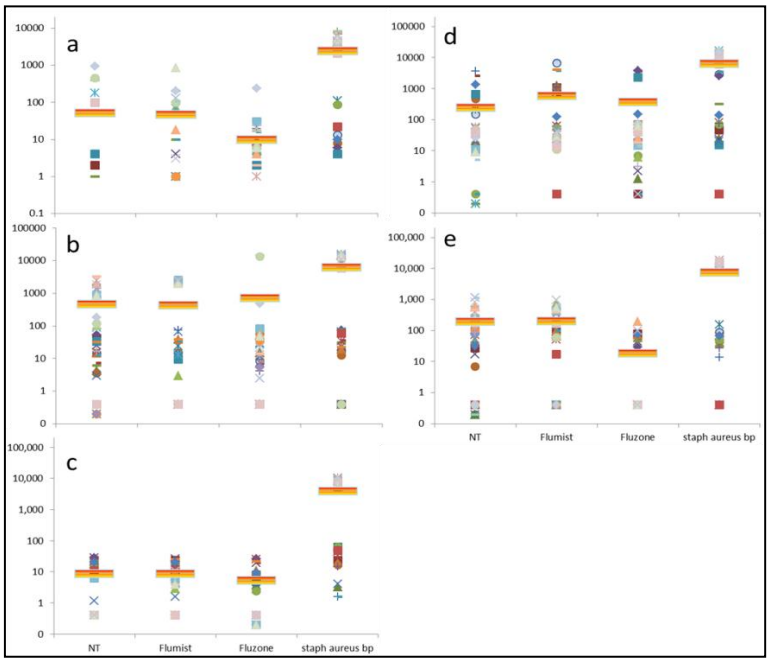

Figure 22: TNF-alpha (pg/ml) production in a) alveolar epithelium, b) nasal epithelium, c) alveolar bilayer, d) A549 cell line, and e) CRL-1848 cell line tissue models.

Secretory factors

The earlier section defined the baseline level of mucosal tissue related secretory cytokine and chemokine innate response. Here, the same idea was revisited with the addition of monocytes and influenza vaccine antigen. The innate cytokine and chemokine section trends for the 10 donors (40 replicates) are summarized in the human tissue model specific heat map shown in Figure 19. For the influenza vaccine antigen, the result show that the A549 and CRL-1848 cell lines are not equivalent to the primary cell MTE modules. The A549 cell line shows a consistent stimulation of all the tested cytokines and chemokines. Whereas, the primary cell based alveolar MTE showed the least level of response. Flumist® was more

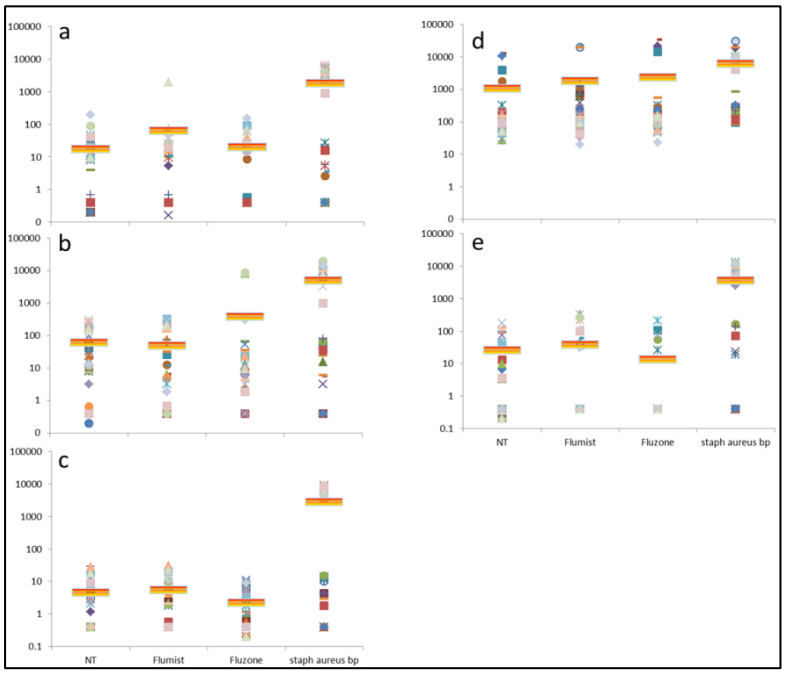

Figure 23: IL-10(pg/ml) production in a) alveolar epithelium, b) nasal epithelium, c) alveolar bilayer, d) A549 cell line, and e) CRL-1848 cell line tissue models.

immunogenic than Fluzone®. A broader dosing study may address the specifics of these differences. For generalized trend overview, the MTE response heat maps were generated by comparing the average stimulation condition cytokine and chemokine levels against the no treatment controls. Figures 20 through 29 and Appendix A1 show the quantified (pg/ml) cytokine levels independently. The flat orange bar represents the treatment condition average for data interpretation for the ten donors.

In general, the primary human tissue model cytokine and chemokine innate response is not comparable to the cell line models. Similarly, the direct comparison of no treatment control condition in the five human tissue models demonstrates this difference in dendritic cell maturation. The addition of an endothelium to the alveolar epithelium does not boost the cytokine and chemokine profiles and in most cases has an immunosuppressive effect when compared against the alveolar epithelium alone tissue model. This demonstrated that the endothelium provides a balance to innate cellular and tissue function to influenza vaccine antigen.

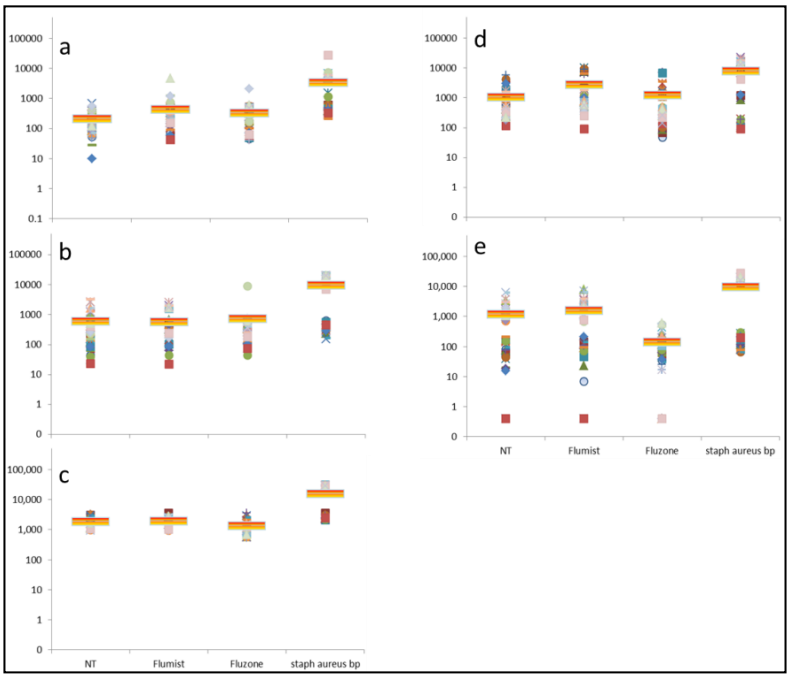

Figure 24: IL-6 (pg/ml) production in a) alveolar epithelium, b) nasal epithelium, c) alveolar bilayer, d) A549 cell line, and e) CRL-1848 cell line tissue models

Overall, we observed the strongest and most consistent innate pro-inflammatory response by the inactive *Staphylococcus aureus* bioparticle treatment conditions. This resulted in a fold increase in the production of TNF-alpha, MIP-1a,-1b along with IL-1b.

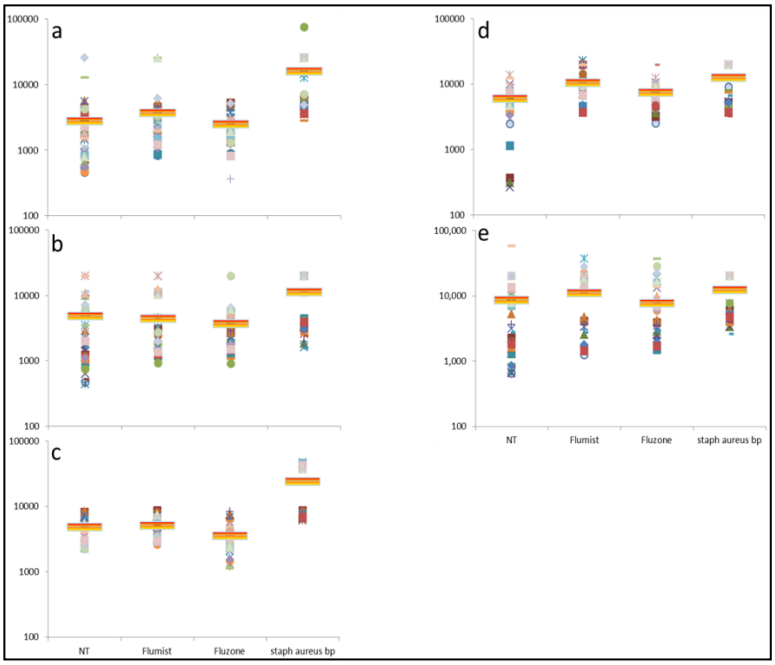

Figure 25: IL-8 (pg/ml) production in a) alveolar epithelium, b) nasal epithelium, c) alveolar bilayer, d) A549 cell line, and e) CRL-1848 cell line tissue models

This innate response profile can be attributed to TLR-4, TLR-2 interaction of Staphylococcus *aureus* bacterial bioparticles (Ritter 2005; Greene, 2005). This positive bacterial antigen condition serves as a study control condition, as low dose influenza vaccine antigen produces a mild tissue response. This bacterial stimulation also induced Interleukin-10 anti-inflammatory cytokine response; Figure 23. This can be attributed to the kinetic sampling and the transient presence of secretory cytokines in the culture media to balance the pro-inflammatory response. Specifically, the alveolar bilayer model compared to alveolar epithelium alone has similar trends, but with a milder to non-existent response to the local tissue related cytokines IL-6, IL-8 and IL-1b (Figure 24, 26, and 29, respectively).

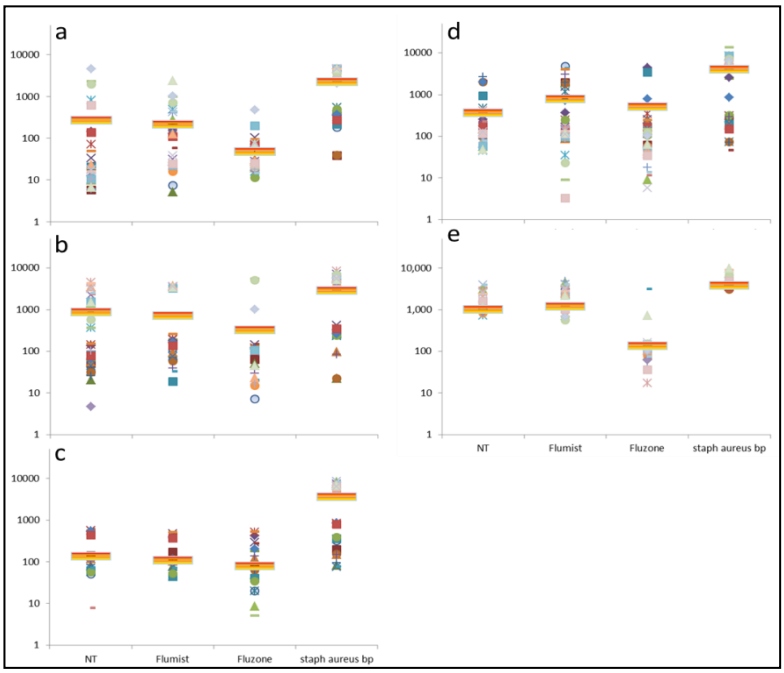

Figure 26: MIP-1b (pg/ml) production in a) alveolar epithelium, b) nasal epithelium, c) alveolar bilayer, d) A549 cell line, and e) CRL-1848 cell line tissue models

Similar trends of interferon gamma induced protein 10 (IP-10) production was observed in alveolar epithelium and CRL1848 cell line for FluMist® and Fluzone® treated cultures. The alveolar bilayer model only showed a similar response to the live attenuated vaccine, FluMist®. However, all ten donors showed a suppressed IP-10 response to Fluzone®, which represents a

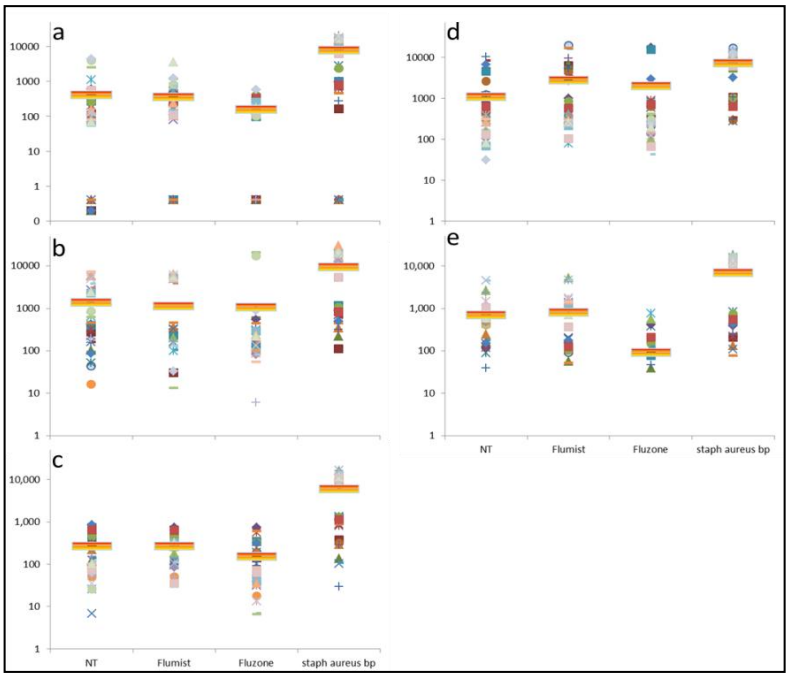

Figure 27: MIP-1a (pg/ml) production in a) alveolar epithelium, b) nasal epithelium, c) alveolar bilayer, d) A549 cell line, and e) CRL-1848 cell line tissue models

dampened interferon gamma activity (not tested in this detection panel). Interferon-alpha 2 was the only interferon family member tested in this study (Figure A4) and its low activity level was attributed to the genomic nature of an attenuated vaccine where a low grade interferon response to the live virus is designed to limit pathogenesis pathways or infection due to vaccination. We hypothesize that the endothelium is involved in balancing the innate response.

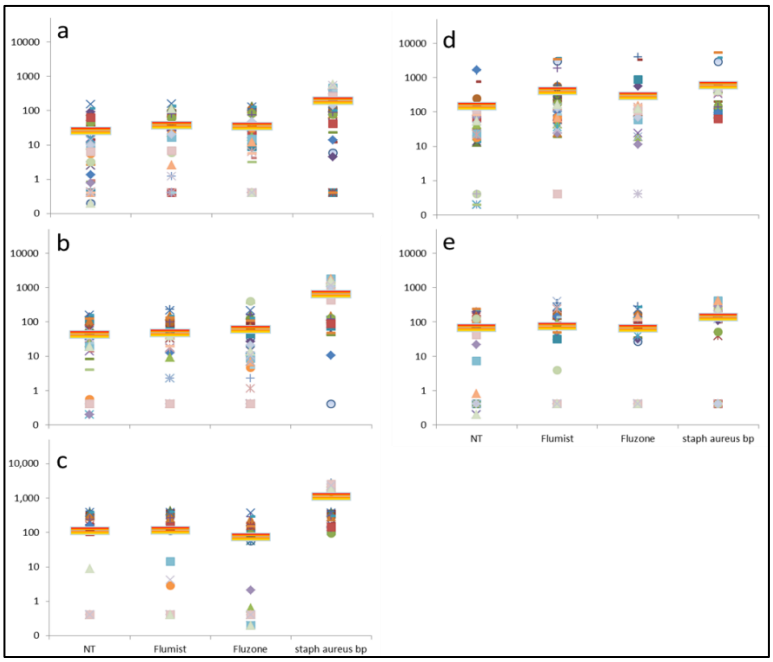

Figure 28: GM-CSF(pg/ml) production in a) alveolar epithelium, b) nasal epithelium, c) alveolar bilayer, d) A549 cell line, and e) CRL-1848 cell line tissue models

Macrophage inflammatory protein beta and GM-CSF show a mild overall response to FluMist®. It is to be noted that our positive control of inactive *Staphylococcus aureus* bioparticle stimulation showed a consistent five to ten fold up-regulation of GM-CSF, MIP-1apha, and MIP-1 beta. In comparison, the FluMIst® and Fluzone® vaccine showed a mild innate response, at the tested dose; Figure 25, 26, 28. These cytokines are involved in macrophage and dendritic cell recruitment to the infection site.

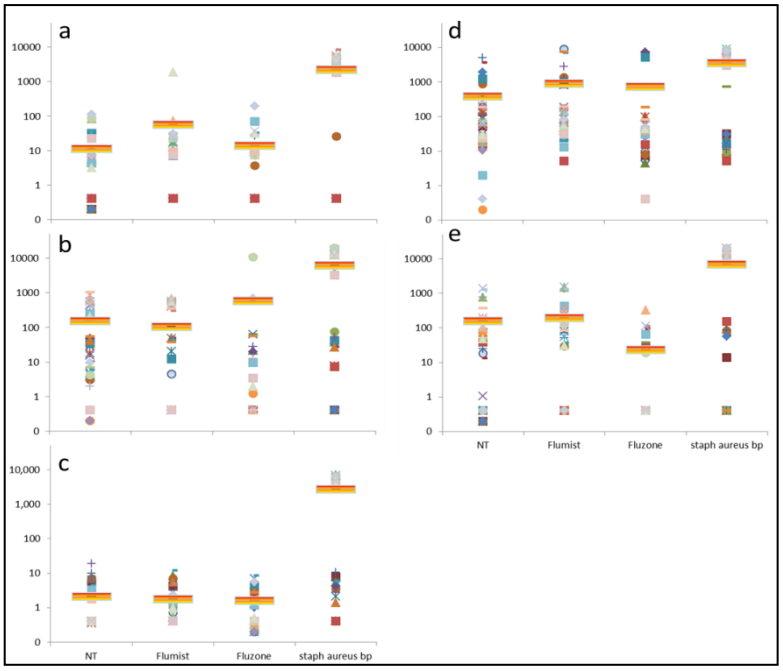

Figure 29: IL-1b (pg/ml) production in a) alveolar epithelium, b) nasal epithelium, c) alveolar bilayer, d) A549 cell line, and e) CRL-1848 cell line tissue models

Overall, we can conclude that the cytokine and chemokine secretory innate response for the primary human cell models was not equivalent to the cell line tissue motifs. There is more data to support this in Appendix A1.

Simultaneous studies on cell surface markers from these models further explore the non-equivalent functional response by the five human constructs.

Antigen presenting cell population (APC) in human tissue models

The innate immune response to influenza antigen was re-visited with the addition of immune cells in the five human MTE tissue modules. The results are summarized in Table 3; the "*" label denotes an overall trend. The immune response was tested in terms of antigen presenting maturation, though the natural selection process of extravasation, and cytokine and chemokine response. This approach builds on the previous section where the innate response was quantified for the MTE tissue module without monocytes. The highest degree of response was observed for the *Staphylococcus Aureus* bacterial antigen, which was am experimental positive control. Flumist® produced a stronger innate immune response than Fluzone® in terms of dendritic cell maturation and cytokine and chemokine production. The A549 and CRL-1848 cell lines produced higher levels of secretory cytokines and chemokines, relative to primary MTE modules. However, the level of

dendritic cell maturation was significantly reduced for the cell lines. These results are in

			Alveolar Epithelium	Nasal Epithelium	Alveolar Bilayer Epithelium / endothelium	A549 Lung Carcinoma	CRL1848 Lung Carcinoma
Airway Tissue Plus Immune Cells Innate Immune Response	DC Phenotype (CD14, HLA-DR)	Bacterial antigen Inactive *Staphylococcus aureus*	+	+	+	+	+
		Influenza vaccine (FluMist®, Fluzone®)	-	-	+	-	-
	Secretory factors	Cytokine and chemokine response Bacterial antigen-inactive *Staphylococcus aureus*	+	+	+	+	+
		Cytokine and chemokine response Influenza vaccine-FluMist®, Fluzone®	-/+*		+/-*	+/-*	

Table 3: Summary of human MTE module mucosal tissue plus immune cell response

agreement with the permeability studies, described in the previous section. This is related to the tissue confluencey and the active process of immune cell extravasation.

The presence of a confluent endothelium promotes the dendritic cell maturation process via the extravasation process, similar to *in vivo* physiology of cell migration through the vasculature. The loss of CD14+ expression in the dendritic cell population is related to antigen uptake and maturation in the antigen presenting cells. This process is enhanced by the presence and relative dose of a variety of antigen. The cell surface marker phenotyping from *the in vitro* MTE cellular harvests serve a measure of tissue

dependent immune cell function. The no treatment control condition provides an average baseline response by various tissue models.

The bilayer model design contains a confluent endothelium, which makes the cellular extravasation process selective through the tissue tight-junctions and not a passive gravity driven process. This APC maturation process is observed in the alveolar bilayer tissue models and more clearly present in the bacterial and viral antigen conditions. This conclusion is supported by the FITC-dextran permeability study (Figure 8). Overall, the alveolar mucosal tissue model is most responsive when directly compared against other tissue motifs. The phenotyping of cell surface markers on the harvested antigen presenting cell population gated on the live cell population expressing HLA-DR+ and CD14- showed maturation in human alveolar bilayer model with the addition of FluMist® and *Staphylococcus aureus* bioparticles (Figure 30).

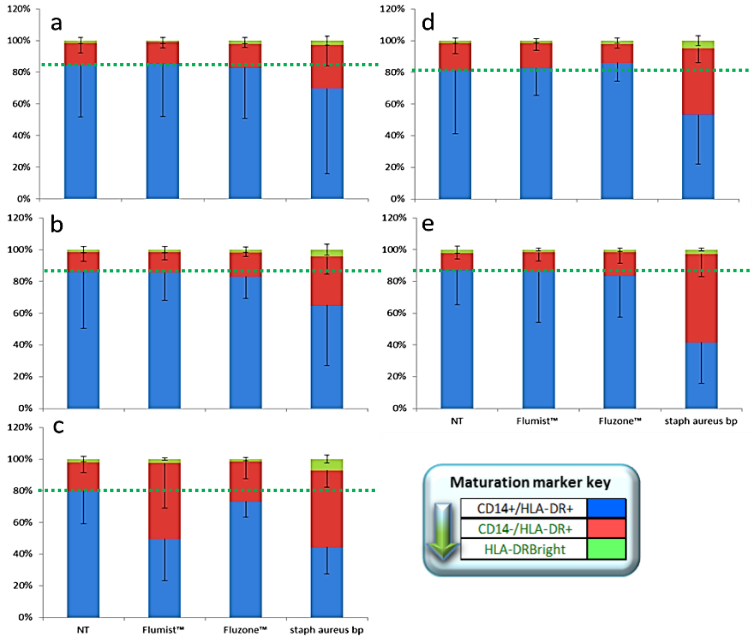

Figure 30: Antigen presenting cell maturation in a) alveolar epithelium, b) nasal epithelium, c) alveolar bilayer, d) A549 cell line, and e) CRL-1848 cell line tissue models.

For the tested cell markers, the Fluzone® treatments showed the mildest maturation profile. Similarly, the CD80+ (Figure 31) and CD83+ (Figure 32) expression in the APC population is

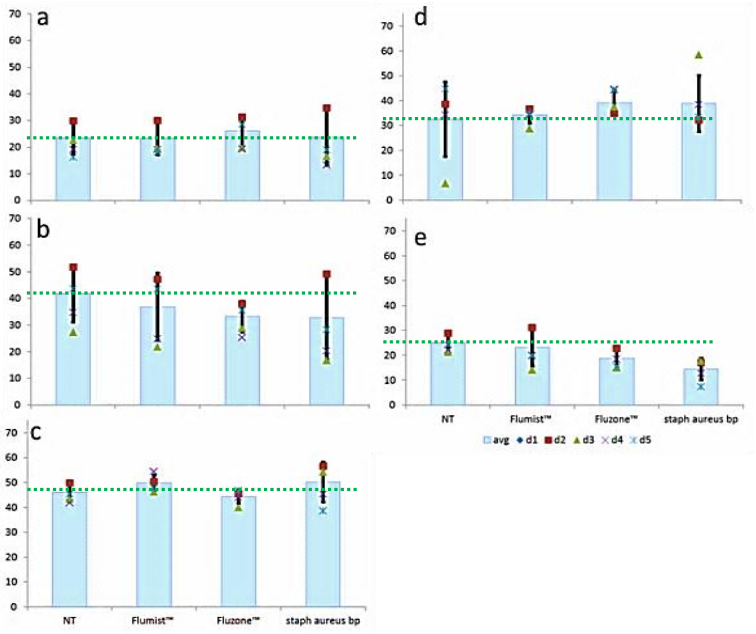

Figure 31: CD80+ expression a) alveolar epithelium, b) nasal epithelium, c) alveolar bilayer, d) A549 cell line, and e) CRL-1848 cell line tissue models.

relatively higher in the alveolar bilayer model compared to other human tissue model. It is to be noted that the vaccine or antigen dose plays a key role in the degree of antigen presenting cell maturation where viability can be compromised at the cost of driving dendritic cell maturation. For the five tested donors (4 replicates per donor), significant dendritic cell maturation was observed in all tissue models with the inactive *Staphylococcus aureus* bioparticle stimulation.

The inter-connected functional role of a variety of cellular populations in the pulmonary mucosa serves as a primary defense interface to pathogen entry. Thus far, we have developed of *in vitro* tissue models to represent local and systemic physiologic responses to different immunologic stimuli. Future studies, will build on the idea of form and function and connect the mode of therapeutic delivery as means to drive immune function to live virus infection. Thus, these initial results serve as a means to guide the influenza and filovirus disease model development.

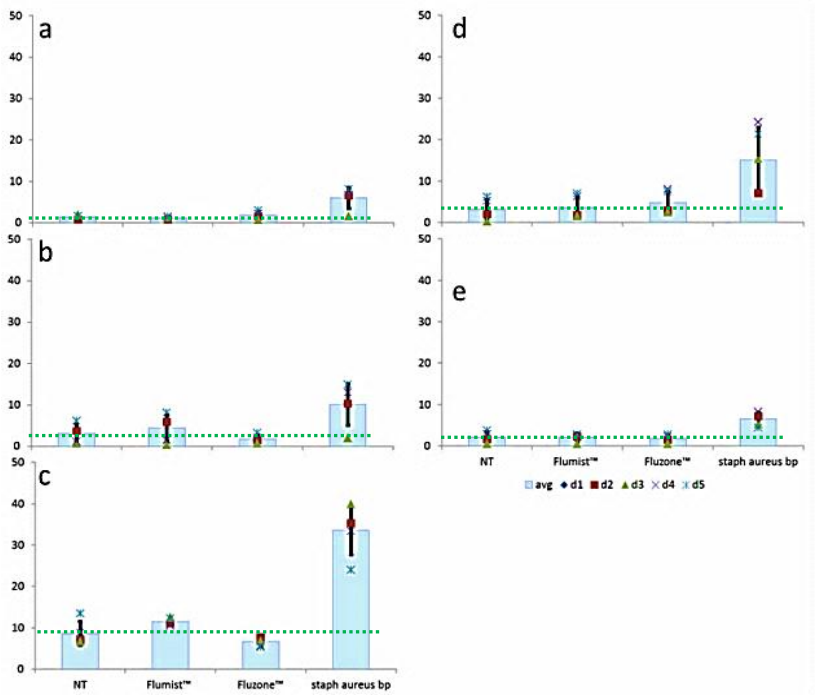

Figure 32: CD83+ expression a) alveolar epithelium, b) nasal epithelium, c) alveolar bilayer, d) A549 cell line, and e) CRL-1848 cell line tissue models.

Part II: Non-Human Primate Tissue Models (specific aim 3.2.1)

Experimental Methods

Tissue culture

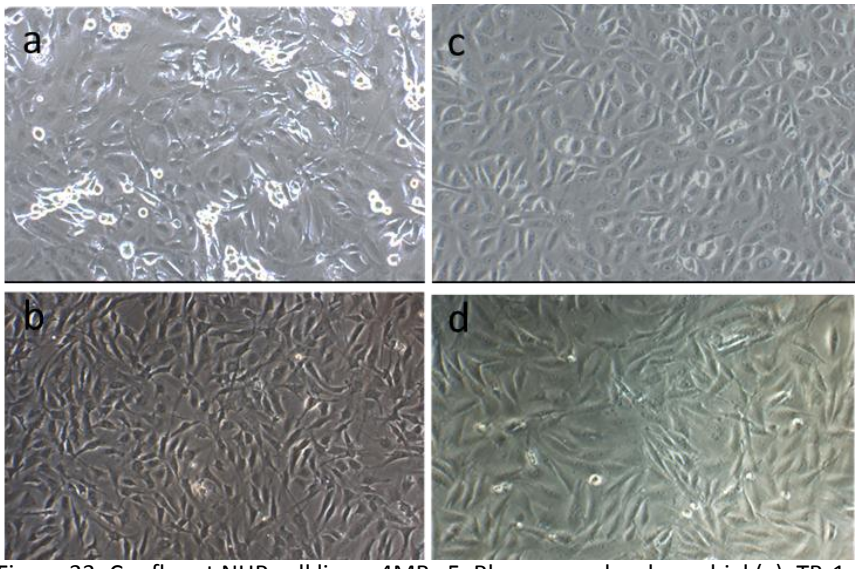

Figure 33: Confluent NHP cell lines: 4MBr-5, Rhesus monkey bronchial (a); TB-1 Lu*, Tadarida brasiliensis)* bat lung (b); Vero, Africa green monkey kidney (c); LA4 mouse lung adenocarcinoma (d).

4MBr-5 Rhesus monkey cell line, Tb1Lu Bat cell line, LA-4 murine cell line and Vero African green monkey cell line were purchased from ATCC and expanded up to passage 8 in the ATCC recommended media formulations. The cultured cell lines were grown in 30% serum containing HAM's FK-12 base media. 4-MBr5 cell line was cultured without EGF after the initial expansion up to passage 8. Media was exchanged every 48hr until confluent. For the cell lines, cell seeding density was 35,000cells/per well. Tissue layer formation was observed between 3-4days for the cell lines. Media was removed from the apical side of tissue constructs and placed on a rocker at a rate of 1/min for 3 hour. The experiments were staggered to take into account the growth rates, so the stimulations were done on differentiated tissue constructs.

Tissue confluencey and viability via confocal microscopy

The NHP tissue models were stained with Calcein AM and DAPI to check for confluencey and detect viable cells.

Vesicle cycling

In vitro vesicle cycling via time-lapse tissue imaging (NHP Tissue Model)*:* FM-143FX, a lipophilic styryl dye, was used to label cellular vesicle membranes. 1ug/ml dye was added to the apical side of live differentiated tissue. Fluorescence microscopy images were captured every 2 minutes for a period of 10-15 minutes for time lapse studies.

Results and discussion

Part II: Non-human primate MTE models

With the help of USAMRIID labs, we identified filo virus infection relevant non-human species and cell lines. Our preliminary experiments show that these cell lines exhibit significantly improved cell line doublings after 4 passages (Figure 33). For 4-MBr5, there is a need for murine EGF in the culture media. These cells also exhibit multilayer behavior with some morphologically distinctive sub-populations that tend to group into clusters. The Tb-1 Lu and the LA4 cell lines have a tendency to grow in patches. However, they do not require growth factors. The Vero cells show the most consistent monolayer formation. However, these cells are not isolated from airway tissue; thus there may be functional and metabolic differences to lung epithelial cells. The rationale for performing the FITC-dextran permeability study in the human and NHP tissue models is as an alternative measure of cellular confluencey. This method provides a general measure of tissue integrity and possibly antigen deposition and delivery to the MTE module.

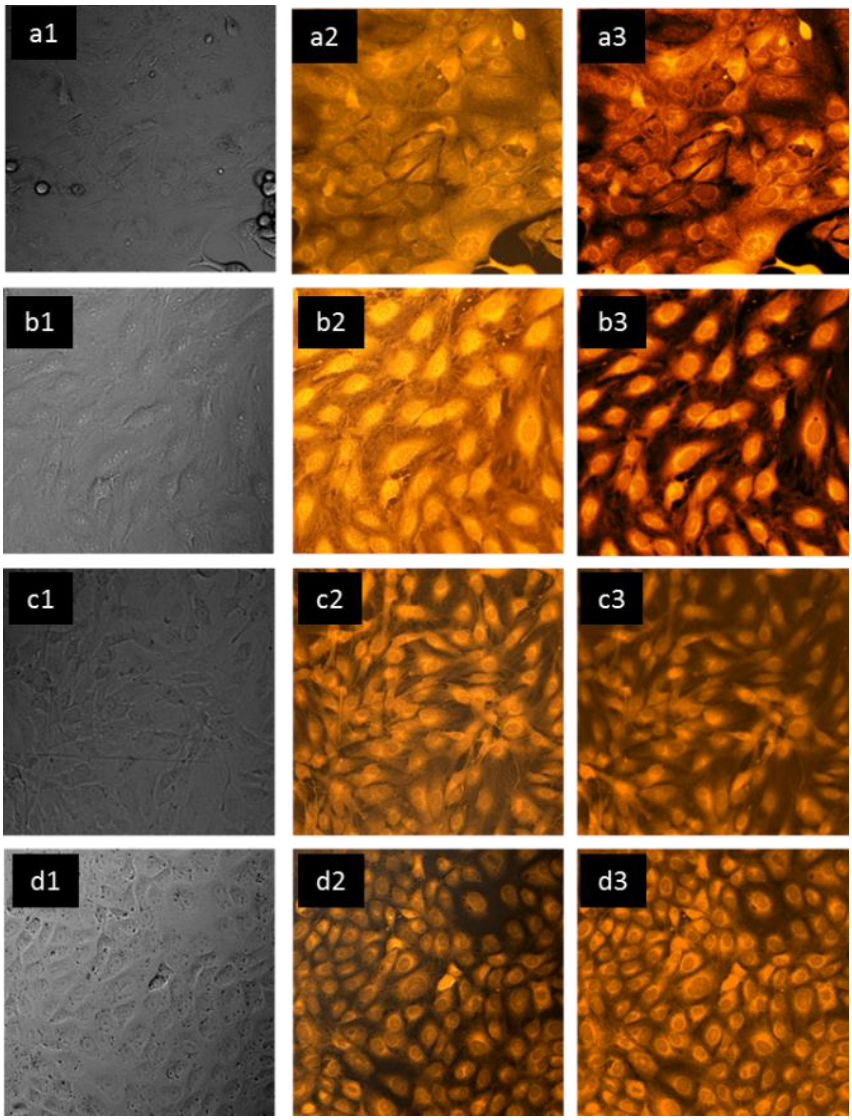

Figure 34: Fluorescence microscopy of NHP cell lines including 4MBr-5, Rhesus monkey bronchial (a); TB-1 Lu*, Tadarida brasiliensis)* bat lung (b); Vero, Africa green monkey kidney (c); LA4 mouse lung adenocarcinoma (d). Phase contrast (1), light plus fluorescent (2), and confocal microscopy (3) images of NHP tissue models show viable cell layers (CalceinAM) with healthy nuclei (DAPI).

For the non-human primate models, we also stained the cells with CalceinAM viability stain and DAPI nuclear stain. Figure 34 shows

the health and general cellular coverage. The phase contrast and fluorescence microscopy images allow for side-by-side comparison of the various cell types. It is to be noted that the 4-Mbr5 cells are perhaps the most diverse in terms of morphology. Based on the irregular tissue morphology, this initiated permeability experiments on the NHP cell lines. Here, controlled molecular weight polymers were introduced to the apical side of the tissue constructs and kinetic sampling of various chambers allows for a quantitative measure of tissue leakiness.

For the NHP cell lines exhibited confluent and viable MTE constructs. These modules were composed of 4MBr-5 (Rhesus monkey bronchial tissue derived), TB-1 Lu *(Tadarida brasiliensis)* bat lung derived), LA4 (mouse lung adenocarcinoma cell line), and Vero (Africa green monkey kidney cell line). Compared to the human tissue models, these cell lines have variable growth rates and some, like the 4-MBr5, require murine EGF. They were weaned off the growth factors over continuous culture. The NHP cell lines produced viable tissue layers. However, 4-MBr5, Tb1Lu and LA-4 cell lines showed non-confluent tissue morphology. This observation was confirmed by the FITC-dextran permeability study. Permeability experiments with fluorescently labeled compounds with controlled molecular weights showed that the NHP cell lines are non-confluent and therefore permit non-specific entry through the mucosal epithelium. This resembles injured or diseased airway physiology. The vesicle cycling experiments, with similar conditions to the human counterparts, show that these NHP cell lines do not exhibit active vesicle formation at the tested dose. This basic airway physiological function is needed for active cellular entry. The following sections discuss the results for each study in detail.

			4-MBr-5 Rhesus Monkey Bronchial	Tb1 Lu Bat Lung	Vero African Green Monkey Kidney	LA-4 Murine Lung Adenocarcinoma
Airway Tissue	Tissue Integrity	Viability	+	+	+	+
		Confluencey (live/dead staining)	+/-	+/-	+	+/-
		High resolution TEM (differentiated epithelium)				
		Short-term FITC Dextran permeability (10KDA, 70KDa, 500KDa)	+	+/-	-	+
	Vesicle / membrane function	Membrane activity (epithelium dye uptake)	-/+	-	-	-/+
		Active vesicle cycling (time-lapse confocal imaging)	-	-	-	-

Table 4: Summary of non-human primate MTE module tissue response

Vesicle cycling in non-human primate tissue models The vesicle cycling and permeability studies for the NHP models designed similar to the human models (Part I). Overall, we can conclude that NHP cells are not as responsive to the FM-143FX membrane stain for vesicle formation (Figure 35; 36). We found the superficial cellular aggregates of the 4-MBr5 more prone to picking up the FM-143FX dye. However, there was no consistency throughout the cell layer. The other cell lines showed some background level of membrane staining. However, there was little indication of vesicle like spherical structures in the cell layers. We are not aware of the ability of these cell types to produce surfactant and mucin proteins. Thus, the lack of staining may be attributed to residual proteins or perhaps a higher concentration or exposure time is needed to get a response similar to the human tissue models.

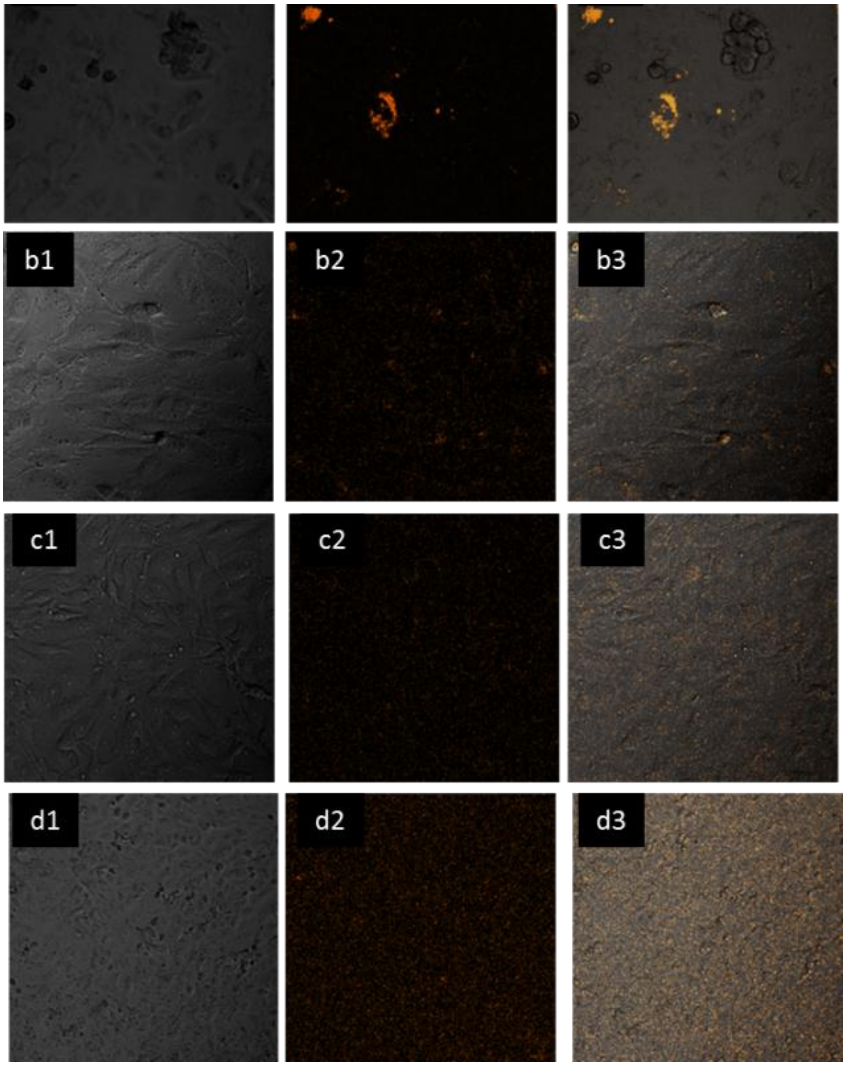

Figure 35: FM-143FX saturation (15min) of cellular membranes of NHP cell lines including 4MBr-5, Rhesus monkey bronchial (a); TB-1 Lu, *Tadarida brasiliensis*-bat lung (b); Vero, African green monkey kidney (c); LA4 mouse lun adenocarcinoma (d).

Time lapse imaging of the vesicle cycling experiments showed the highest level of staining at 2 minute time interval (Figure35, 36). However, our previous experience with the human tissue models showed a significantly higher level of activity. Thus our

observation suggests a difference between the human and non-human tissue models in terms of membrane associated vesicle activity.

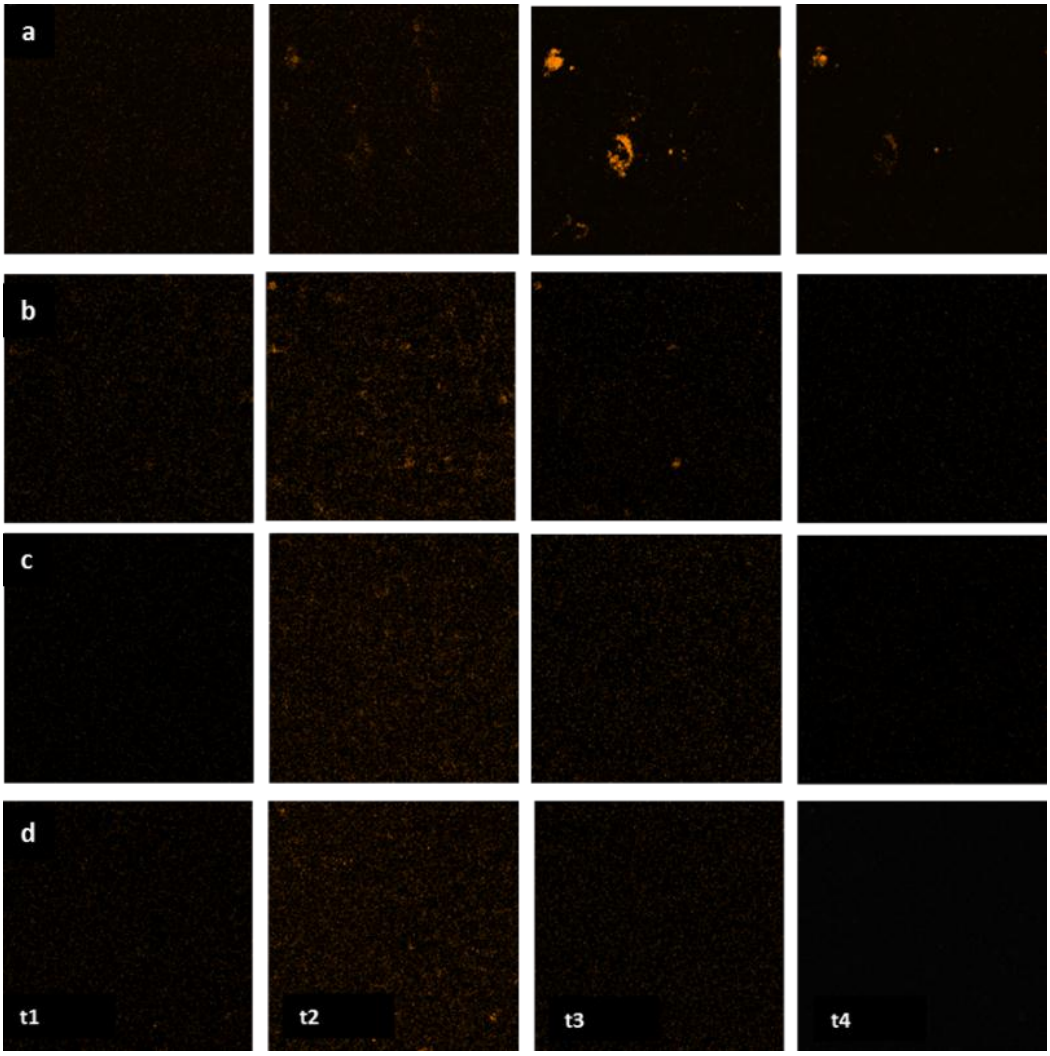

Figure 36: NHP cell line vesicle cycling in 2 minute intervals 4MBr-5, Rhesus monkey bronchial (a); TB-1 Lu*, Tadarida brasiliensis)* bat lung (b); Vero, Africa green monkey kidney (c); LA4 mouse lung adenocarcinoma (d).

Non-human primate tissue “leakiness” or permeability studies

The permeability studies were designed to address the qualitative visual of massive gaps in tissue confluencey as observed by phase contrast and live cell staining; Figure33; 34. The FITC-dextran experiments with three different molecular weights were designed to characterize the confluencey thorough measurement of short term “leakiness” of the tissue constructs. For direct comparison to human models, the basal media was used to measure the concentration of FITC dextran molecules (10Ka, 70KDa, 500KDa). This served as the most reliable measure of permeability since non-specific binding to the transwell material, and attachment or metabolism of the molecule by the cells was not measured.

The basal FITC-dextran measure indicates the most non-confluent tissue constructs and were composed of human CRL-1848 and NHP 4-MBr5 cell lines. This is shown by the blue line graph in Figures 37 for the NHP cells. These findings confirm the previous qualitative confocal imaging results in which gaps were observed in the cultured tissue CRL-1848 and NHP 4-MBr5 cell lines.

Vero cells tissue showed the highest impermeability to all molecular weights of FITC dextran, similar the alveolar bilayer model. The lack of FITC-dextran permeation through the in vitro cultured constructs resembles a healthy airway mucosa (Briot, 2008; Bayat, 2000, Gurey, 1998). However, Vero cell line originates from kidney tissue from African Green Monkey. (AAll the other NHP cell lines, including LA-4, 4-MBr5 and Tb-1Lu, showed FITC-dextran permeation profiles and displayed higher well-to-well variance in the basal and apical supernatants. The 10KDa FITC dextran (smallest MW) showed the highest degree of permeability in the NHP models. However, there was no apparent trend for the 70KD or 500KDa molecular weights. Based on these results, we cannot draw any conclusion or trends on FITC-dextran molecular weight and tissue permeability.

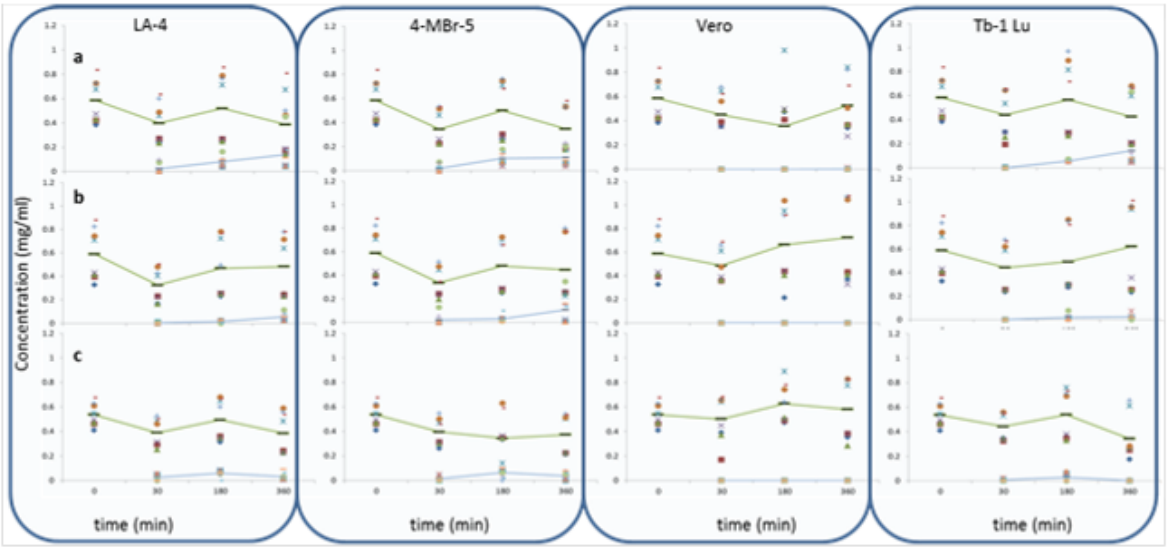

Figure 37: FITC-dextran permeability in NHP tissue models a) 10KDa, b) 70KDa, c) 500KDa (green=apical

KEY RESEARCH ACCOMPLISHMENTS:

PART I: Human airway tissue models (specific aims 3.2.1; 3.3.1)

1. We have demonstrated distinct differences between populating alveolar tissue models with primary airway nasal cells and human A549 and CRL848 cell lines.

   a. Upper and lower airway tissue models with primary epithelial cells: These tissue constructs show a differentiated nasal and alveolar primary epithelial cells with microvilli structures on the apical side of the tissue along with surfactant and lipid containing vesicles. The high resolution electron microscopy suggests that the primary cell tissue constructs are actively producing and releasing vesicles with endosomes, lipids and lamellar bodies associated with surfactant release.

   b. Cell line airway tissue models: The A549 and CRL848 human cell lines also show differentiated microvilli at the apical side, and numerous vesicles were observed throughout the tissue. However, these vesicles are empty and do not contain lamellar bodies or lipids.

2. Vesicle Cycling: The confocal microscopy of FM-143FX demonstrates active vesicle formation and transport from the alveolar and nasal epithelium and the alveolar bilayer model with both primary epithelial and endothelial cells. The cell line tissue models of A549 and CRL848 do not exhibit the same level of vesicle formation and transport function.

3. Tissue Permeability: The degree of tissue “leakiness” of the five human constructs was quantified through FITC-dextran permeability studies. The least degree of permeability or the highest level of confluencey was observed in the alveolar bilayer models. This is of relevance to passive vs. active antigen and cellular transport through the cell layer.

4. Tissue Innate Secretory Immune Response in the Epithelial Constructs: The innate cytokine and chemokine response in terms of TLR agonist activity demonstrates highest function from the TLR3 agonist, followed by TLR4 and TLR2. The addition of filovirus GP antigen showed a dampening effect on macrophage chemotactic protein-1 production. Whereas, Macrophage inflammatory protein-1beta showed a modest up-regulation.

5. Genomic Response in the Human Airway Constructs: The results indicate that the primary upper (nasal) and lower (alveolar) airway primary cell based *in vitro* constructs do not have equivalent gene expression profiles to human airway cell

lines (A549, CRL-848). This further demonstrates the stromal cell contribution to the tissue function.

a. We have begun to identify baseline gene expression of Pattern Recognition Receptor (PRR) associated genes.

i. The cellular membrane associated Toll-like Receptor glycoprotein activity was induced and identified by the introduction of complimentary TLR agonists. Seven TLR genes associated with viral and bacterial entry were identified per tissue model system.

ii. The cytosolic PRR activity was identified by characterizing RIG-I and NOD-1 response.

b. For the primary airway cell tissue models, the alveolar bilayer showed relatively higher gene expression with the TLR agonist related genes and other intracellular PRR. In most cases, this was also observed for the tested inactivated filovirus strains. This may be of relevance for developing *in vitro* models that mimic *in vivo* physiology of pathogen or therapeutic antigen delivery from the alveolar epithelial mucosa to the microvasculature for cellular recruitment and induction of a broader systemic response.

c. For the cell lines, CRL-848 showed the higher differential PRR related genomic activity with the introduction of the selected filovirus strains. In comparison, the primary cells have a dampened expression of the tested PRR genes similar to in vivo pathology. We plan to explore this further with future studies relating to the added complexity of immune cell interactions.

d. For the defense mechanism related mucosal protein, the alveolar bilayer model showed surfactant protein-C, -D production along with MUC1. There was little to no response to the inactive filovirus in the primary epithelial models. The addition of the endothelium to the alveolar epithelial mucosa produced a mild defense protein response. CRL-848 produced MUC1, MUC5AC, SFPC, and SFPC. We speculate the variation between primary cells and cells lines is due to the mucoepidermoid carcinoma origins of the cell lines.

e. For genomic studies, the epithelial cell containing tissue models were tested with inactive filovirus strains (*Sudan, Marburg, Ebola, and Bundibugyo*) without the addition of immune cells. Nonetheless, we have observed tissue related expression of host defense genes like Suppressor of Cytokine Signaling (SOCS1) in the cell lines and the primary cell tissue models. It is to be noted that the response in the primary cell tissue models is to a lesser degree. The related interferon response is also dampened in the primary cells. The TNF and TYK2

genes were up-regulated for the primary cells. The human cell line models showed irregular trends as the SOCS1 levels were up-regulated with significant IFNG, TNF, MYD88 and IRF3 activity were generally highest for the CRL-1848 cell line. We plan to explore viral entry with the addition off immune cells like antigen presenting cells as it relates to immune suppression and related biological queues to better understand infection to design *in vitro* models that mimic animal physiology.

6. Innate Response in the Airway Tissue Models with the Addition of Immune cells: The complexity of the upper and lower airway constructs was increased by the addition of monocytes. The secretory cytokine and chemokine levels in the culture supernatants and the cell surface markers in the antigen presenting cell population show differences between the five human tissue models.

   a. The *Staphylococcus aureus* bioparticles produced the most consistent TLR-4 and TLR-2 related pro-inflammatory response with fold increase in the production of TNF-alpha, MIP-1a,-1b along with IL-1b relative to the no treatment control. The bioparticle stimulation showed a consistent five to ten fold up-regulation of GM-CSF, MIP-1apha, and MIP-1 beta.

   b. The influenza vaccine antigen produces a mild tissue response when compared against the *Staphylococcus aureus* antigen control. The interferon gamma induced protein 10 (IP-10) levels in the alveolar epithelium were similar to the CRL1848 cell line for FluMist® and Fluzone® treated cultures. The alveolar bilayer model showed a similar response to the attenuated vaccine, FluMist®.

   c. All ten donors showed a suppressed IP-10 response to Fluzone®, which may be correlated with reduced interferon gamma activity. Macrophage inflammatory protein beta and GM-CSF show a mild overall response to FluMist®; these cytokines are involved in macrophage and dendritic cell recruitment to the infection site.

   d. The alveolar bilayer model showed relatively higher degree of dendritic cell maturation, in terms of HLA-DR and CD14 expression. The impermeability of FITC-dextran in the alveolar model demonstrates the tissue confluencey needed to drive the extravasation process. Thus, the observed DC maturation is attributed to active cellular activity and not gravity driven transport of monocytes through an open sieve tissue motif.

Part II: Non-human Primate Tissue Models (specific aim 3.2.1)

For the NHP cell lines of interest, we demonstrated confluent and viable in-vitro cultured constructs made of 4MBr-5 (Rhesus monkey bronchial tissue derived), TB-1 Lu *(Tadarida brasiliensis)* bat lung derived), LA4 (mouse lung adenocarcinoma cell line), and Vero (Africa green monkey kidney cell line). Compared to the human tissue models, these cell lines have variable growth rates and some, like the 4-MBr5, require murine EGF. They were weaned off the growth factors over continuous culture.

1. Vesicle cycling experiments with similar conditions to the human counterparts show that these NHP cell lines do not exhibit active vesicle formation at the tested dose. This basic airway physiological function is needed for active cellular entry.

2. Permeability experiments with fluorescently labeled compounds with controlled molecular weights showed that the NHP cell lines are non-confluent and therefore permit non-specific entry through the mucosal epithelium. This resembles injured or diseased airway physiology.

Overall Project Summary Table: Relative comparison of phenotypic and cellular function

			NHP cell line tissue model				Primary human airway models			Human cell line models	
			4-MBr-5 Rhesus Monkey Bronchial	Tb1 Lu Bat Lung	Vero African Green Monkey Kidney	LA-4 Murine Lung Adenocarcinoma	Alveolar Epithelium	Nasal Epithelium	Alveolar Bilayer Epithelium / endothelium	A549 Lung Carcinoma	CRL1848 Lung Carcinoma
Airway Tissue	Tissue Integrity	Viability	+	+	+	+	+	+	+	+	+
		Confluencey (live/dead staining)	+/-	+/-	+	+/-	+	+	+	+	+/-
		High resolution TEM (differentiated epithelium)					+	+	+	-/+	-/+
		Short-term FITC Dextran permeability (10KDA, 70KDa, 500KDa)	+	+/-	-	+	+/-	+/-	-	+	+
	Vesicle / membrane function	Membrane activity (epithelium dye uptake)	-/+	-	-	-/+	++	++	++	+/-	+/-
		Active vesicle cycling (time-lapse confocal imaging)	-	-	-	-	++	++	++	-	-
	Gene expression	PRR: TLR gene expression- TLR agonists					+/-	+/-	++	+/-	-/+
		PRR: TLR expression- Irradiated filovirus interaction					-/+	-	+/-	-/+	++
		Cytosolic PRR: RIG-I and NOD1- inactive filovirus					-	-/+	++	-	++
		Surfactant protein genes expression- inactive filovirus					-/+	-/+	+/-	+/-	+/-
		Mucin protein gene expression- inactive filovirus					-	-/+	+/-	+	+
	Secretory factors	Cytokine and chemokine response- TLR agonist-3,-4					+/-	+/-	-/+	+	+
Airway Tissue Plus Immune Cells Innate Immune Response	DC Phenotype (CD14, HLA-DR)	Bacterial antigen Inactive *Staphylococcus aureus*					+	+	+	+	+
		Influenza vaccine (FluMist®, Fluzone®)					-	-	+	-	-
	Secretory factors	Cytokine and chemokine response Bacterial antigen- inactive *Staphylococcus aureus*					+	+	+	+	+
		Cytokine and chemokine response Influenza vaccine- FluMist®, Fluzone®					-/+*		+/-*	+/-*	

*Please refer to heat map Table 1 for class / family specific cytokine and chemokine response trends

"+" denotes a positive response; "-"denotes a negative response; combination of "+" and "-"denotes relative response

REPORTABLE OUTCOMES:

1. Presentation Title: Evaluation of *In Vitro* Tissue Models of Upper and Lower Airway

Authors: Ayesha Mahmood, John Dye, Eric Mishkin, William Warren

Biomedical Engineering Society 2013 Annual Meeting, Seattle, Washington.

CONCLUSION:

This report summarizes the developmental work of the MIMIC MTE module using primary human and non-human primate cells and cell lines, of relevance to filovirus infection. In the first year of the program, we have demonstrated morphological and cellular functional differences between the primary human upper and lower airway tissue to A549 and CRL848 cell lines in terms of tissue morphology, vesicle cycling, cytokine and chemokine secretory factors, gene expression and innate immune response with the addition of immune cells; see Project Summary Table for a quick summary. Overall, each tissue model is unique in terms of both morphology and function. The transcriptomic evaluation of the mucosal tissue models further supports that the alveolar bilayer tissue model exhibits desirable function for PRR receptors, mucin and surfactant protein, along with a host of viral entry related genes. For the human cell lines, we report superior function of CRL848 tissue model. The human models are being developed further for antigen presenting cell activation studies to better understand the role of the mucosal tissue and antigen delivery mode to meet the overall program objective of building filo virus and influenza infection disease models.

A differentiated epithelium is critical for mucosal function. For the lower airways, the Type II alveolar epithelial cells serve as “pseudo antigen presenting cells” due to their ability to pick-up and transfer foreign matter to the local and systemic circulation. These comparative experiments with primary upper and lower airway tissue models and cell lines were designed to examine tissue morphology, permeability, vesicle cycling and innate tissue response to selected antigen on interest for respiratory mucosa (Feherenbach, 2001; Herzog, 2008). The data suggests that the primary cells are more functional in terms of producing more specialized vesicle structures. Along with the presence of a differentiated mucosa the presence of microvilli, healthy cellular organelles including nuclei, golgi and endoplasmic reticulum is observed. The primary alveolar epithelium showed active endocytosis process with a variety of vesicle structures with lamellar bodies, lipids or endosomes. The presence of lamellar bodies in vesicular structures is indicative of surfactant or mucin presence which is considered an important barrier function to contain pathogen entry. The vesicle cycling process via florescent dye labeling also demonstrated the vesicle cycling ability of the epithelium. The primary nasal epithelial model, representing the upper airway, showed similar morphology with the exception of the presence of relatively larger number of lipid filled vesicles; surfactant vesicles are generally produced in the lower airway where it is required for improving surface tension for the alveoli during the breathing process. The presence of these specialized vesicle structures was missing in the A549 and CRL848 cell line models. Similarly, these cell line models show minimal vesicle formation in the presence of FM-143FX; the dye did stain cellular membrane (considered background fluorescence). The human MTE morphology and vesicle cycling experiments demonstrate that the primary cell based modules mimic *in vivo* local tissue morphology

in terms of the presence of “pseudo-APC” Type II epithelial cell morphology and vesicle transport processes (Feherenbach, 2001; Herzog, 2008).

To better understand the difference between secreted cellular by-products and cellular gene specific activity, as it relates to pathogen entry, we have demonstrated exogenous vs. endogenous activity. The kinetics of cytokine release is tied into innate inflammatory response for the local vascular network (endothelium) or the tissue epithelium and leads to subsequent cellular processes like surfactant production and leukocyte recruitment. The protective effect of surfactant protein on innate cytokine response at the site of infection (Clark, 2002; King, 2011), may be an explanation for the slightly dampened cytokine response by the alveolar bilayer model. We have also identified specific genes related to pattern recognition receptors (TLR family, NOD1 and suppressive RIG-1), interferon responsive genes (SOCS1, STAT1, and JAK2) and genes known for pathogen defense mechanisms (IFN, TNF, IRF3) and pulmonary defense mechanism surfactant related genes (SFT-C,-D, MUC-1,-5AC). In comparison to the primary cell models, the cell lines are more consistent at producing innate cytokines by TLR-3, TLR-4 and TLR2/TLR1 agonists; these cells are selected based on a compromise between growth and function. The innate response in terms of secreted cytokines and chemokines from the primary nasal and alveolar epithelial cell models and A549 cell line showed stimulation by TLR3, TLR2/1 and TLR4 in the form of chemotactic cytokines IP-10 and RANTES; these cytokines are involved in the recruitment of leukocytes including antigen presenting cells like monocytes, DCs, macrophages along with T cells to the inflammation site. Low level secretory activity for TLR 7, 8, and 9 was also observed from the alveolar models. It is interesting to note the slightly dampened activity of the bilayer alveolar model compared to the alveolar epithelium alone. The genomic data suggests the same. Here the TLR agonist related activity also demonstrates differences in the sub-cellular endogenous and excretory cellular mechanisms, as more TLR related genes are activated with the addition of endothelium. The kinetics and degree of cellular processes related to cytokine and chemokine secretion and sampling suggest that the genomic data provides a more accurate snapshot of cellular activation of TLR-2,-3,-4,-7,-8,-9 for the alveolar bilayer model, where the weak secretory activity is supplemented with fold increase in gene expression.

The alveolar bilayer model showed relatively higher degree of dendritic cell maturation. The impermeability of FITC-dextran in the alveolar model demonstrates the tissue confluencey needed to drive the extravasation process. These finding are in accord in vivo studies where FITC dextran measurement in BAL fluid after intravascular administration has been recognized as a measure of lung acute lung injury or disease related tissue permeability (Briot, 2008; Bayat, 2000, Gurey, 1998). Thus, the observed DC maturation in the alveolar bilayer MTE is attributed to active cellular activity and not gravity driven transport of monocytes through an open sieve tissue motif. The next steps for the human tissue models will require the testing of more donors to expand this work further.

Our experimental results demonstrate that the alveolar bilayer tissue model exhibits the highest degree of response in terms of antigen presenting cell maturation via selective cellular extravasation through the epithelium and endothelium layers, vesicle cycling and defense surfactant protein genomic expression. However, the cytokine and chemokine response, with the addition of immune cell population, is still relatively milder in the alveolar bilayer model, when compared to A549 and CRL-1848. The relatively higher cytokine and chemokine profiles by the cell lines can be attributed to the cellular origin; this is a repeat observation from our previous studies without the immune cells. The MTE cell lines were isolated from pulmonary carcinoma. The continuous culture of cell lines results in population functional drift away from the *in vivo* and primary cell source. The degree of antigen presenting cell maturation is relatively lower for these cell line tissue models, suggesting that the pronounced secretory factors are produced by the cell line tissue constructs and cannot be directly attributed to the immune cell interaction. The physiological relevance (Table 5) of the MTE modules suggests the primary cells are biomimetic in nature. The alveolar bilayer MTE outperforms the other tested MTE due to its antigen uptake, permeability and selective / immunologically relevant function. Thus, this module is a good starting point for viral infection related disease model studies.

	PART I				PART II				
	NHP cell line tissue model				Primary human airway models			Human cell line models	
	4-MBr-5 Rhesus Monkey Bronchial	Tb1 Lu Bat Lung	Vero African Green Monkey Kidney	LA-4 Murine Lung Adenocarcinoma	Alveolar Epithelium	Nasal Epithelium	Alveolar Bilayer Epithelium / endothelium	A549 Lung Carcinoma	CRL1848 Lung Carcinoma
In vivo resemblance to differentiated mucosal morphology	✗	✗	✗	✗	✓	✓	✓		
Biomimetic FITC dextran permeability	✗	✗	✓	✗			✓		
Physiologically relevant active vesicle cycling	✗	✗	✗	✗	✓	✓	✓	✗	✗
High degree of TLR gene expression to TLR agonists							✓		
High degree of cytokine and chemokine secretion								✓	✓
Selective cytokine and chemokine secretion					✓	✓	✓		
High degree of antigen presenting cell maturation							✓		

Table 5: Generalized physiological relevance of the nine MTE modules.

For the non-human primate tissue models, thus far, we have demonstrated viable tissue with minimal vesicle cycling ability. The FITC-dextran study in the NHP tissue models

confirmed the presence of a non-confluent epithelium in 4-MBr-5 Rhesus Monkey, LA-4 murine, and Tb-1Lu bat cell line, as described in the previous quarterly report. Of the NHP cell line tissue models. Vero African green monkey cell line shows the least permeability; however, this is a kidney cell line and therefore is not recommended for lung cell based tissue models. All the NHP cell lines (Tb1Lu Bat cell line, LA-4 murine cell line, Vero African green monkey, and 4MBr-5 Rhesus monkey cell line) showed little to no vesicle cycling when compared against the primary human tissue models. Thus, the permeability study results build on differences between human and non-human cellular response profiles. Similar to human models, there was no direct correlation between FITC-dextran molecular weight and the permeability readout.

Future studies for this program will entail antigen cell population priming via droplet and liquid phase delivery. To this end, we will begin with nebulizers and then transition into the Vitrocell system based on positive experimental findings. The antibody primed MTE will be infected with live influenza infection. We anticipate the live virus MOI to significantly affect the functional readouts related to neutralization and replication *in vitro*. The models will require some developmental work for live filovirus infections. We will pursue the simplest and most practical methodology for recommendations to the USAMRIID labs. Any adjustments to the plan of work will be based on experimental findings and joint agreement to abandon or pursue alternative avenues. We plan to help our collaborators with the transfer of human MTE to the USAMRIID labs in the near future.

REFERENCES

Ariki S, Nishitani C, Kuroki Y. Diverse functions of pulmonary collectins in host defense of the lung. J Biomed Biotechnol. 2012;2012:532071.

Bayat S, Anglade D, Menaouar A, Martiel JL, Lafond JL, Benchetrit G, Grimbert FA, In vivo measurement of lung capillary-alveolar macromolecule permeability by saturation bronchoalveolar lavage, Crit Care Med 2000 Aug; 28(8):2937-42.

Briot R, Bayat S, Anglade D, Martiel JL, Grimbert F, Monitoring the capillary-alveolar leakage in an A.R.D.S. model using broncho-alveolar lavage, Mircrocirculation, 2008 April; 15(3):237-49.

Clark H Palaniyar N, Strong P, Edmonson J, Hawgood S, Reid KB Surfactant Protein D reduces alveolar macrophage apoptosis in vivo. J Immunol 2002 Sep 15;169(6):2892-9.

Feherenbach H Alveolar epithelial type II cell: defender of the alveolus revisited, Respir Res 2001; 2(1):33-46

Greene CM, McElvaney Toll-like receptor expression and function in the airway epithelial cells Arch Immunol Ther Exp 53, 418-427, 2005.

Griber SC, Richardson WM, Sodhi CP, Hackam DJ No longer an innocent bystander: epithelial toll-like receptor signaling in the development of mucosal inflammation Mol Med 14 (9-10): 645-59, 2008.

Gurey BP, Nelson S, Viget N, Fialdes P, Summer WR, Dobard E, Beaucaire G, Mason CM, Fluirescein-labeled dextran concentration is increased in BAL fluid after ANTU-induced edema, J Appl Physiol, 1998 Sept; 85(3):842-8.

Herzog EL, Brody AR, Colby TV, Mason R, Williams MC, Knowns and unknowns of the alveolus Proc Am Thorac, 2008, Sept 15; 5(7): 778-82

King BA, Kingma PS, Surfactant protein D deficiency increases lung injury during endotoxemia.Am J Respir Cell Mol Biol . 2011 May;44(5):709-15.

Lau SK, Weiss LM, Chu PG. Differential expression of MUC1, MUC2, and MUC5AC in carcinomas of various sites: an immunohistochemical study. Am J Clin Pathol. 2004 Jul;122(1):61-9.

Li Y, Dinwiddie DL, Harrod KS, Jiang Y, Kim KC. Anti-inflammatory effect of MUC1 during respiratory syncytial virus infection of lung epithelial cells *in vitro*. Am J Physiol Lung Cell Mol Physiol. 2010 Apr;298(4):L558-63.

Mogensen TH. Pathogen recognition and inflammatory signaling in innate immune defenses. Clin Microbiol Rev. 2009 Apr;22(2):240-73

Opitz B, van Laak V, Eitel J, Suttorp N. Innate immune recognition in infectious and noninfectious diseases of the lung. Am J Respir Crit Care Med. 2010 Jun 15;181(12):1294-309.

Ritter M, Mennerich, D, Weith, A, Seither, P Characterization of Toll-like receptors in primary lung epithelial cells: strong impact of the TLR3 ligand Poly (I:C) on the regulation of Toll-like receptors, adaptor proteins and inflammatory responseJ Inflamm 2005 Nov 29;2:16.

Schleh C, Rothen-Rutishauser BM, Blank F, Lauenstein HD, Nassimi M, Krug N, Braun A, Erpenbeck VJ, Gehr P, Hohlfeld JM. Surfactant Protein D modulates allergen particle uptake and inflammatory response in a human epithelial airway model. Respir Res. 2012 Feb 1;13:8.

Vareille M, Kieninger E, Edwards M, Regamey N, Clinical Mirobiology Reviews, The Airway Epithelium: Soldier in the Fight against Respiratory Viruses, January 2011 vol. 24(1), 210-229.

Xiang M, Fan J. Pattern recognition receptor-dependent mechanisms of acute lung injury. Mol Med. 2010 Jan-Feb;16(1-2):69-82.

Yamamoto M, Sato S, Mori K, Hoshino K, Takeuchi O, Takeda K, Akira S. Cutting edge: a novel Toll/IL-1 receptor domain-containing adapter that preferentially activates the IFN-beta promoter in the Toll-like receptor signaling. J Immunol. 2002 Dec 15;169(12):6668-72.

Yang W, Peter JI, Williams RO 3rd Inhaled nanoparticles—a current review Int J Pharm 356 (1-2):239-47, 2008.

APPENDICES

A0: Filovirus morphology

A1: Quantitative PCR data and supporting cytokine and chemokine in the human lung tissue models

A3: Appendix 2: 2013 Biomedical Engineering Society Meeting presentation documentation

Appendix: A0

Virus High resolution Transmission Electron Microscopy

The virus suspension was negatively stained with 2% phosphotungstic acid prior to visualization on EM grids. High resolution transmission electron microscopy was used for comparing the primary and cell line tissue models.

Results

High resolution transmission microscopy of inactive virus strains confirmed the presence of filovirus-like morpholgy in the suspensions used for the human tissue model stimulation. We confimed the heterogeneous viral morphology and the presence of classic rod-like and shepard's hook structures shown in Figure 1 below. This serves as a crude measure of the presence of virus in the stimulation cultures.

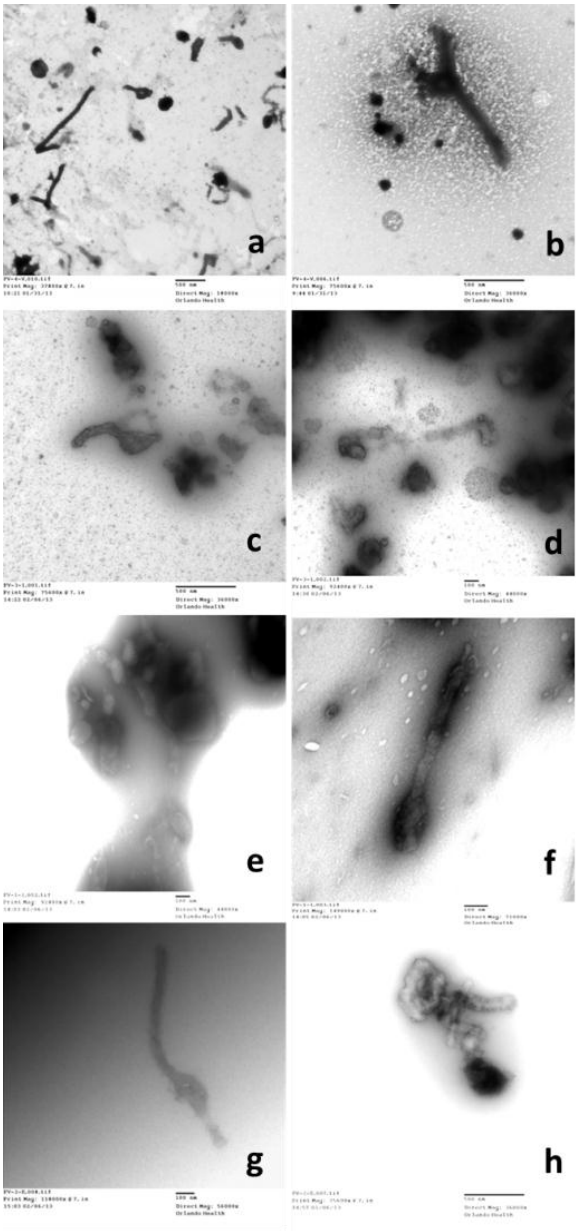

Figure A0: Electron microscopy images of filovirus strains: *Sudan* SUDV012010AK (a,b), Marburg MARV5Nov2009 (c,d); *Bundibugyo* BDBV1Jun2010 (e,f); *Ebola* EBOV'95Iot1 (g,h)

Appendix: A1
qPCR Graphs

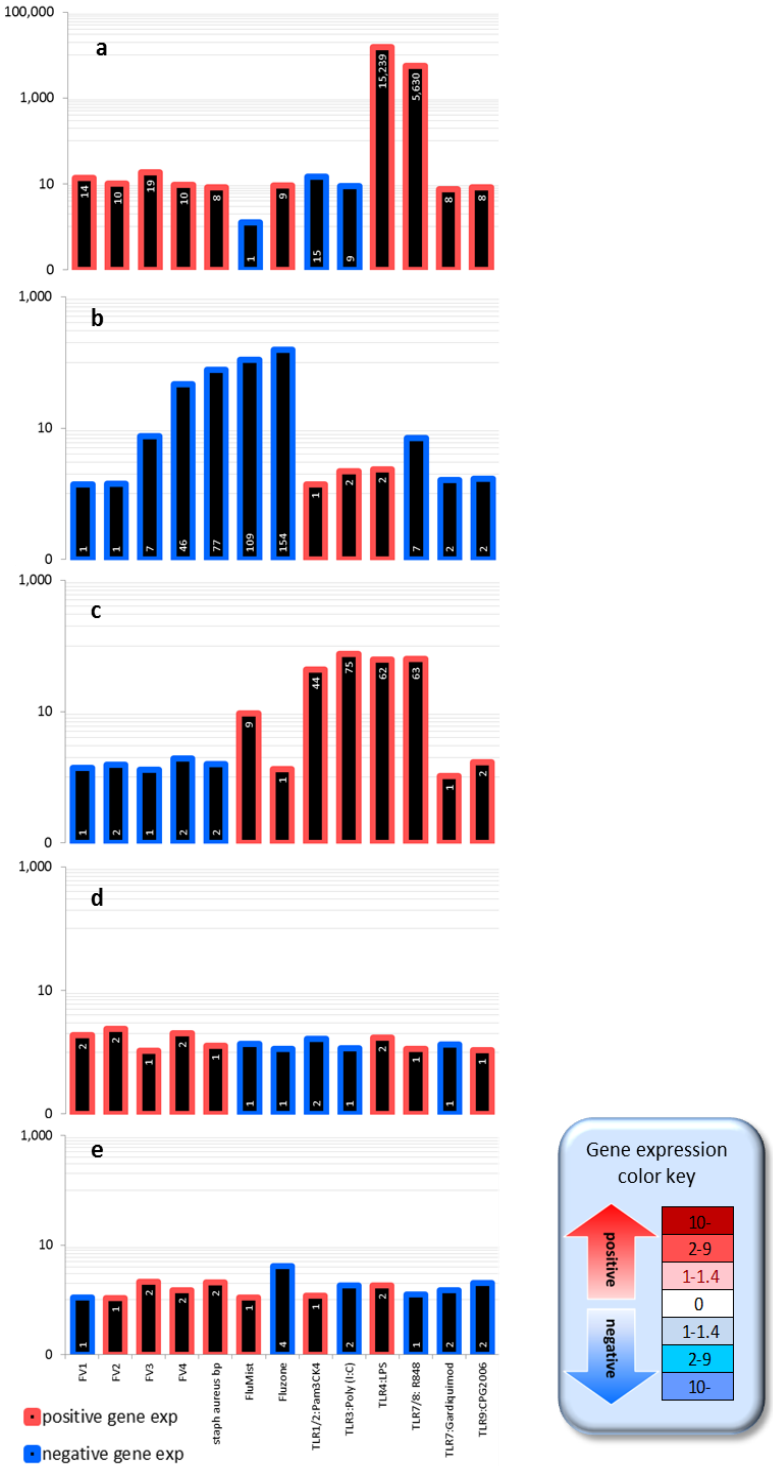

Figure A1: TLR1 expression in human tissue models a) alveolar epithelium, b) nasal epithelium, c) A549 cell line, d) CRL848 cell line, e) alveolar epithelium/endothelium

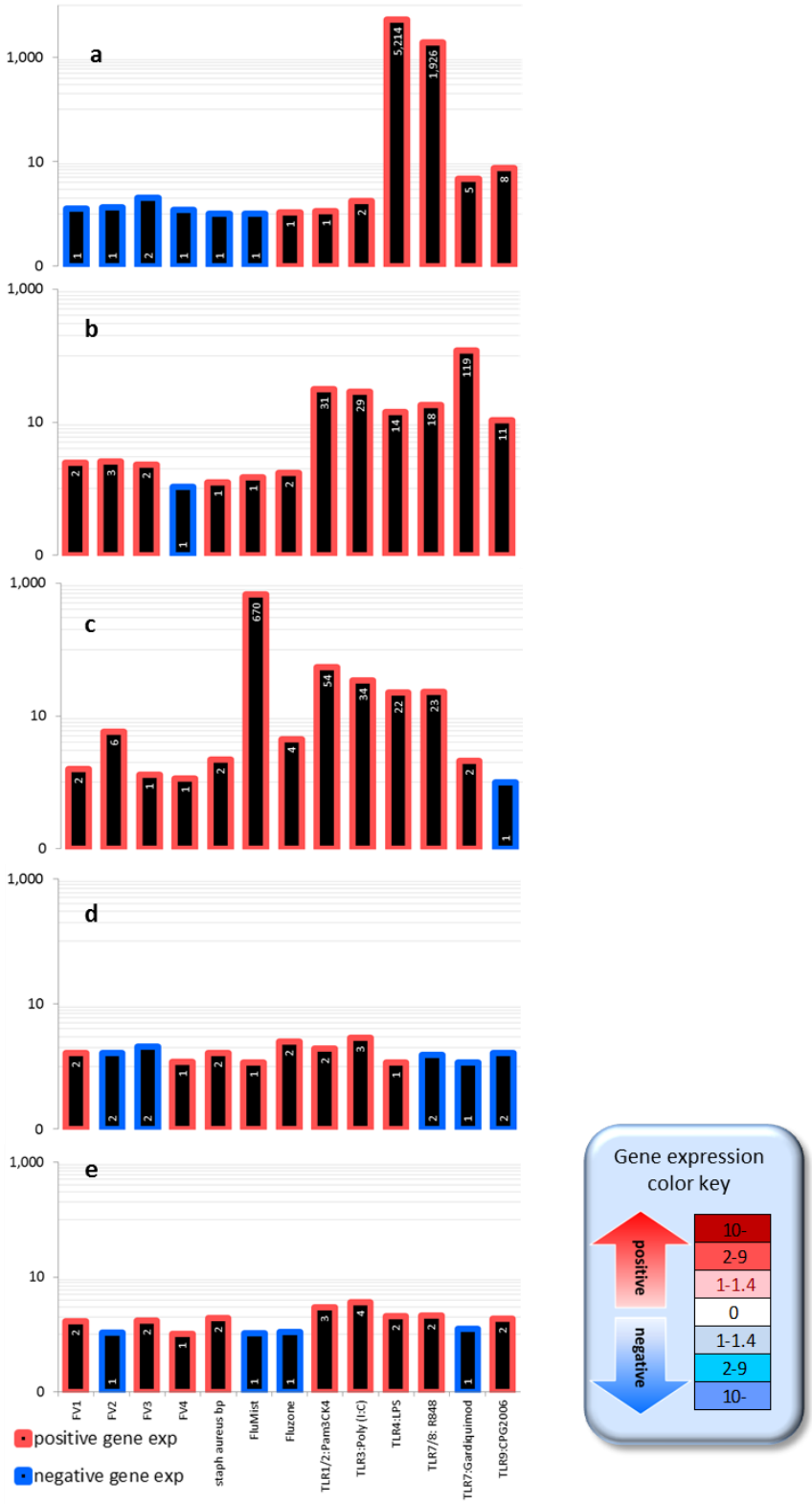

Figure A2: TLR2 expression in human tissue models a) alveolar epithelium, b) nasal epithelium, c) A549 cell line, d) CRL848 cell line, e) alveolar epithelium/endothelium

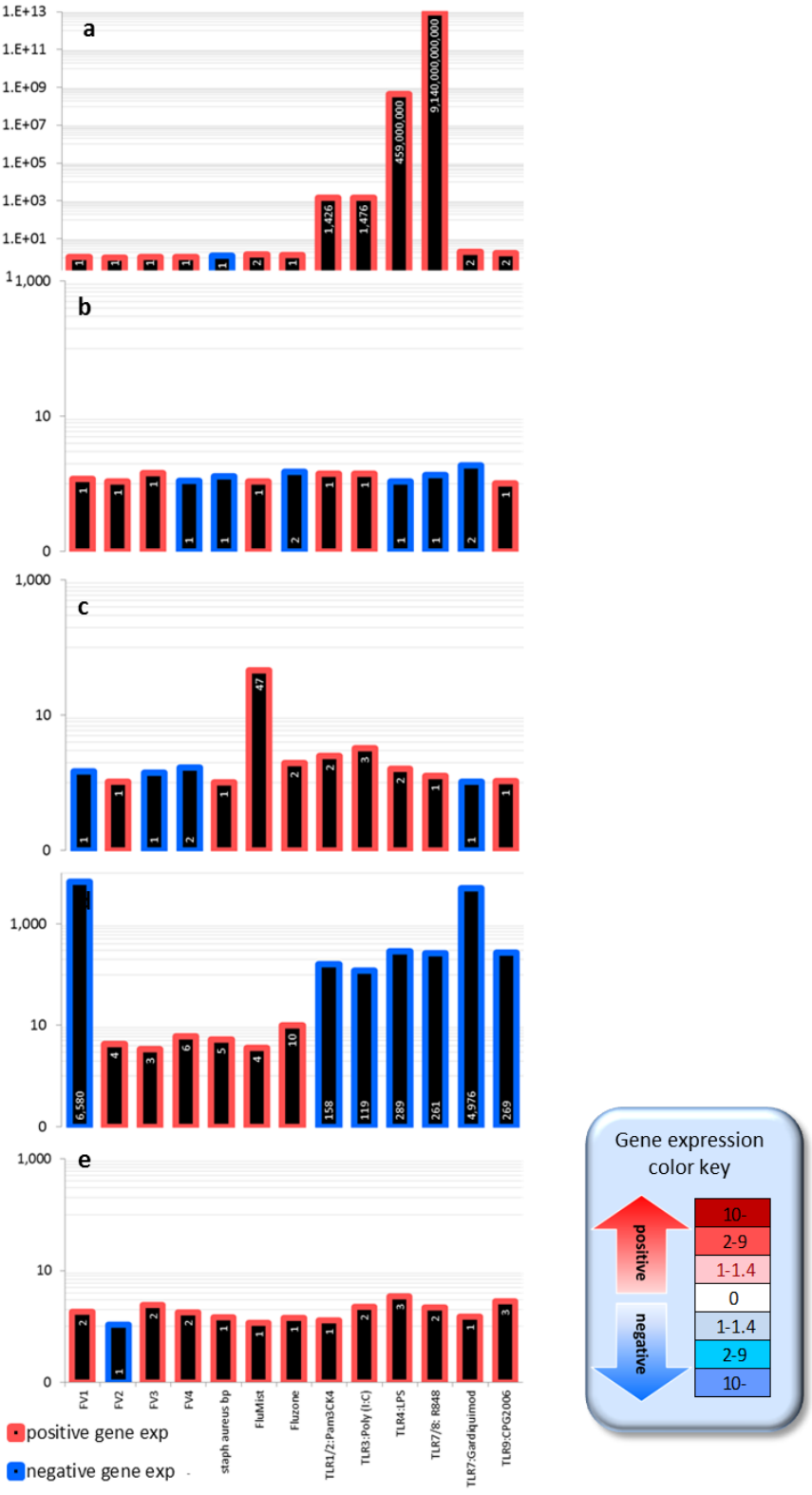

Figure A3: TLR3 expression in human tissue models a) alveolar epithelium, b) nasal epithelium, c) A549 cell line, d) CRL848 cell line, e) alveolar epithelium/endothelium

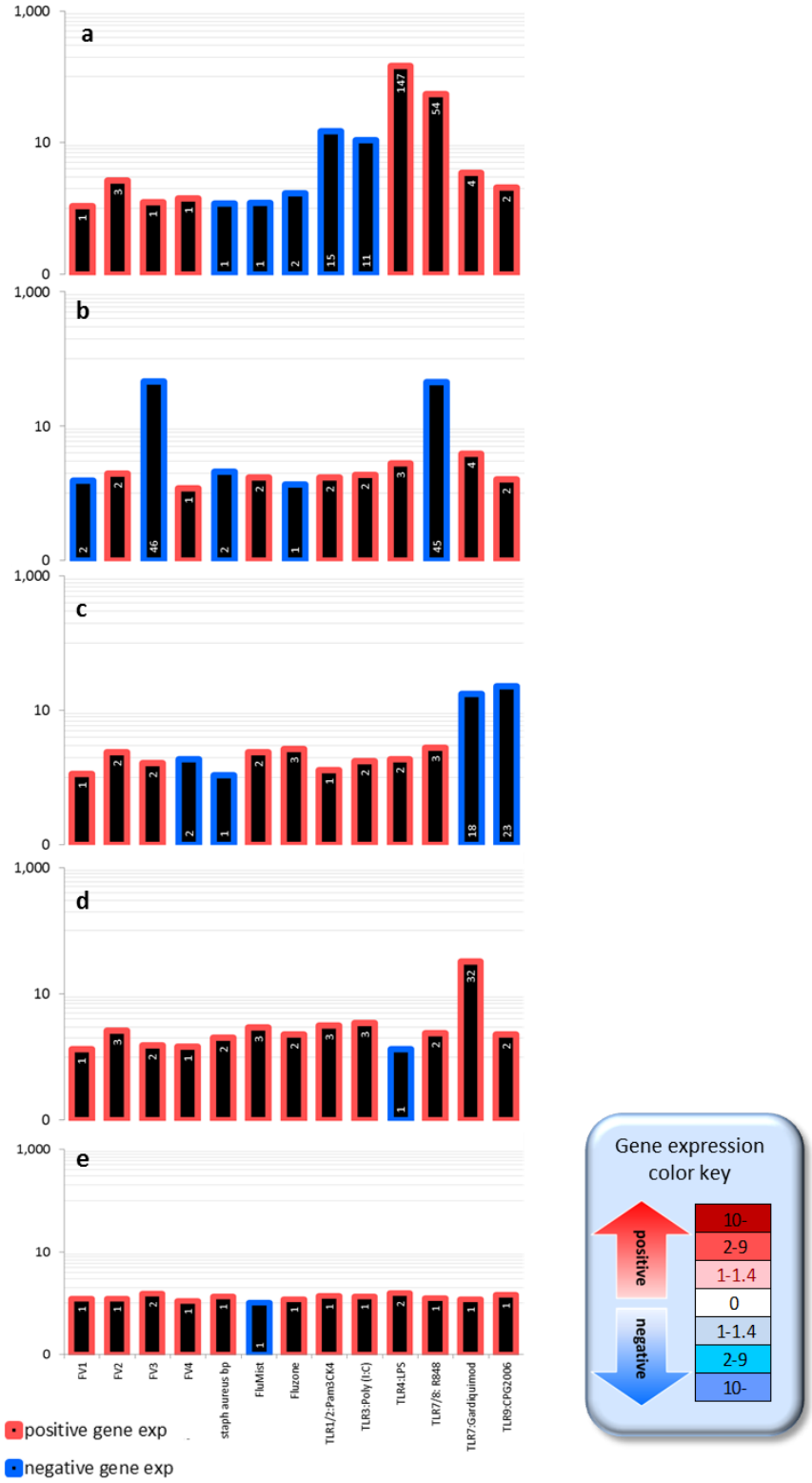

Figure A4: TLR4 expression in human tissue models a) alveolar epithelium, b) nasal epithelium, c) A549 cell line, d) CRL848 cell line, e) alveolar epithelium/endothelium

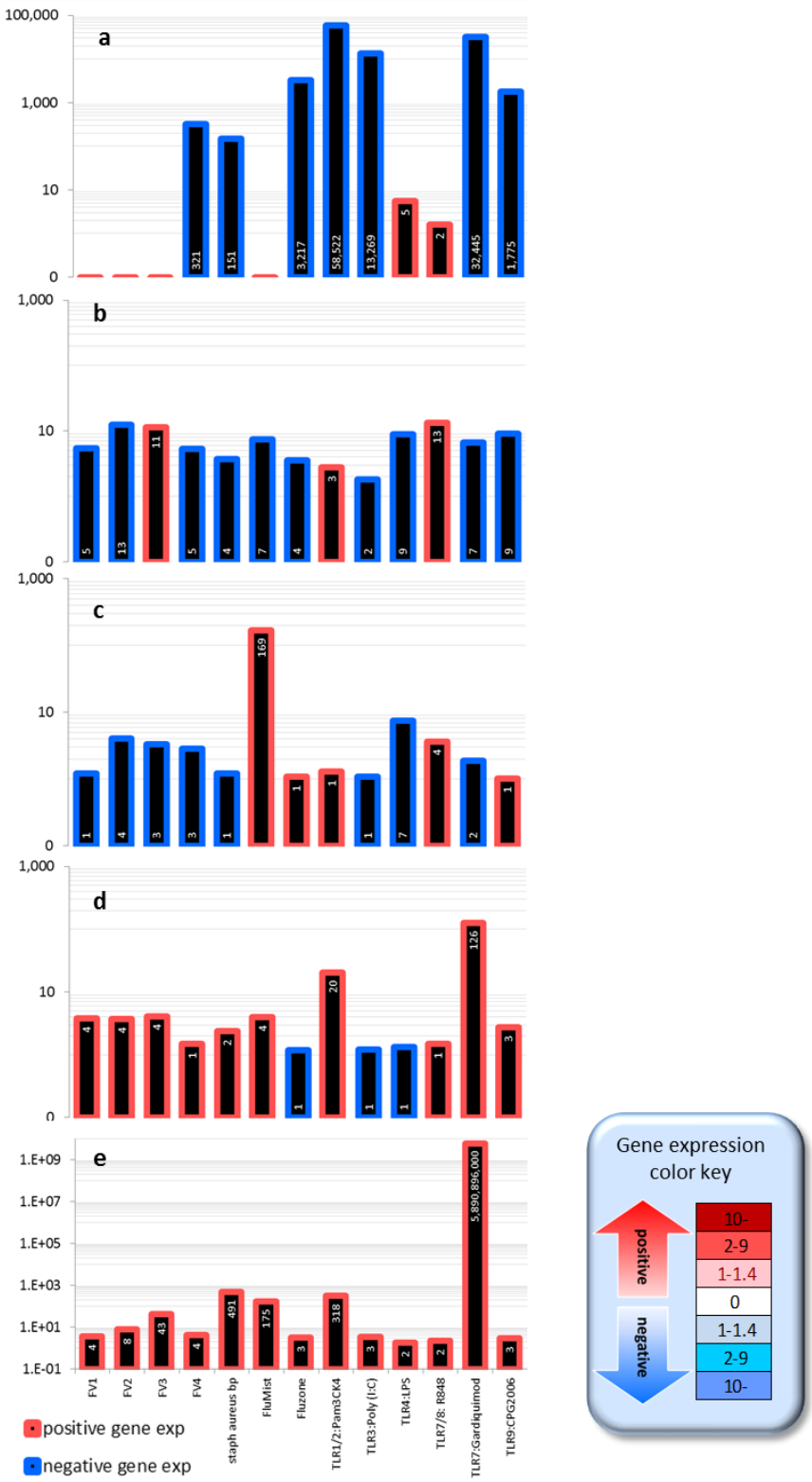

Figure A5: TLR7 expression in human tissue models a) alveolar epithelium, b) nasal epithelium, c) A549 cell line, d) CRL848 cell line, e) alveolar epithelium/endothelium

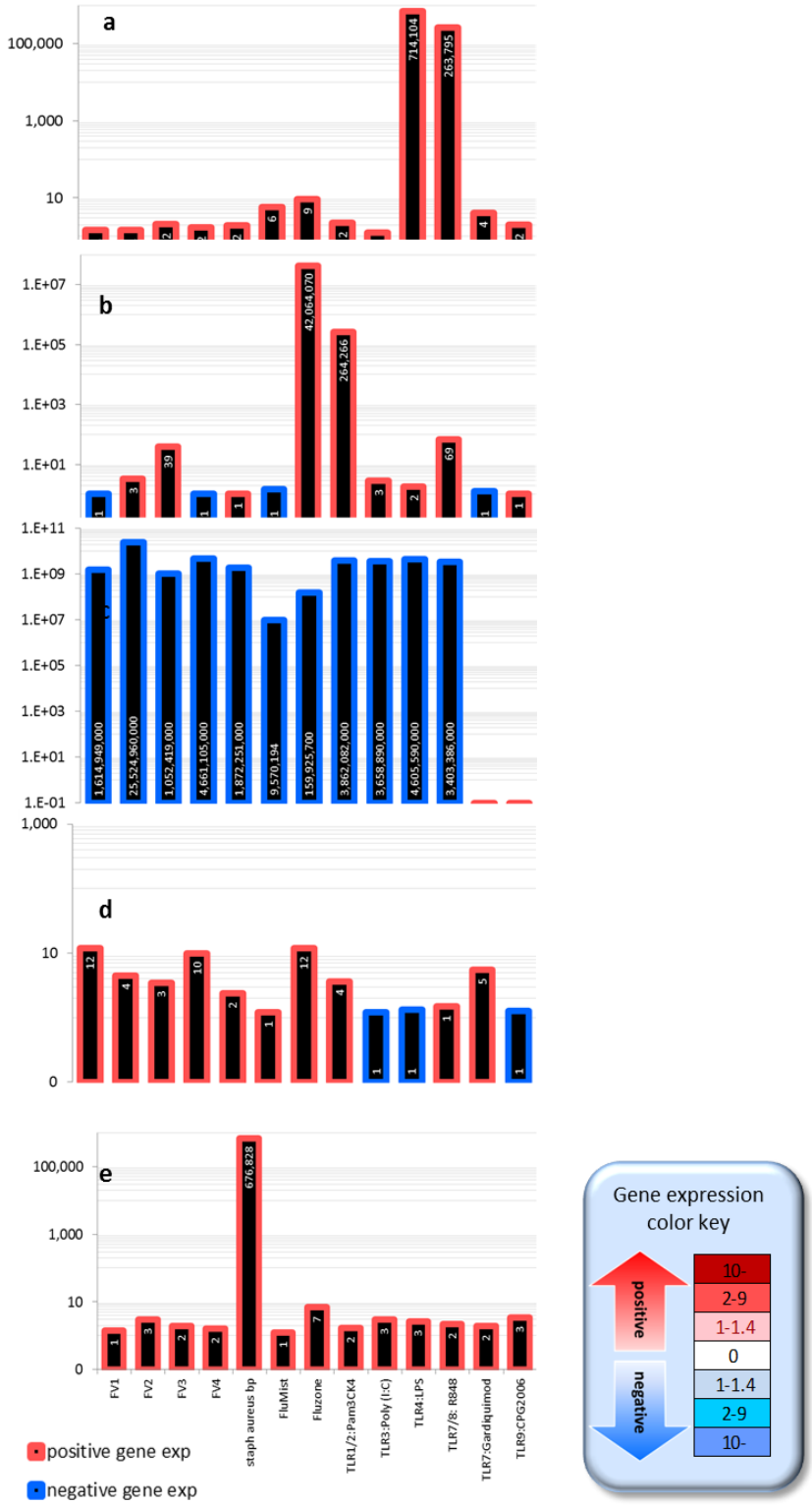

Figure A6: TLR8 expression in human tissue models a) alveolar epithelium, b) nasal epithelium, c) A549 cell line, d) CRL848 cell line, e) alveolar epithelium/endothelium

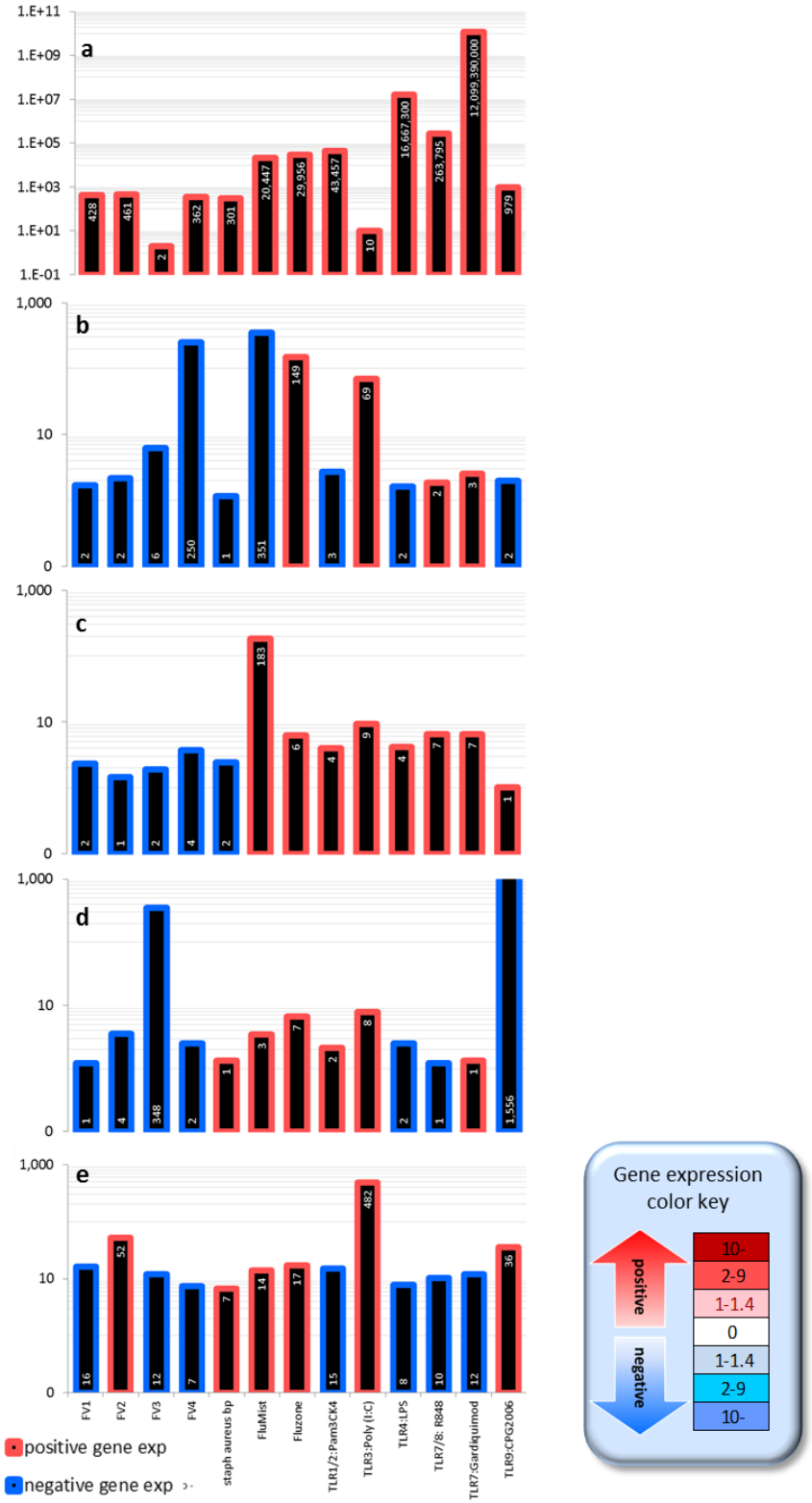

Figure A7: TLR9 expression in human tissue models a) alveolar epithelium, b) nasal epithelium, c) A549 cell line, d) CRL848 cell line, e) alveolar epithelium/endothelium

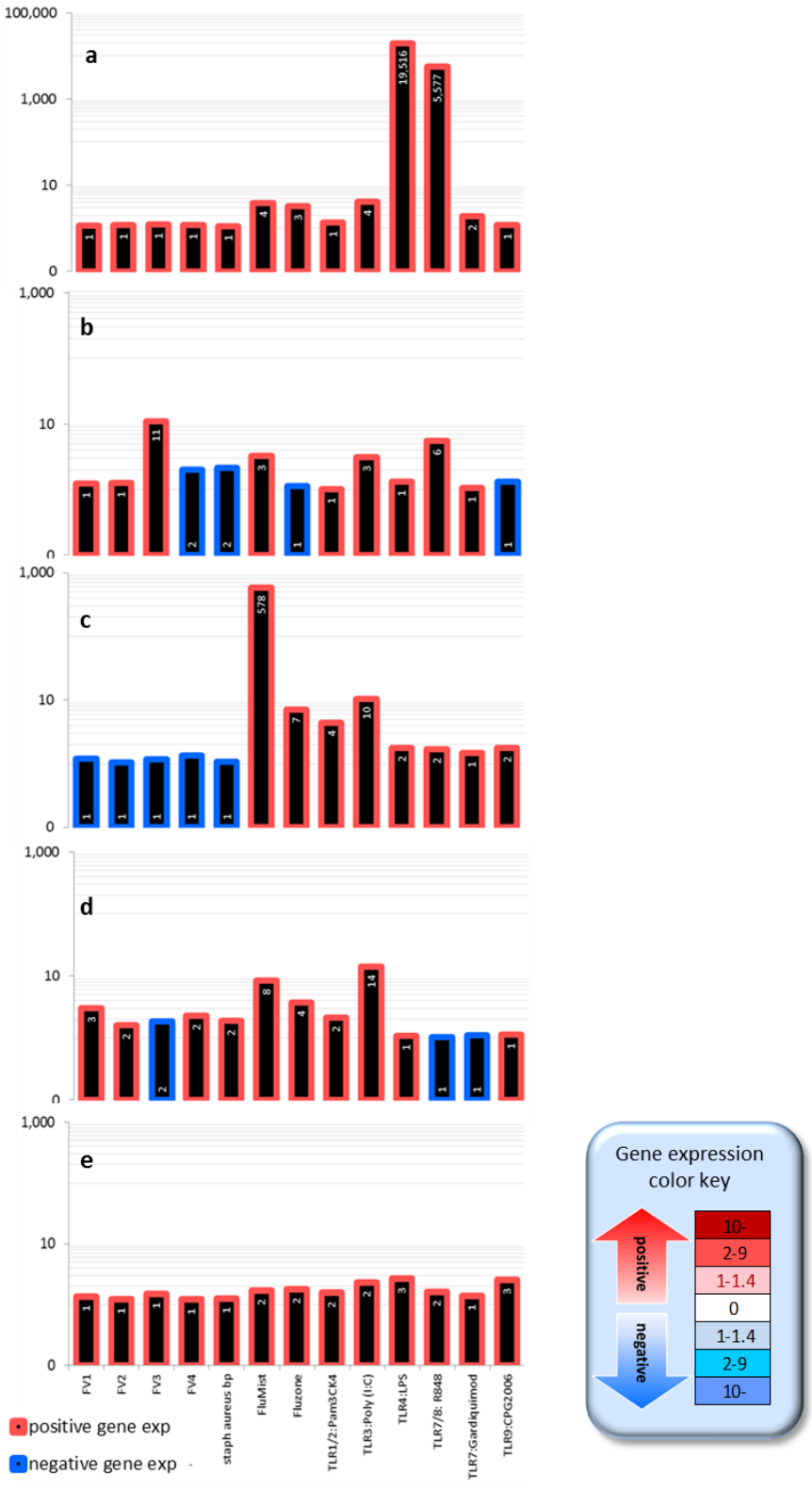

Figure A8: DDX58 expression in human tissue models a) alveolar epithelium, b) nasal epithelium, c) A549 cell line, d) CRL848 cell line, e) alveolar epithelium/endothelium

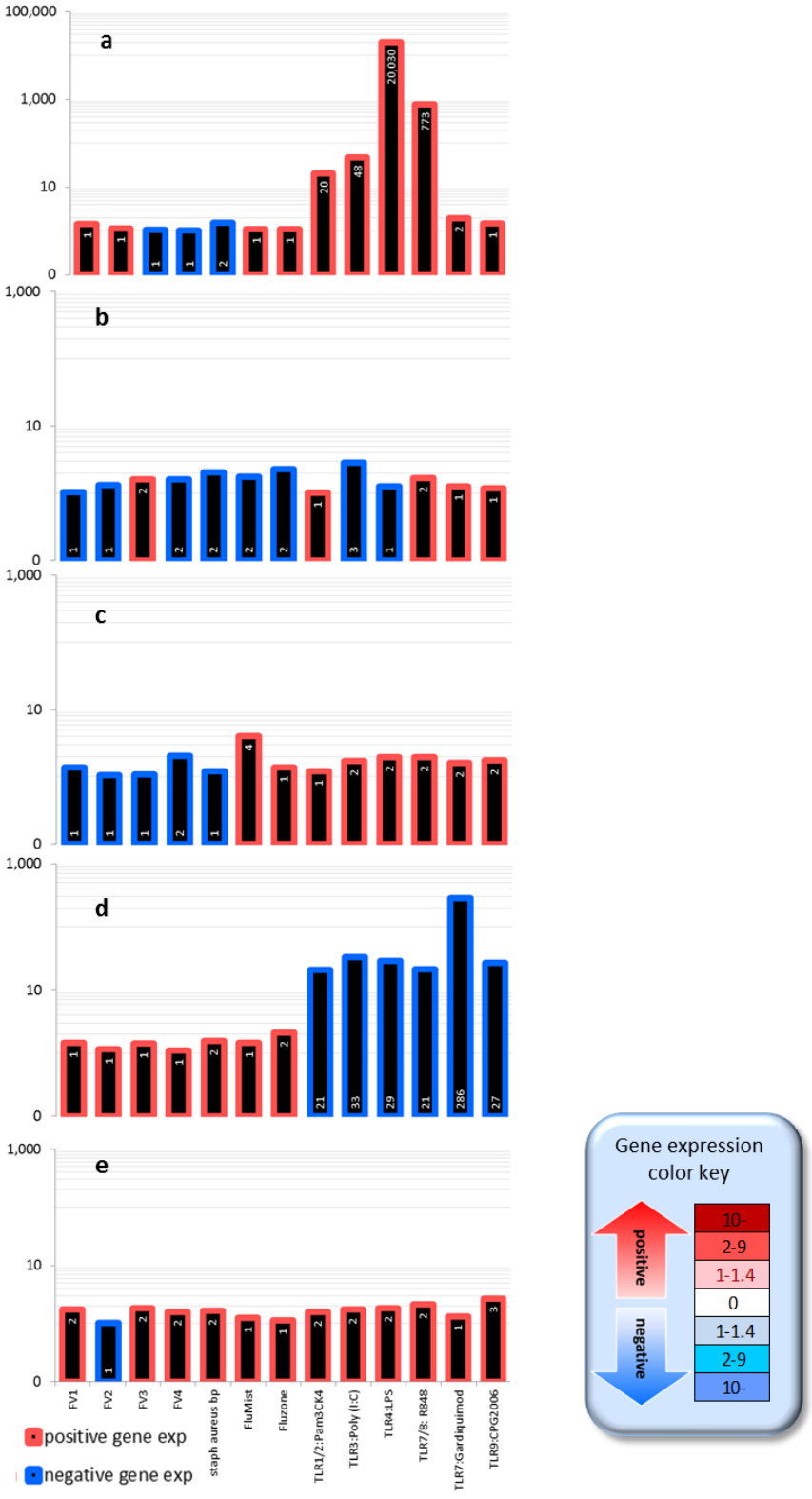

Figure A9: NOD1 expression in human tissue models a) alveolar epithelium, b) nasal epithelium, c) A549 cell line, d) CRL848 cell line, e) alveolar epithelium/endothelium

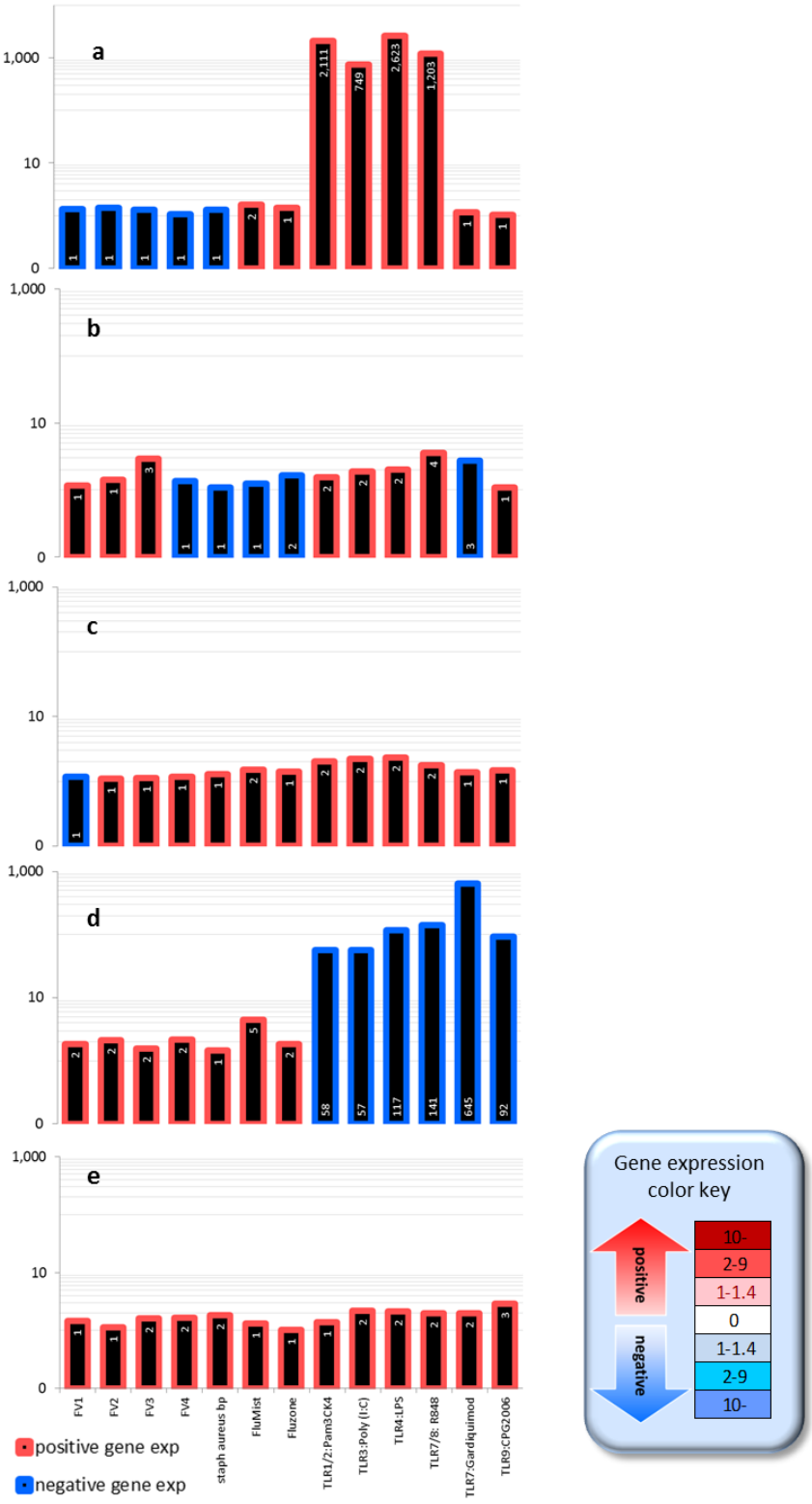

Figure A10: MUC1 expression in human tissue models a) alveolar epithelium, b) nasal epithelium, c) A549 cell line, d) CRL848 cell line, e) alveolar epithelium/endothelium

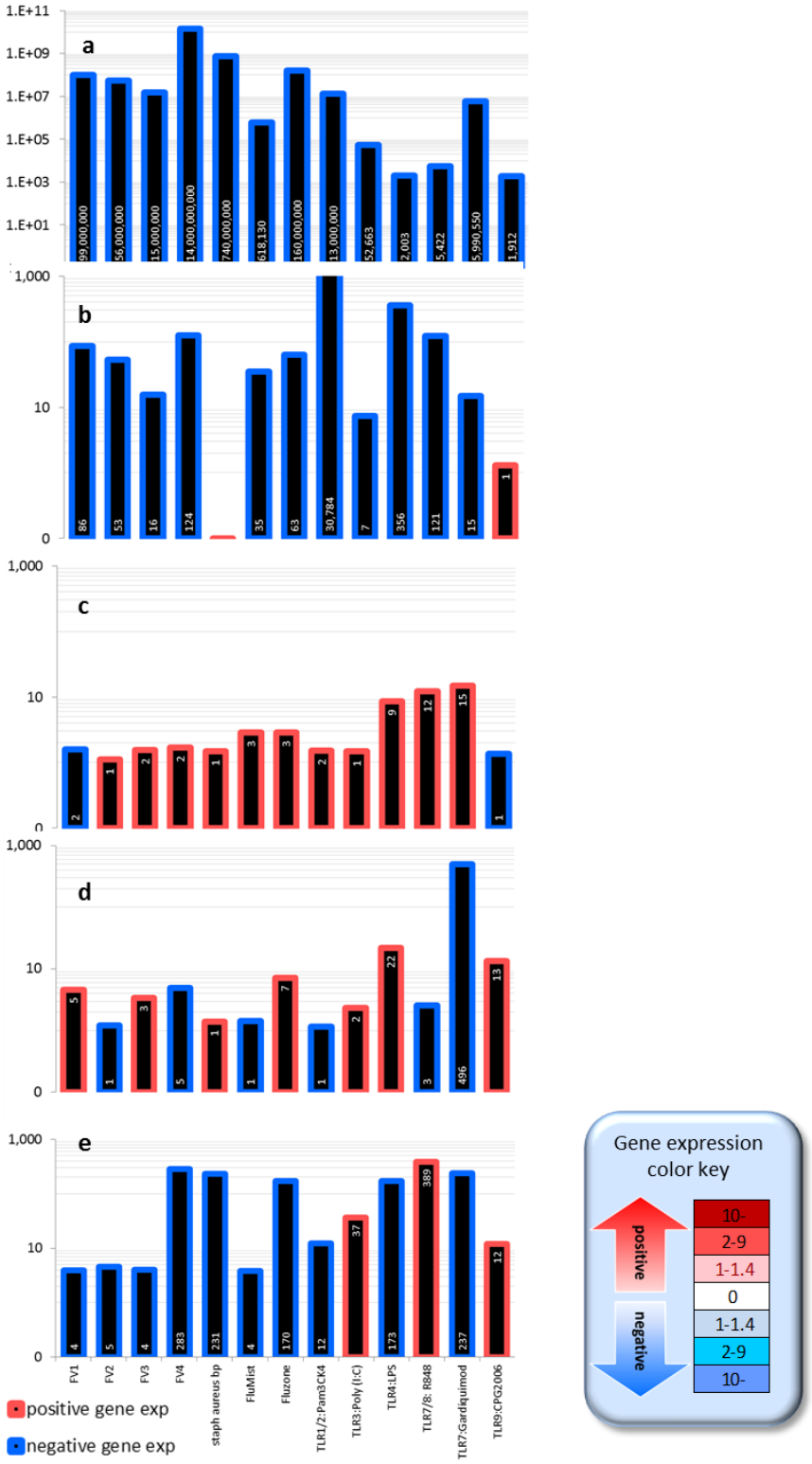

Figure A11: MUC5AC expression in human tissue models a) alveolar epithelium, b) nasal epithelium, c) A549 cell line, d) CRL848 cell line, e) alveolar epithelium/endothelium

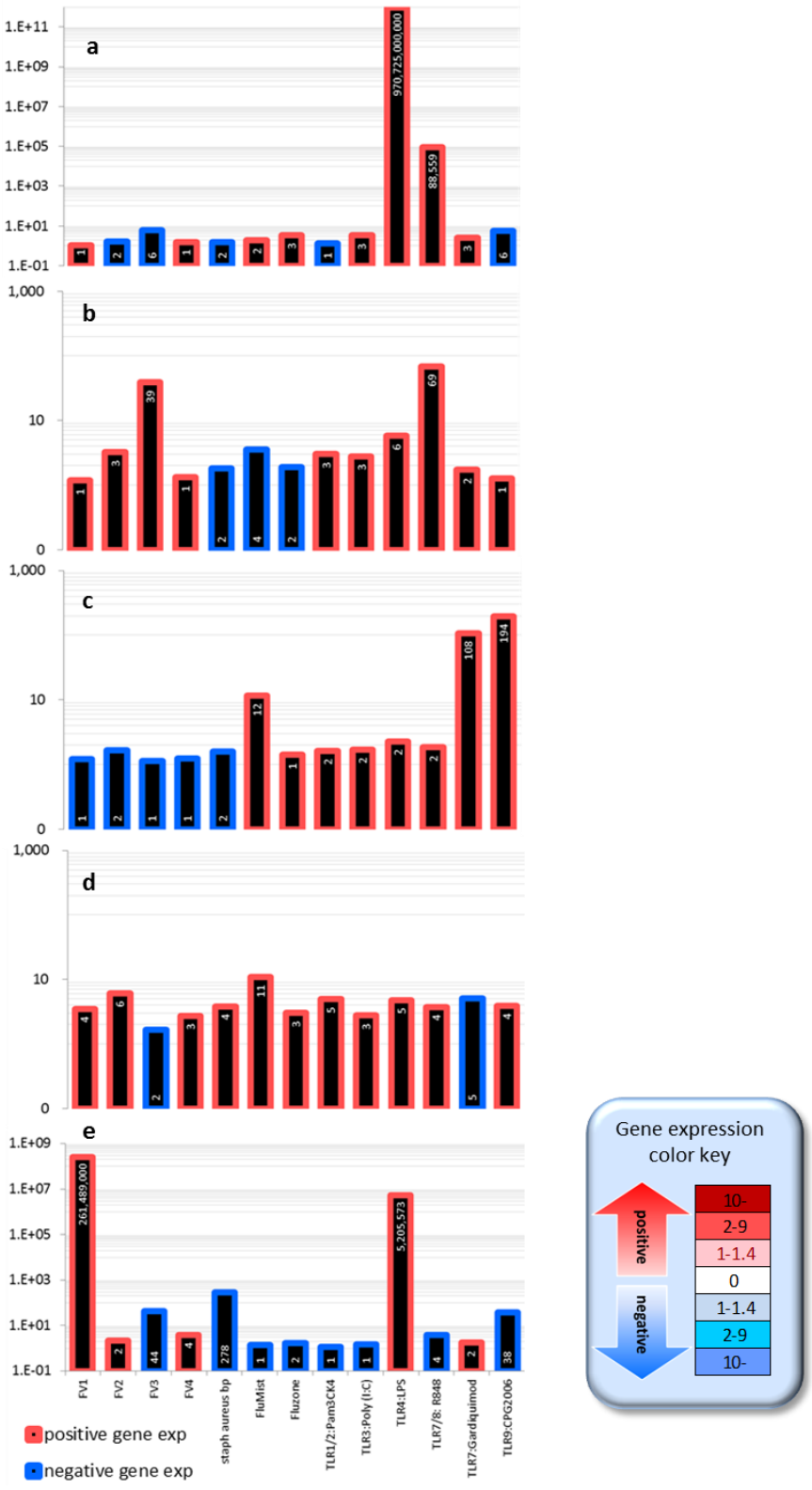

Figure A12: SFPD expression in human tissue models a) alveolar epithelium, b) nasal epithelium, c) A549 cell line, d) CRL848 cell line, e) alveolar epithelium/endothelium

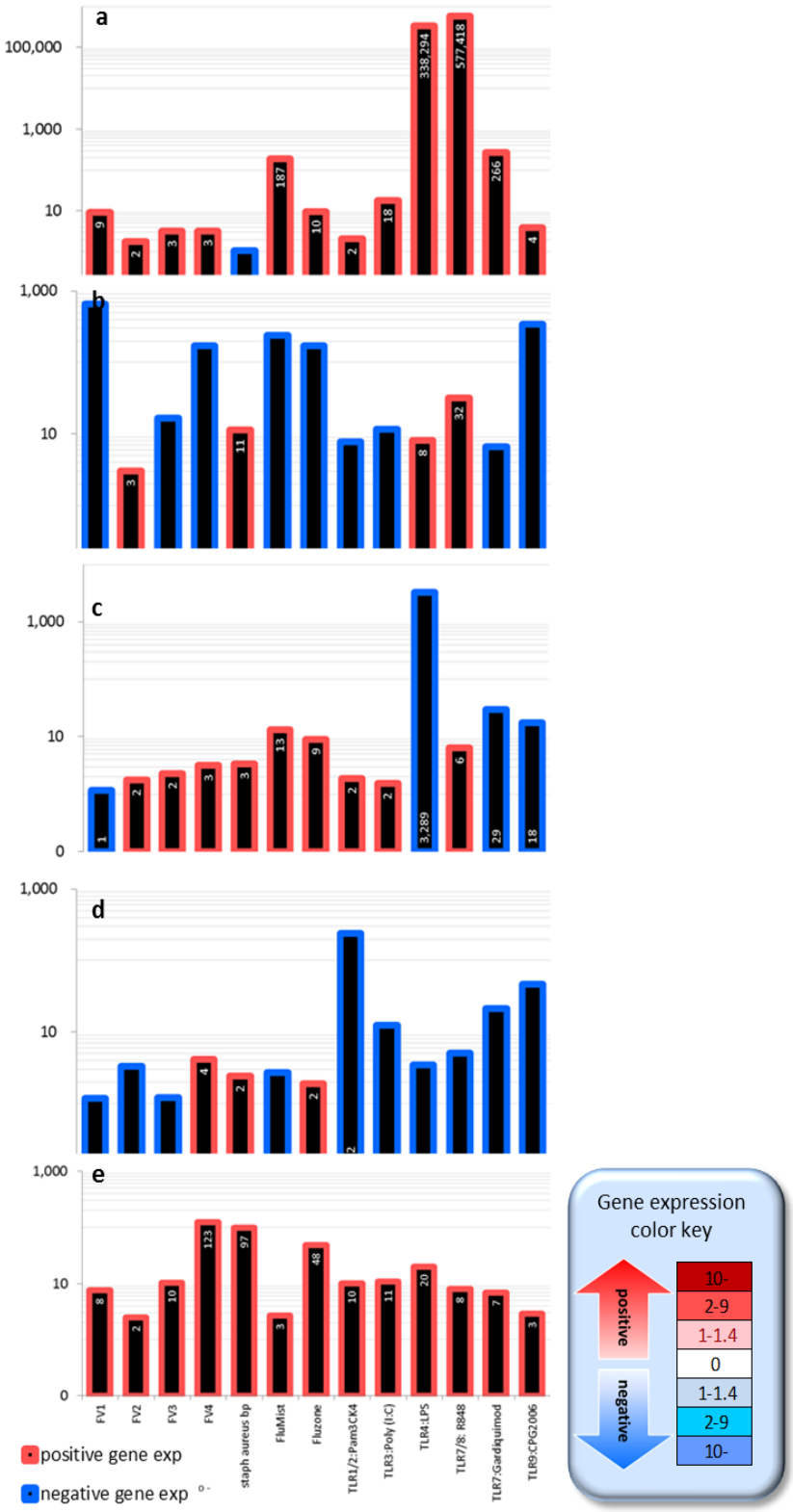

Figure A13: SFPC expression in human tissue models a) alveolar epithelium, b) nasal epithelium, c) A549 cell line, d) CRL848 cell line, e) alveolar epithelium/endothelium

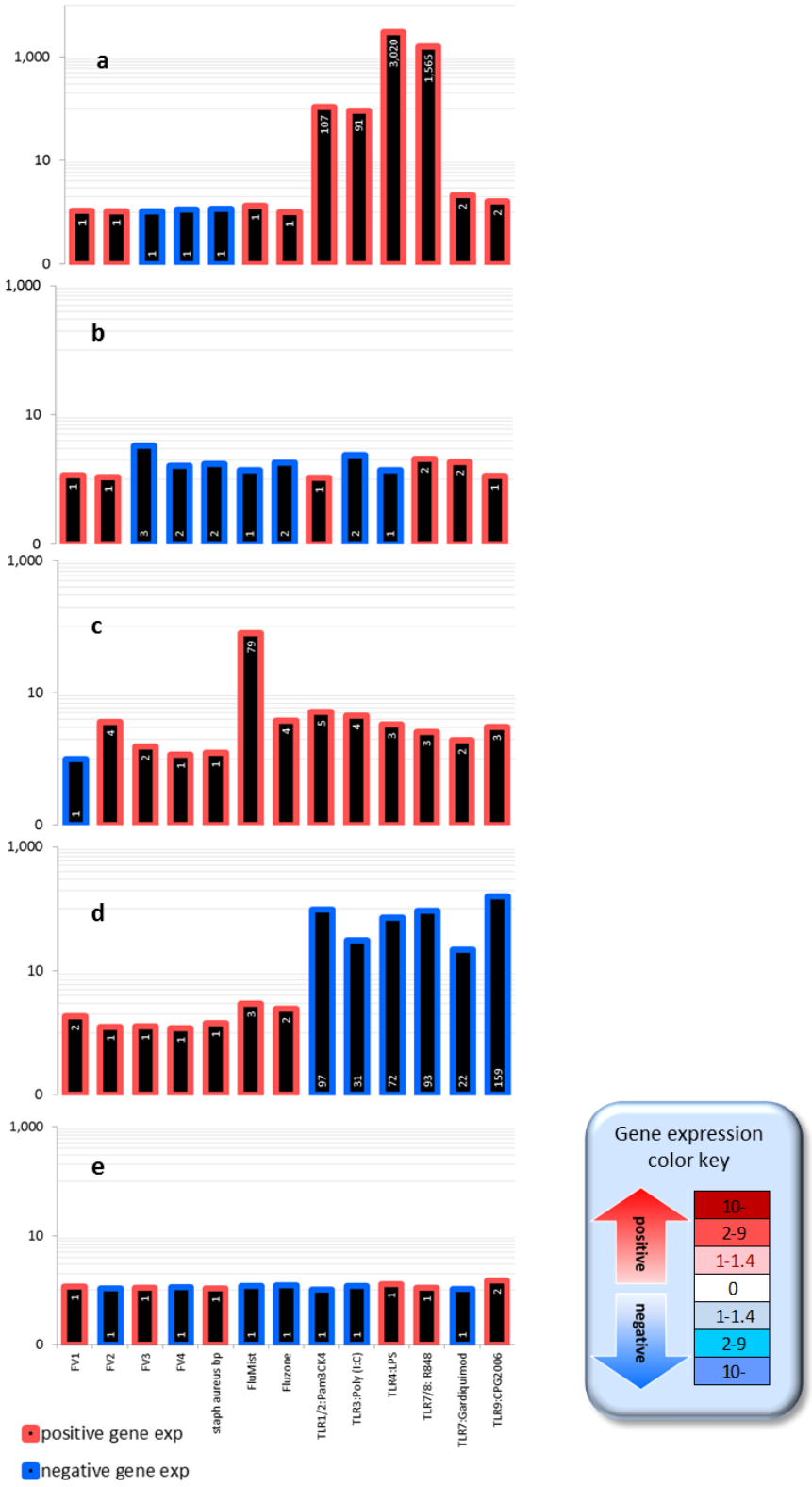

Figure A14: SOCS1 expression in human tissue models a) alveolar epithelium, b) nasal epithelium, c) A549 cell line, d) CRL848 cell line, e) alveolar epithelium/endothelium

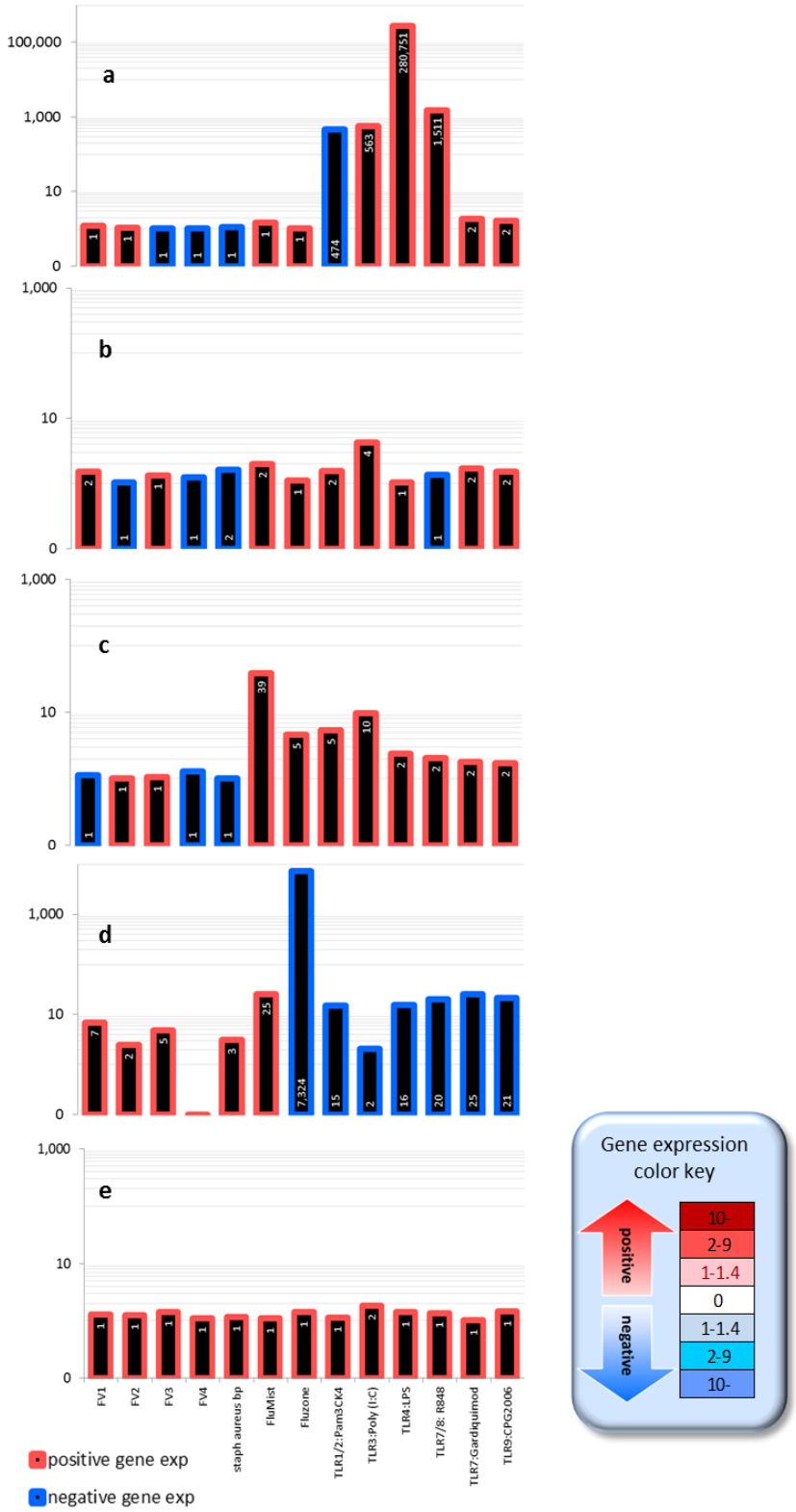

Figure A15: STAT1 expression in human tissue models a) alveolar epithelium, b) nasal epithelium, c) A549 cell line, d) CRL848 cell line, e) alveolar epithelium/endothelium

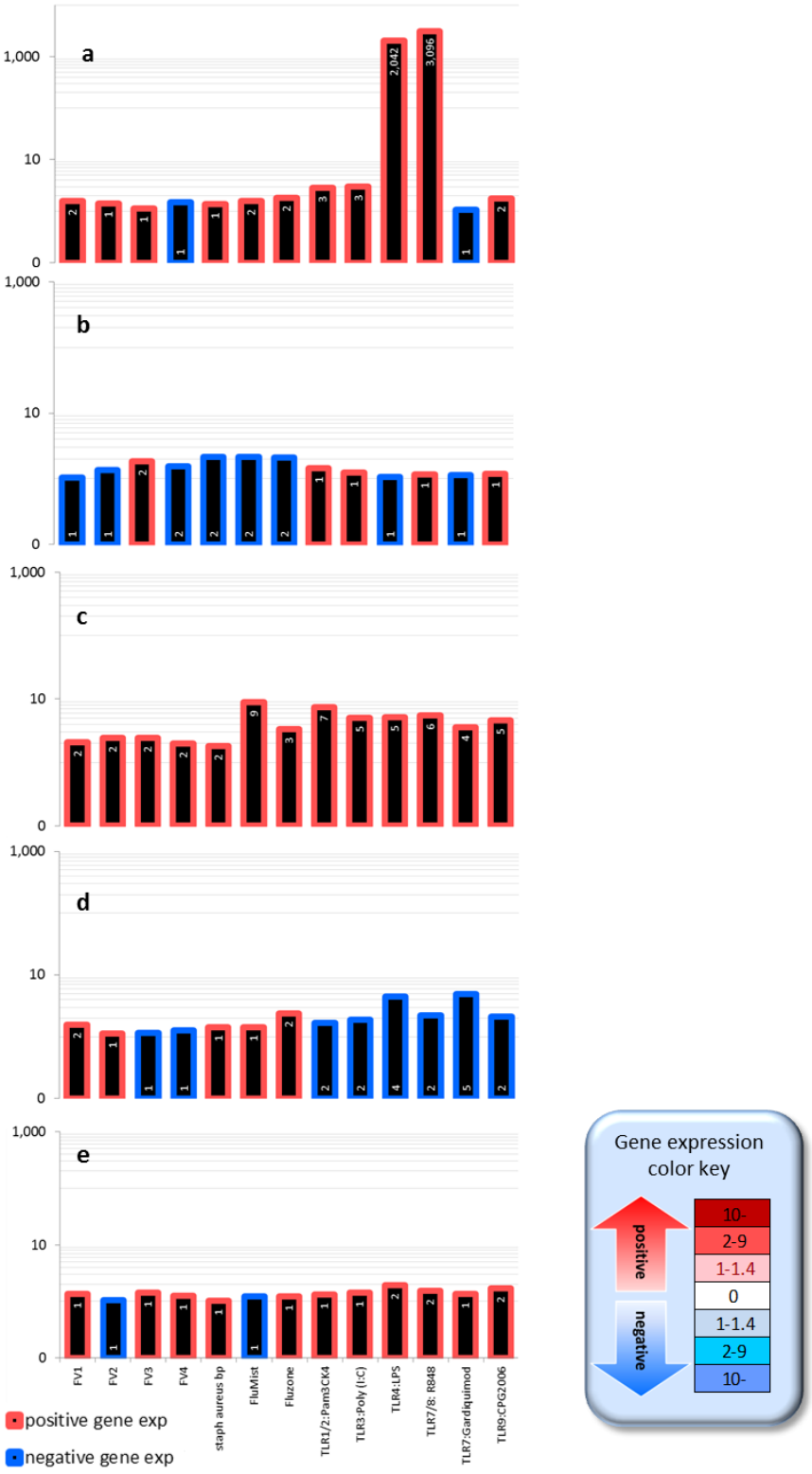

Figure A16: JAK2 expression in human tissue models a) alveolar epithelium, b) nasal epithelium, c) A549 cell line, d) CRL848 cell line, e) alveolar epithelium/endothelium

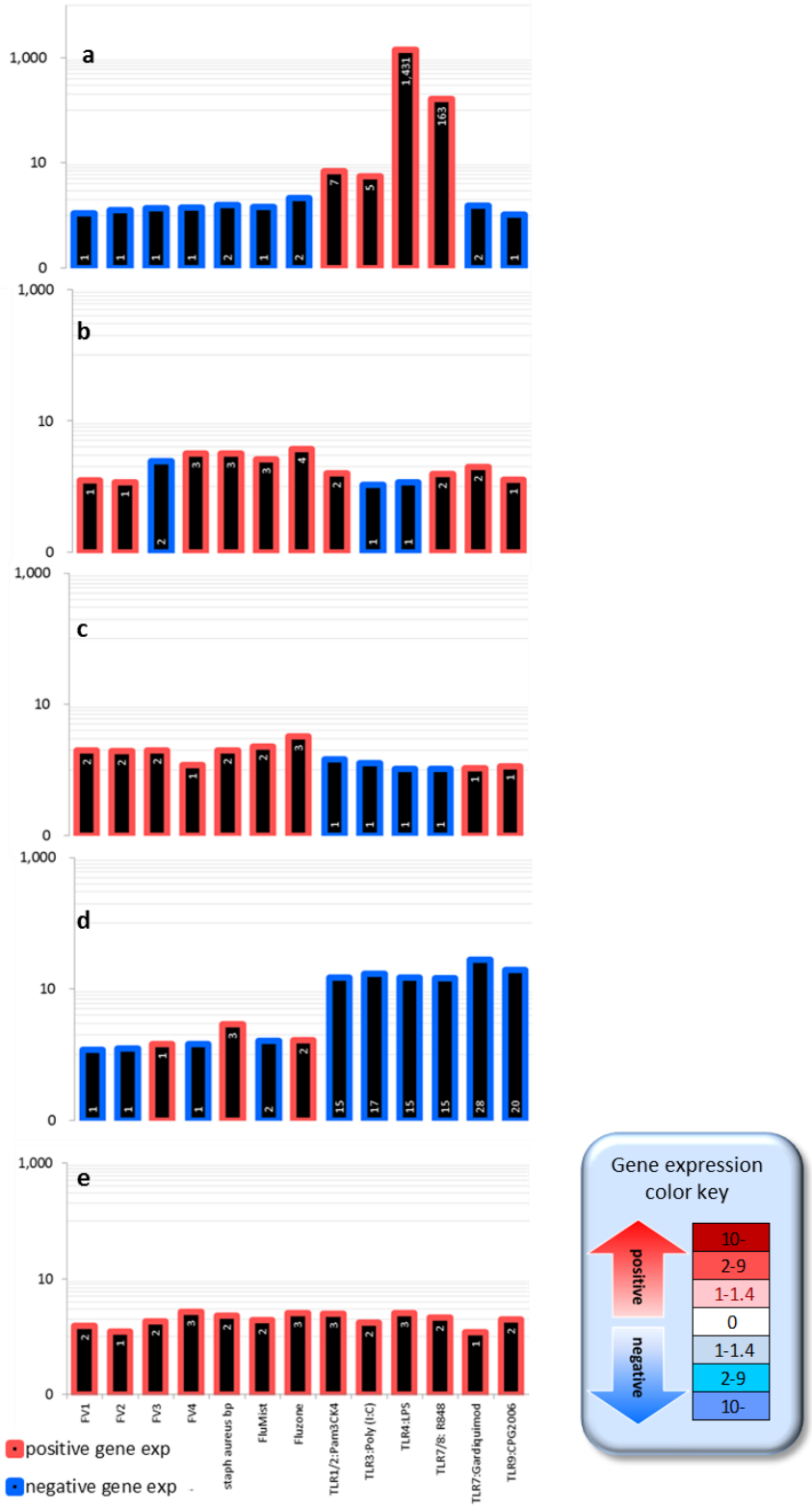

Figure A17:TYK2 expression in human tissue models a) alveolar epithelium, b) nasal epithelium, c) A549 cell line, d) CRL848 cell line, e) alveolar epithelium/endothelium

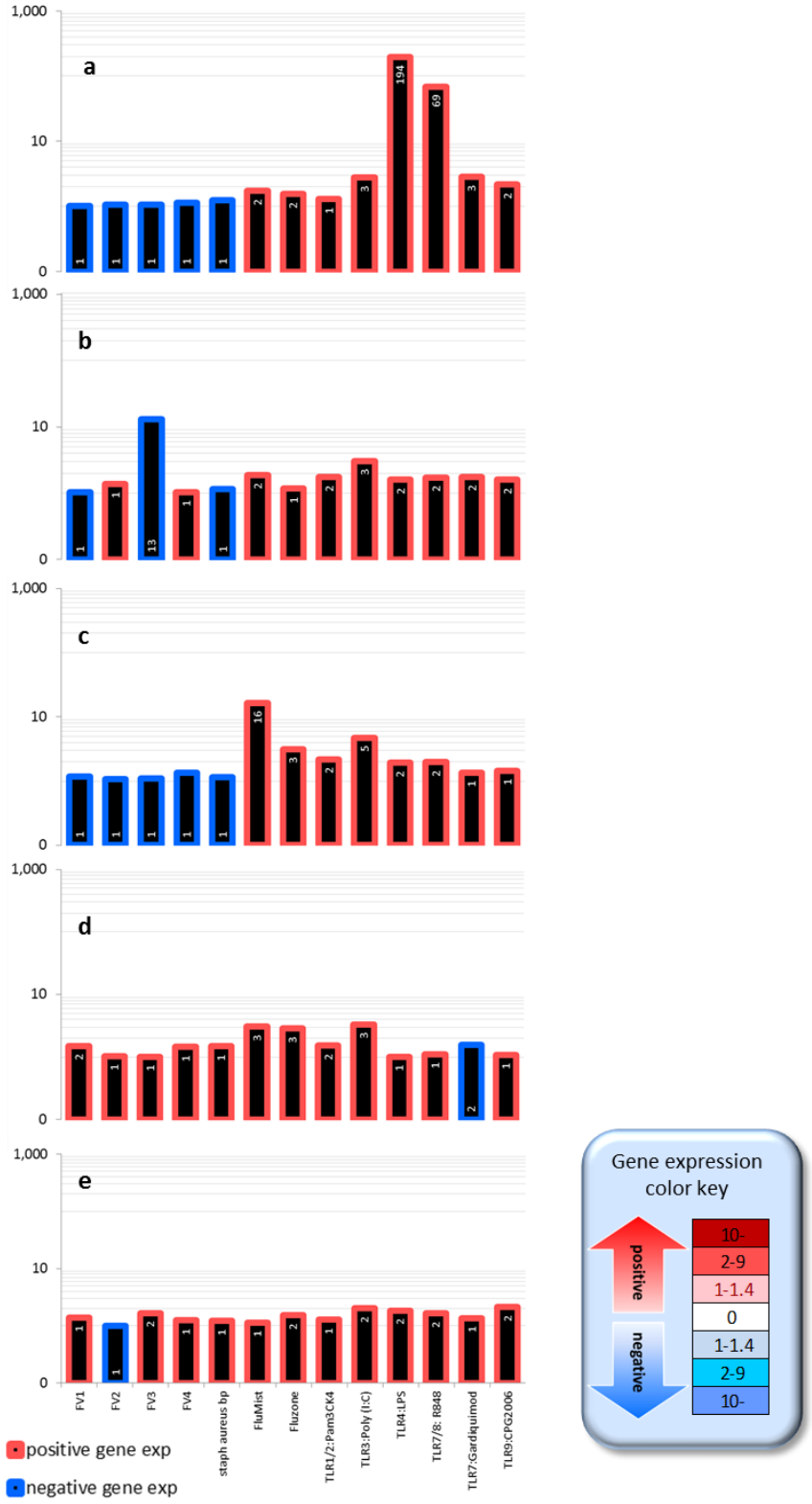

Figure A18: EIF2AK expression in human tissue models a) alveolar epithelium, b) nasal epithelium, c) A549 cell line, d) CRL848 cell line, e) alveolar epithelium/endothelium

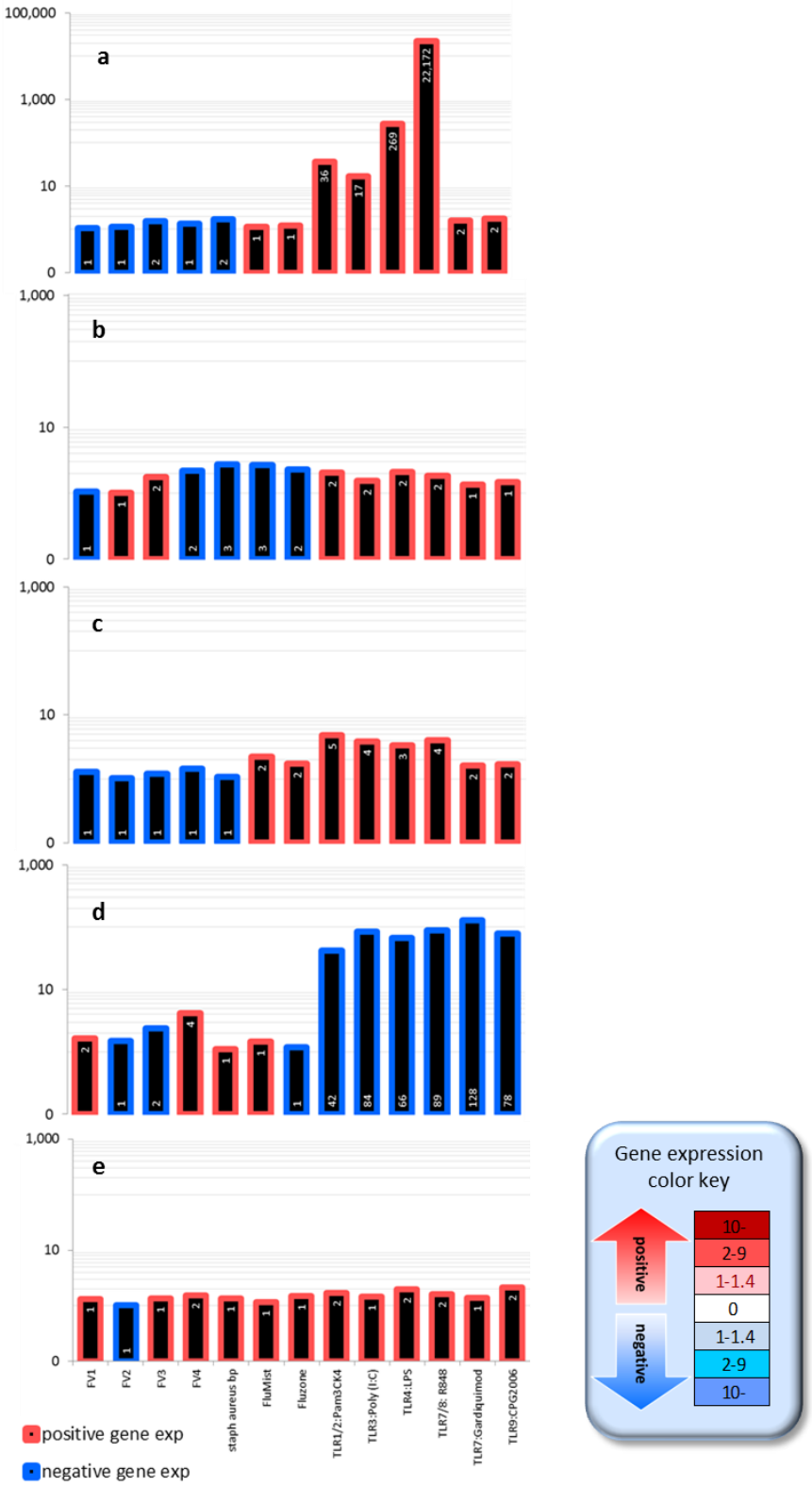

Figure A19: IFNAR2 expression in human tissue models a) alveolar epithelium, b) nasal epithelium, c) A549 cell line, d) CRL848 cell line, e) alveolar epithelium/endothelium

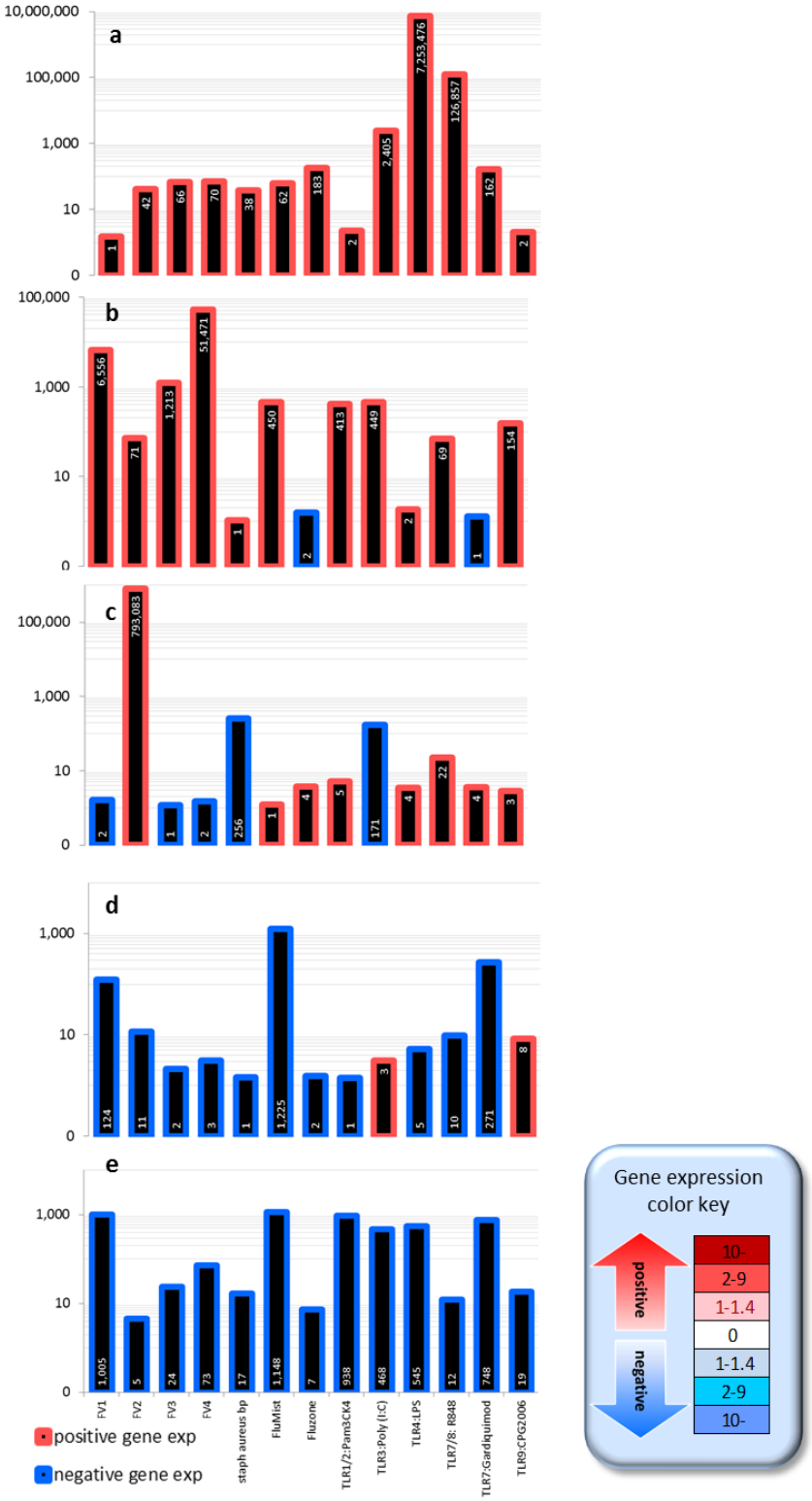

Figure A20: IFNB1 expression in human tissue models a) alveolar epithelium, b) nasal epithelium, c) A549 cell line, d) CRL848 cell line, e) alveolar epithelium/endothelium

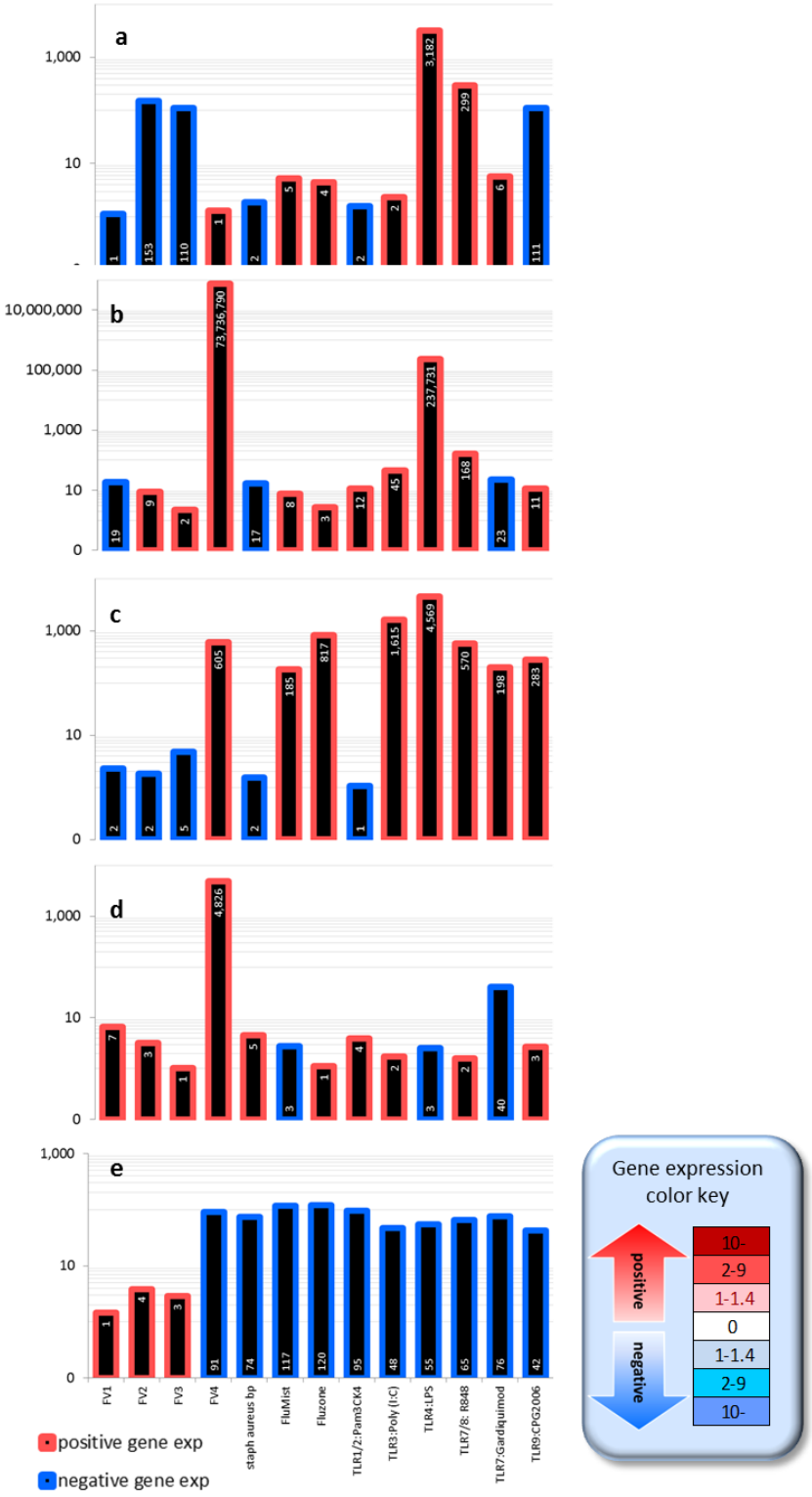

Figure A21: IFNG expression in human tissue models a) alveolar epithelium, b) nasal epithelium, c) A549 cell line, d) CRL848 cell line, e) alveolar epithelium/endothelium

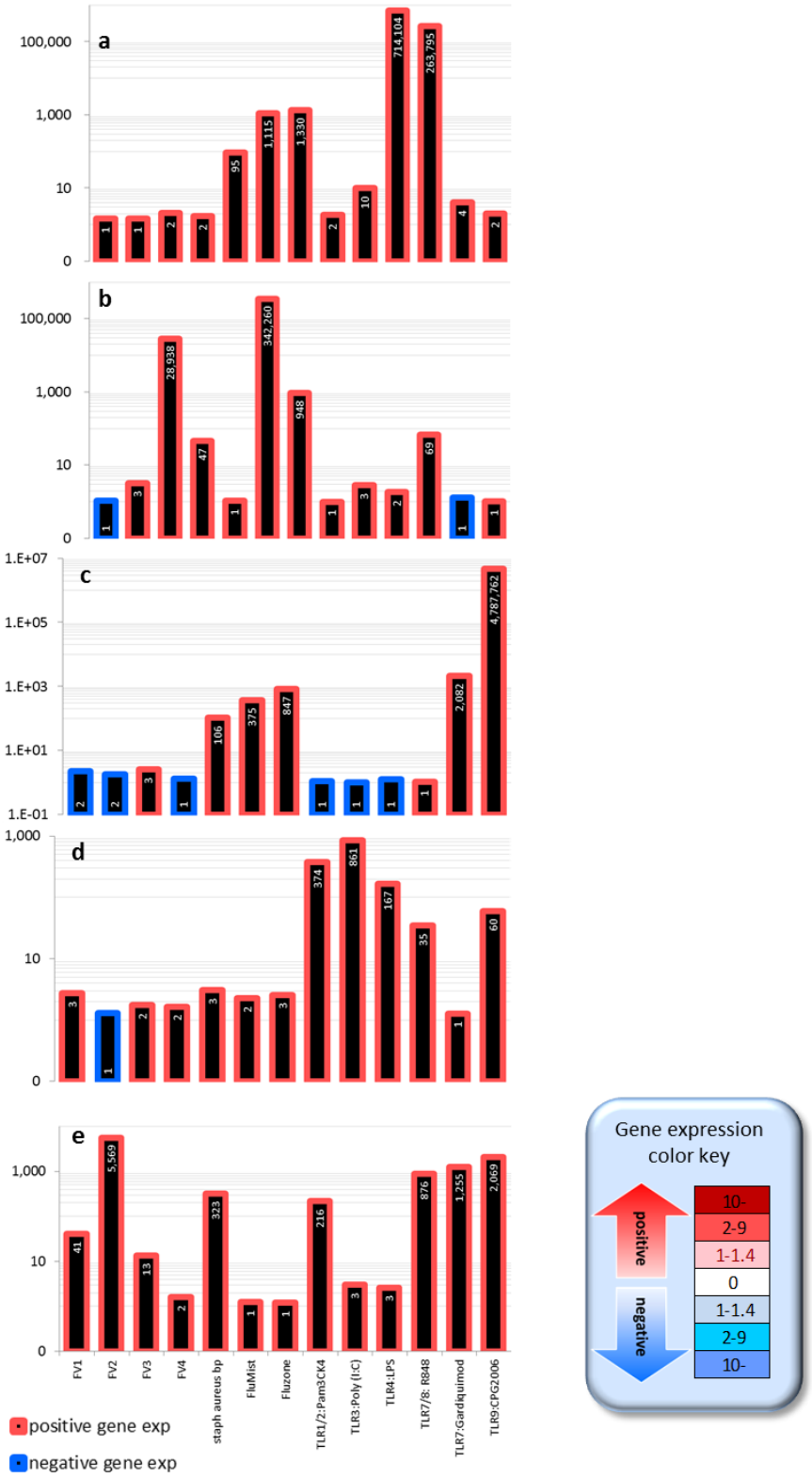

Figure A22: TNF expression in human tissue models a) alveolar epithelium, b) nasal epithelium, c) A549 cell line, d) CRL848 cell line, e) alveolar epithelium/endothelium

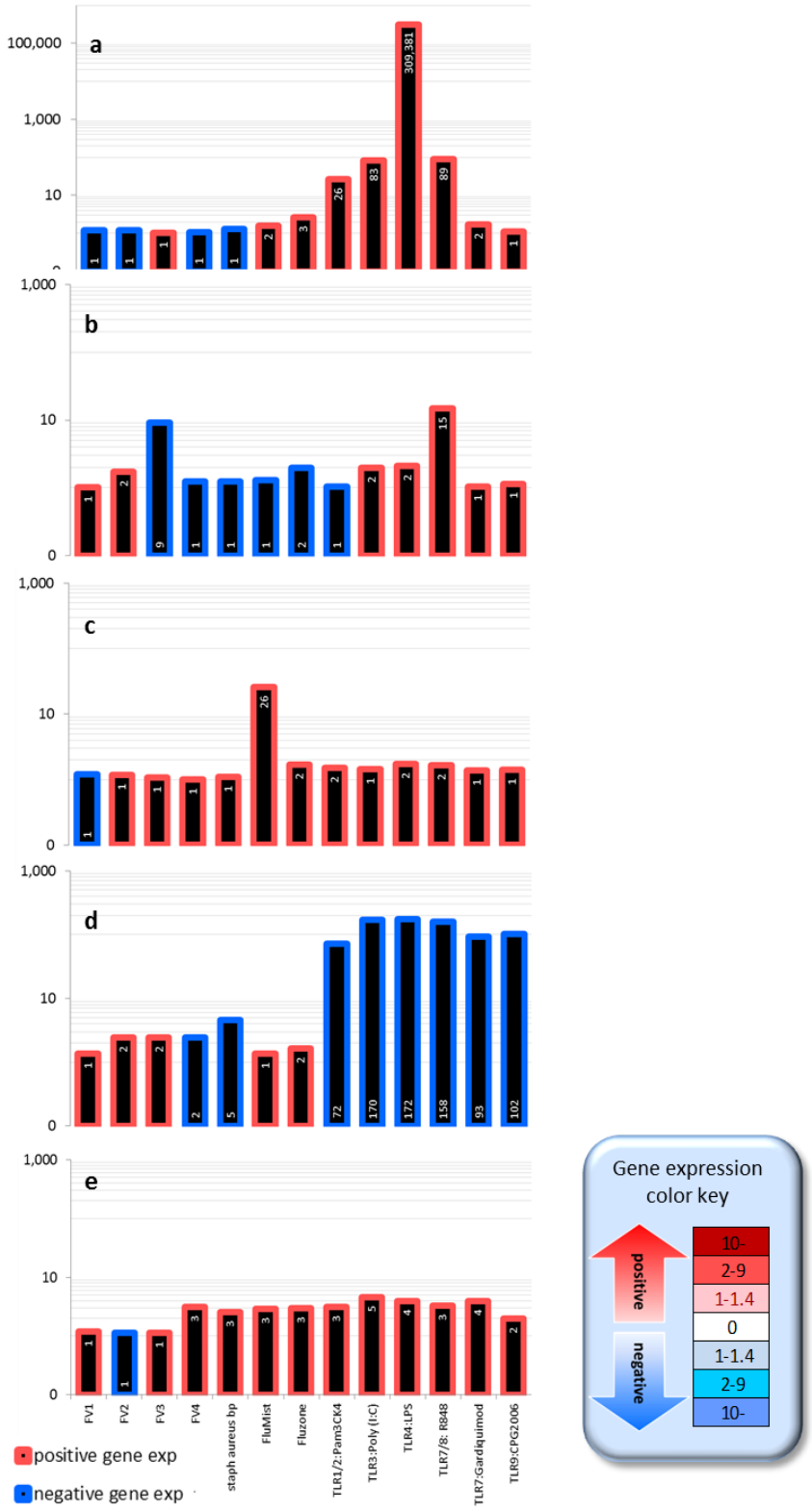

Figure A23: IRF3 expression in human tissue models a) alveolar epithelium, b) nasal epithelium, c) A549 cell line, d) CRL848 cell line, e) alveolar epithelium/endothelium

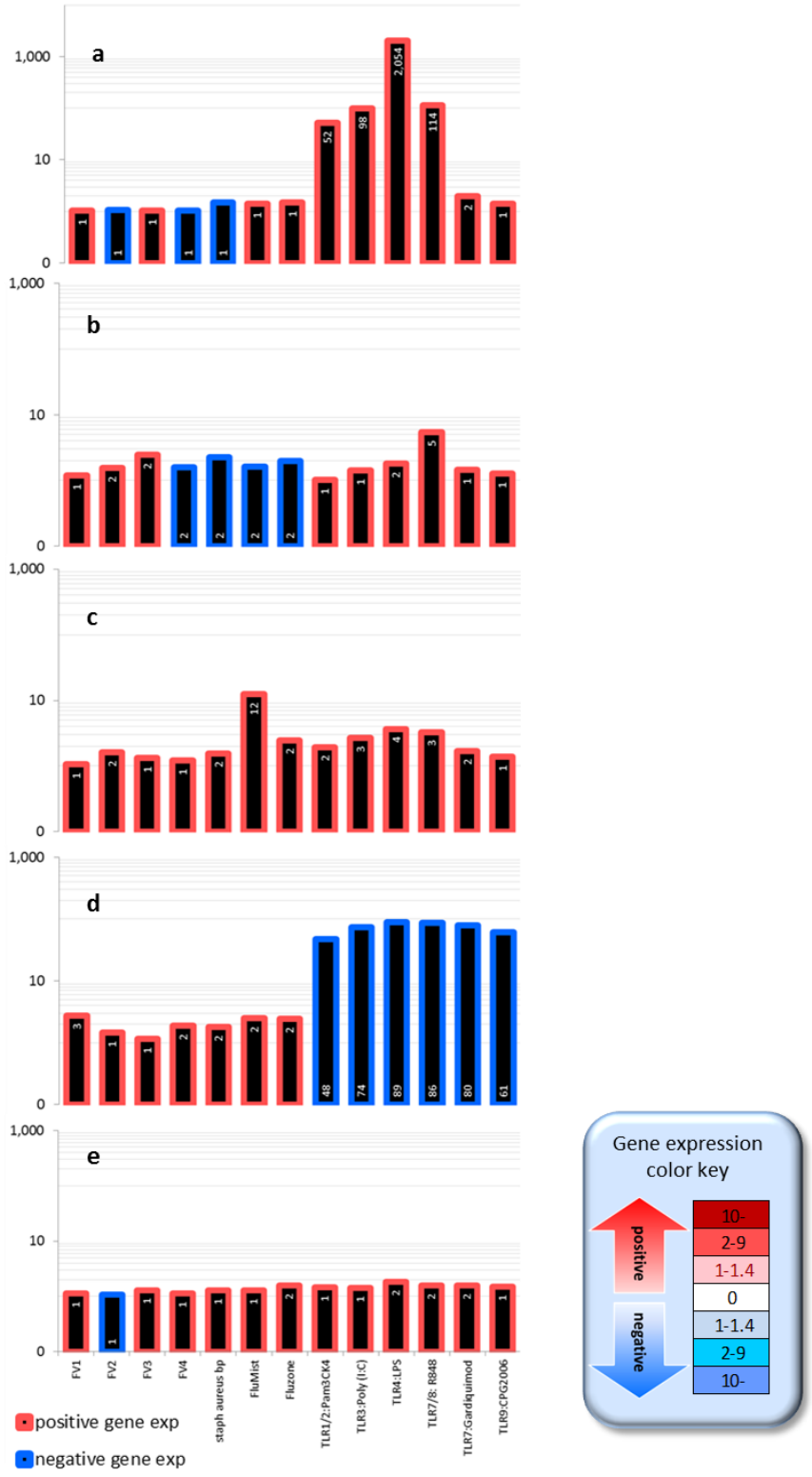

Figure A24: TICAM1 expression in human tissue models a) alveolar epithelium, b) nasal epithelium, c) A549 cell line, d) CRL848 cell line, e) alveolar epithelium/endothelium

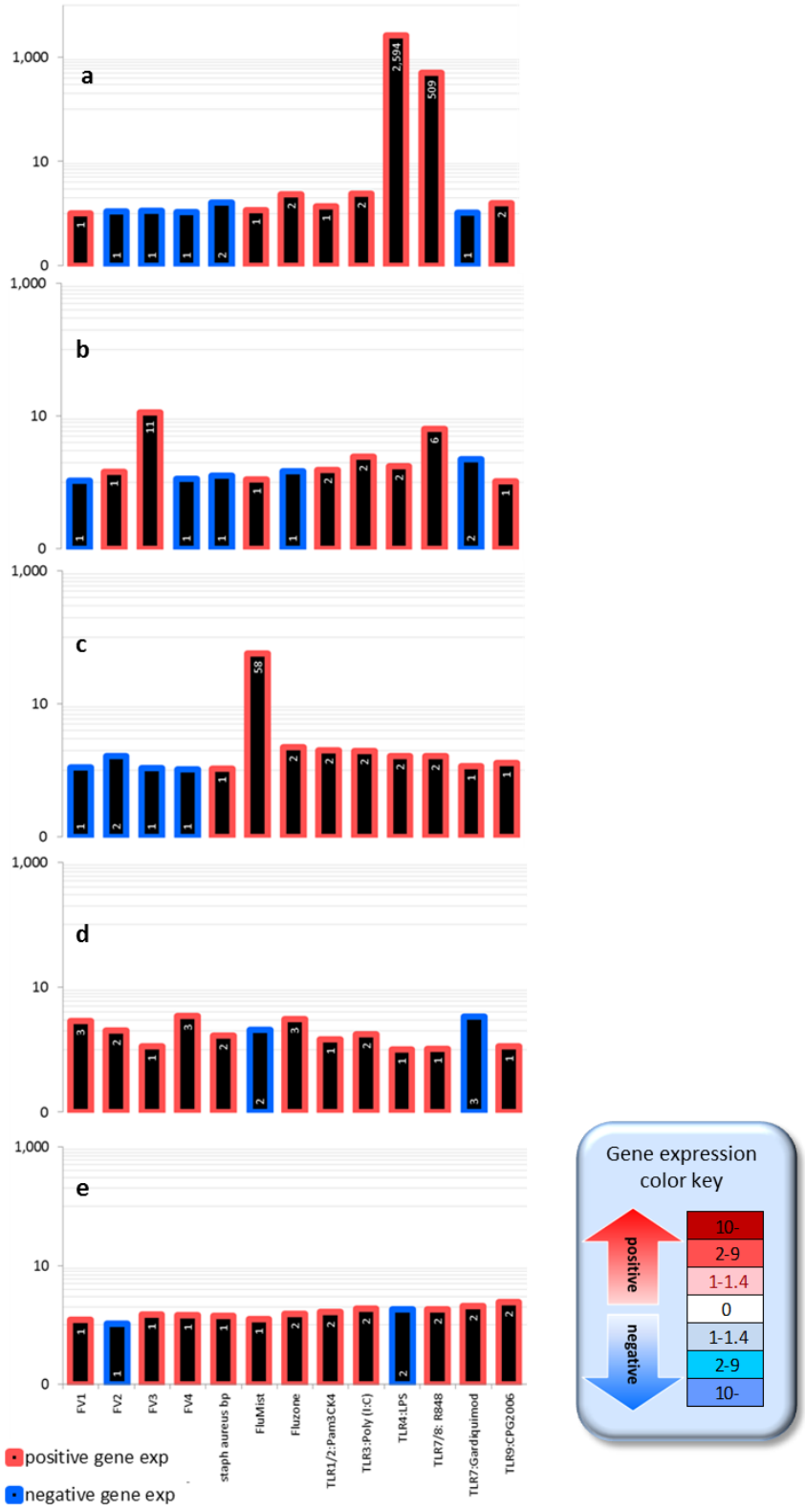

Figure A25: MYD88 expression in human tissue models a) alveolar epithelium, b) nasal epithelium, c) A549 cell line, d) CRL848 cell line, e) alveolar epithelium/endothelium

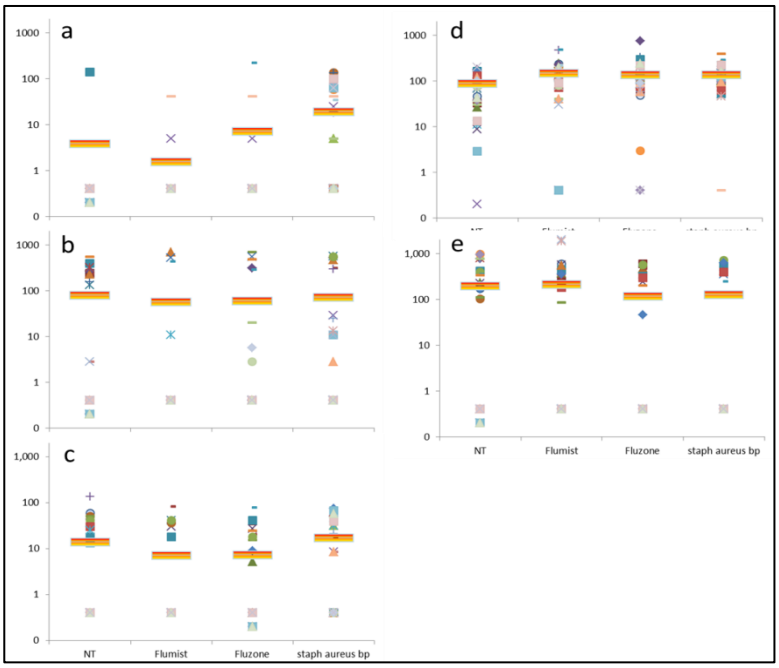

Figure A26: IFN-alpha2 (pg/ml) production in a) alveolar epithelium, b) nasal epithelium, c) alveolar bilayer, d) A549 cell line, and e) CRL-1848 cell line tissue models.

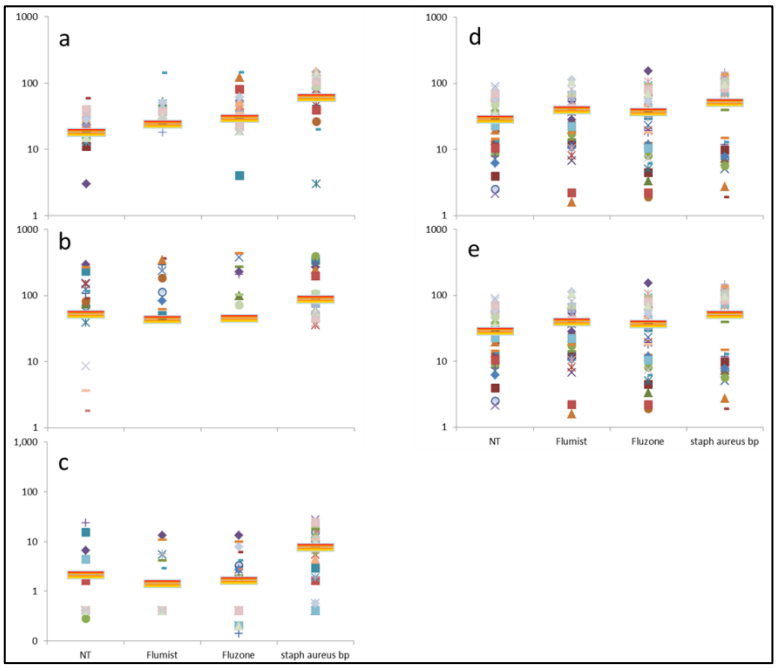

FigureA27: IL-12 (p40) (pg/ml) production in a) alveolar epithelium, b) nasal epithelium, c) alveolar bilayer, d) A549 cell line, and e) CRL-1848 cell line tissue models.

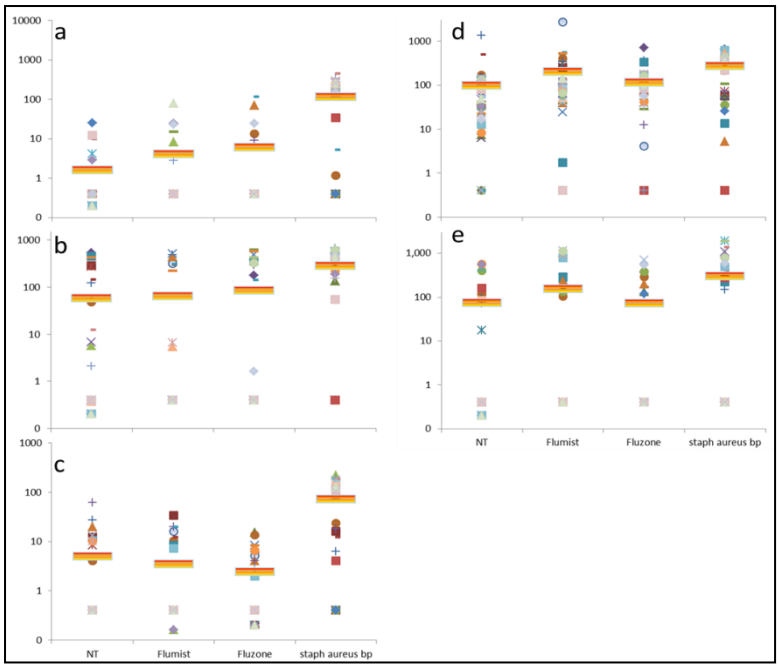

Figure A28: IL-1a(pg/ml) production in a) alveolar epithelium, b) nasal epithelium, c) alveolar bilayer, d) A549 cell line, and e) CRL-1848 cell line tissue models.

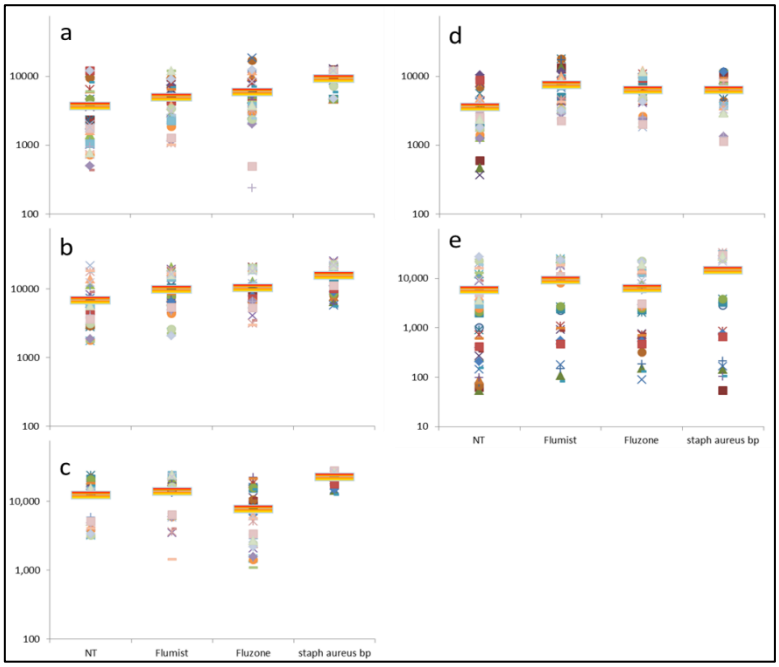

Figure A29: MCP-1(pg/ml) production in a) alveolar epithelium, b) nasal epithelium, c) alveolar bilayer, d) A549 cell line, and e) CRL-1848 cell line tissue models.

Appendix 2: Presentation documentation

Annual 2013 Biomedical Engineering Society meeting, Seattle, WA

Evaluation of *in vitro* Tissue Models of Upper and Lower Airway

Avesha Mahmood[1], John Dye[2], Eric Mishkin[1], William Warren[1]
Sanofi Pasteur Vaxdesign Campus[1], United States Army Medical Research Institute for Infectious Disease [2]

Introduction: The lung airway epithelial surface comprises one of the largest mucosal surfaces for pathogen entry. From the nasopharnyx to the lower airway alveoli, respiratory surfaces are equipped with defense mechanisms against large and small foreign matter which are known to directly interact with pulmonary mucosa and vascular endothelium (Yang, 2008). During this process, Toll-like receptors are an essential part of the pattern recognition receptor family involved in triggering a genomic response along with release of cytokines and chemokines to attract leukocytes to initiate an innate response (Griber, 2008). Based on homogenous genomic selection in cell lines, we anticipate variations in the primary and cell line tissue models on morphological, cellular and genomic levels. We plan to exploit these variations to select for pathogen specific models for infection, expansion and pre-clinical therapeutic preparation and evaluation.

Materials and Methods: Tissue models consisting of primary human nasal and alveolar cells (Promocell), A549 (ATCC) and CRL-848 (ATCC) were prepared with cell type specific media and matrix. Three sets of two constructs were set-up for each model. FV1 (Sudan-lot012010AIK), FV2 (MAR-lot 5Nov2009), FV3(EBOV-95-lot1), FV4 (BDBV-lot1Jun2010) were tested (100ng/ml); inactive whole virus strain were provided by USAMRIID labs. TLR agonists including Pam3CSK4, Poly(I:C), LPS, R848, Gardiquimod, and CpG2006 were tested at 50ng/ml. Besides LPS (Sigma), all TLR agonists were purchased from Invivogen. 2010-2011 Flumist (live attenuated) and Fluzone (inactive intramuscular) were tested at 1:500 dilution of the vaccine. Staphylococcus aureus bioparticles were also tested ($1e^6$bp/ml). For high resolution TEM, the tissue was fixed (2.5% gluteraldehyde), stained with OsO_4 (1hr)/ uranyl acetate (1hr). Samples were later dehydrated (ethanol, propylene oxide) and then embedded in Epon resin. Cut resin blocks were stained with uranyl acetate and lead citrate. The virus suspension was negatively stained with 2% phosphotungsitic acid for TEM. Vesicle cycling function was characterized via time-lapse imaging (2min intervals) of FM-143FX (1ug/ml, Invitrogen). Millipore 14-plex kits were used to quantify cytokine levels in culture supernatants (24hr). The analytes included Interleukin-1a,-1b,-6,-8,-10,-12(p40),-12(p70), GM-CSF, MCP-1, MIP-1a, MIP-1b, MDC, IP-10, IFN-a2, and TNF-a. RNAeasy kit was used to isolate RNA from the tissue constructs.

Results and Discussion: High resolution TEM imaging showed that the primary airway constructs exhibit differentiated cells of Type I and Type II morphology with healthy organelles and vesicle structures with lamellar bodies (surfactant) or lipids. The cell line tissue models were highly vescularized, with hollow vesicles and multinucleated cells. Time lapse fluorescence microscopy also confirmed greater activity in the primary tissue models in terms of vesicle formation and cycling in the nasal and alveolar tissue cellular membranes. In comparison to the primary cell models, the cell lines were more consistent at producing innate cytokines by TLR-3, TLR-4 and TLR2/TLR1 agonists; these cells are selected based on a compromise between growth and function. In comparison to the cell line models, the primary epithelial models showed overall higher levels of IL-6 and IL-8 with modest response by the alveolar models and a similar TLR2/1, TLR3 and TLR4 activity from the primary nasal epithelium. The alveolar epithelium alone generated a dampened macrophage chemotactic protein (MCP-1) response in the presence of filovirus antigen. In contrast the alveolar bilayer tissue showed a significant increase in macrophage inflammatory protein-1 production.

Conclusions: The evaluation of intrinsic differences and similarities between primary human cells and cell lines holds the potential for custom tissue models to study controlled biological systems for pathogen entry, processing, expansion and therapeutic delivery. Overall, our results indicate that the primary alveolar and nasal tissue models have different cellular morphology and function, relative to human cell lines. We plan to increase complexity in the system by exploring the mode of delivery via homogenous, gravity flow and aerosolized delivery with or without the addition of immune cells. Thus our in vitro system can be used for the evaluation of inter and intra-cellular responses including the mode of delivery and understanding of basic to complex cellular function of the upper and lower human airway.

Acknowledgements: This work was funded by USAMRIID, W81XWH-12-2-0071

References:

Yang W, Peter JI, Williams, Int J Pharm 356 (1-2):239-47, 2008
Griber SC, Richardson WM, Sodhi CP, Hackam DJ Mol Med 14 (9-10): 645-59, 2008